The Investigation of a New Time - of - Flight Mass Spectrometer

Toru Sakurai

Institute of Physics, Colledge of General Education, Osaka University

Contents

1. INTRODUCTION

Investigation of the structural elucidation of large molecules by mass spectrometry has become more widespread with the development of new ionization techniques. Field Desorption (FD) ionization was the first technique of exhibiting mass spectra of thermally labile compounds [1-1]. With the advent of Laser Desorption (LD) in 1968 [1-2], Secondary Ion Mass Spectrometry (SIMS) in 1973 [1-3], Plasma Desorption (PD) in 1974 [1-4], Fast Atom Bombardment (FAB) in 1981 [1-5], and subsequent developments, generation of large ions in this decade has become routine. The possibility of analysis of intractable compounds, such as peptides, lipids and proteins, has become apparent.

While these techniques made it possible to generate large ionic species, the instrumentation used for the mass spectrometric analysis of these compounds has begun to show its limitations.

Magnetic deflection instruments are the most common type of mass spectrometer used for the analysis of large molecules, but there is a relationship between the mass and the magnetic flux density such that:

$$\frac{M}{Z} = 4.82 \times 10^7 \frac{B^2 R^2}{V}$$

(1-1)

where M is the mass of the ion (dalton), Z is the charge (e), B

is the magnetic flux density (T), R is the radius of the magnet (m) and V is the acceleration voltage (volt). It can be seen that to increase the maximum mass to charge ratio analyzed by such a machine, either B or R must be increased, or V must be decreased. In an electromagnet cored with a ferromagnetic material, the magnetic flux density, B, has an upper limit (1.8T with Fe magnets and 2.3T with cobalt-alloy), therefore, an increment of B is not really viable. Reduction of the accelerating potential, V, leads to a decrease in ion extraction efficiency, and hence, a loss in sensitivity. The only feasible option, therefore, is to increase R, the radius of the magnetic sector. To double the radius requires a eight fold increase in weight of the magnet. This suggests difficulty in the construction of a large instrument.

Other types of mass spectrometers include Quadrupole mass filters (Q-filter) and Fourier Transform Ion Cyclotron Resonance instruments (FT-ICR). Q-filters are usually limited to around 1,000 dalton mass range, but recent reports suggest that this could be extended to as high as 3,000 dalton in the near future. This still does not bring them within the mass range that is currently proving to be of interest.

FT-ICR instruments are again limited by the strength of the magnetic field employed, even though super-conducting magnets are used. Recent developments have illustrated the mass range of current machines to be as high as 3,000 dalton. The theoretical mass range for FT-ICR is unlimited, but the technique is still very much in its infancy, and such instruments are very expensive, concluding the limitations.

The other option left open is that of Time-of-Flight Mass Spectrometry, and it is this area that will be considered in more detail.

Time-of-Flight (TOF) Mass Spectrometry was first postulated in 1946 [1-6]. Stephens suggested that, after acceleration from an ion source, ions having different M/Z values would possess different velocities, and consequently separate into groups spread out in space. From the time taken to travel a known distance, and if the acceleration voltage is known, the mass to charge ratio of the ions can be calculated as:

$$\frac{M}{Z} = 1.93 \times 10^8 \frac{V \, T_f^2}{L_f^2}$$

(1-2)

where V is the acceleration voltage (volt), T_f is the flight time (s), and L_f is the flight length (m).

Several improvements of the instrumentation of TOF mass spectrometers have been achieved, attending high resolving power in such systems.

In 1955, Wiley et al. improved the resolution of a TOF mass spectrometer with a new electron impact (EI) ion source [1-7]. The development utilized a special alignment of two electric fields in the ion source and a technique of delayed ion extraction.

A further attempt to improve resolution was suggested by Mamyrin et al. in 1973 [1-8], where an electric field was used to 'reflect' the ions in their flight path. This was in order

to compensate for energy distribution among ions generated in the ion source.

Poschenrieder (1971) proposed the use of a sector field to achieve angular isochronous and energy isochronous focusing, in order to improve resolution [1-9]. Spatial focusing should also be achieved to increase sensitivity. The principles of the multiple focusing were thus established.

TOF mass spectrometry has two advantages in the principle of mass measurement, which are:

1) The mass range of TOF instruments is theoretically unlimited, but, in practice, is limited only by the ionization technique capable of generating large ions.

2) TOF mass spectrometers detects all ions from low to high mass successively, and no ions are lost, because no scanning process is necessary. All ions produced are used in subsequent analysis, therefore the technique has a possibility to reduce sample consumption.

On the other hand, poor mass resolution and poor ion transmission of the TOF mass spectrometer have been responsible for restricting the widespread use of this technique for routine analysis. These problems arise from several origins inherent in TOF mass measurements as described in the following:

1) Mass resolution:

-4-

* Finite ionization time

    The pulse width of ionization time determines the mass

    resolution. If ions are generated over a relatively long

    time, then a considerable loss in resolution will result.

* Energy spread of ions

    Ions are generated with a distribution of energies. For a

    system with good resolution, energy isochronous focusing

    must be achieved.

* Divergence angle and entrance position of ions

    Ions flight different paths in the analyzer among their

    initial conditions, therefore the flight times are

    different. Isochronous focusing related to aperture angle

    and position should be met.

* Time resolution in the detection system

    It directly restricts the mass resolution of the TOF

    system. The technique of fast electric circuits is also

    needed in the detection and time measuring system.

2) Ion transmission:

   * Beam divergence

       If an analyzer has no spatial focusing action, the diver-

       gent ions will travel further than ions on a mean path,

       thus the beam diverges to a large spread at the detector.

       This leads to a loss in sensitivity. For a high transmis-

       sion efficiency, stigmatic focusing must be achieved.

   * Energy spread of ions

       Ions having different energies should be led to the

  .   detector, therefore spatial energy focusing should also be

required for the TOF system.

The purpose of this thesis is the investigation and the development of a high performance TOF mass spectrometer, which satisfies high resolution and high transmission, simultaneously. In order to solve the problems of TOF mass spectrometer, ion-optical designs of toroidal electric sectors for the analyzer are studied. A new TOF mass spectrometer consisting of four electric sectors is constructed and examined.

The results of the investigation are described in this thesis as follows:

The third-order approximations for the calculation of particle flight times in drift spaces, toroidal electric sectors, and quadrupole lenses are achieved. The influences of fringing fields are also considered. The results are given in Chapter Two.

The ion optics of multiple focusing TOF instruments, those consisting of toroidal electric sectors, are investigated in Chapter Three. The symmetrical arrangement is introduced in the ion-optical design. A lot of multiple focusing systems are found, and the relative merits and demerits of them are discussed. The doubly symmetrical system consisting of four electric fields is proposed.

In Chapter Four, the construction of the proposed TOF mass spectrometer is described. The pulse operations of two different kinds of ion sources (EI and SIMS) are also given.

The results of the experiments of the TOF mass spectrometer are given in Chapter Five. The ion-optical characteristics of

resolution and transmission of the system are investigated by using an EI ion source. The TOF mass spectra of peptides are obtained with good resolution using a secondary ion source for SIMS analysis.

REFERENCES

1-1. H.D. Beckey, Int. J. Mass Spectrom. Ion Phys., $\underline{2}$ (1969) 500.

1-2. P.G. Kistemaker, G.J.Q. van der Peyl and J. Haverkamp, in H.E. Morris, Ed., 'Soft Ionization Biological Mass Spectrometry,' Heyden: London (1981) pp 120-136.

1-3. A. Benninghoven, Surf. Sci., $\underline{35}$ (1973) 427.

1-4. D.F. Torgerson, R.P. Skowronski and R.D. Macfarlane, Biochem. Biophys. Res. Commun., $\underline{60}$ (1974) 616.

1-5. M. Barber, R.S. Bordoli, R.D. Sedgwick and A.N. Tyler, J. Chem. Soc. Chem. Commun., (1981) 325.

1-6. W.E. Stephens, Phys. Rev., $\underline{69}$ (1946) 691.

1-7. W.C. Wiley and I.H. McLaren, Rev. Sci. Instrum., $\underline{26}$ (1955) 1150.

1-8. B.A. Mamyrin, V.I. Karataev, D.V. Shmikk and V.A. Zagulin, Sov. Phys. JETP, $\underline{37}$ (1973) 45.

1-9. W.P. Poschenrieder, Int. J. Mass Spectrom. Ion Phys., $\underline{6}$ (1971) 413, Int. J. Mass Spectrom. Ion Phys., $\underline{9}$ (1972) 357.

2. CALCULATION OF PARTICLE FLIGHT TIMES TO A THIRD-ORDER APPROXIMATION

2-1. General description

The kinetic energy of a charged particle with mass m and velocity v is given by:

$$\frac{1}{2} m v^2 = Z V \qquad (eV) \tag{2-1}$$

where Z is the charge (e) and V is the acceleration voltage (volt). Therefore, the velocity, v, of the ion is calculated by the following relationship:

$$v = 1.39 \times 10^4 \left(\frac{Z V}{M}\right)^{\frac{1}{2}} \qquad (m/s) \tag{2-2}$$

where M is the mass of ion (dalton). The flight time, T_f, of an ion which travels a length L_f (m) is given by L_f/v as:

$$T_f = 72.0 L_f \left(\frac{M}{Z V}\right)^{\frac{1}{2}} \qquad (\mu s) \tag{2-3}$$

In a TOF mass spectrometer, the flight length, L_f, is a constant dependent upon the design of the system. If only the flight time of an ion is measured, the mass to charge ratio, M/Z, can be obtained by the relation of Eq. 2-3.

In a real ion beam, the kinetic energy of the ions is not homogeneous, an energy distribution caused by the ionization process exists, therefore, the flight times of ions with the same M/Z value may differ. In addition, ion flight paths differ within the analyzer due to different initial conditions of motion at the entrance to the analyzer. The spatial deviation and divergent angle of the ions from the optic axis raise the differences of flight times, even though they have the same M/Z value. Consequently, the resolution of a TOF mass spectrometer decreases by using such an ion beam.

In order to improve the resolution of a time-of-flight mass spectrometer, the use of a toroidal electric sector in the flight region was first proposed by Bakker [2-1] and Poschenrieder [1-9]. The electric sector acts as an energy analyzer, therefore ions having relatively high energies pass along an outer, bigger radius curve in the electric sector. The high energy particles travel a greater distance, therefore, the total flight times are independent of their energies, if a special arrangement of an electric sector is achieved. Such independence in flight times is called 'isochronous focusing' on the analogy of spatial focusing of an ordinary particle spectrometer. The schematic drawings of the isochronous focusing by an electric sector with respect to the spreads of energy and angle of ions are shown in Fig. 2-1. The isochronous focusing condition of a TOF system with an electric sector can be searched, if the flight times of ions in such ion-optical devices are calculated. By using the paraxial ion optics, the flight times of ions can be expressed by power series expan-

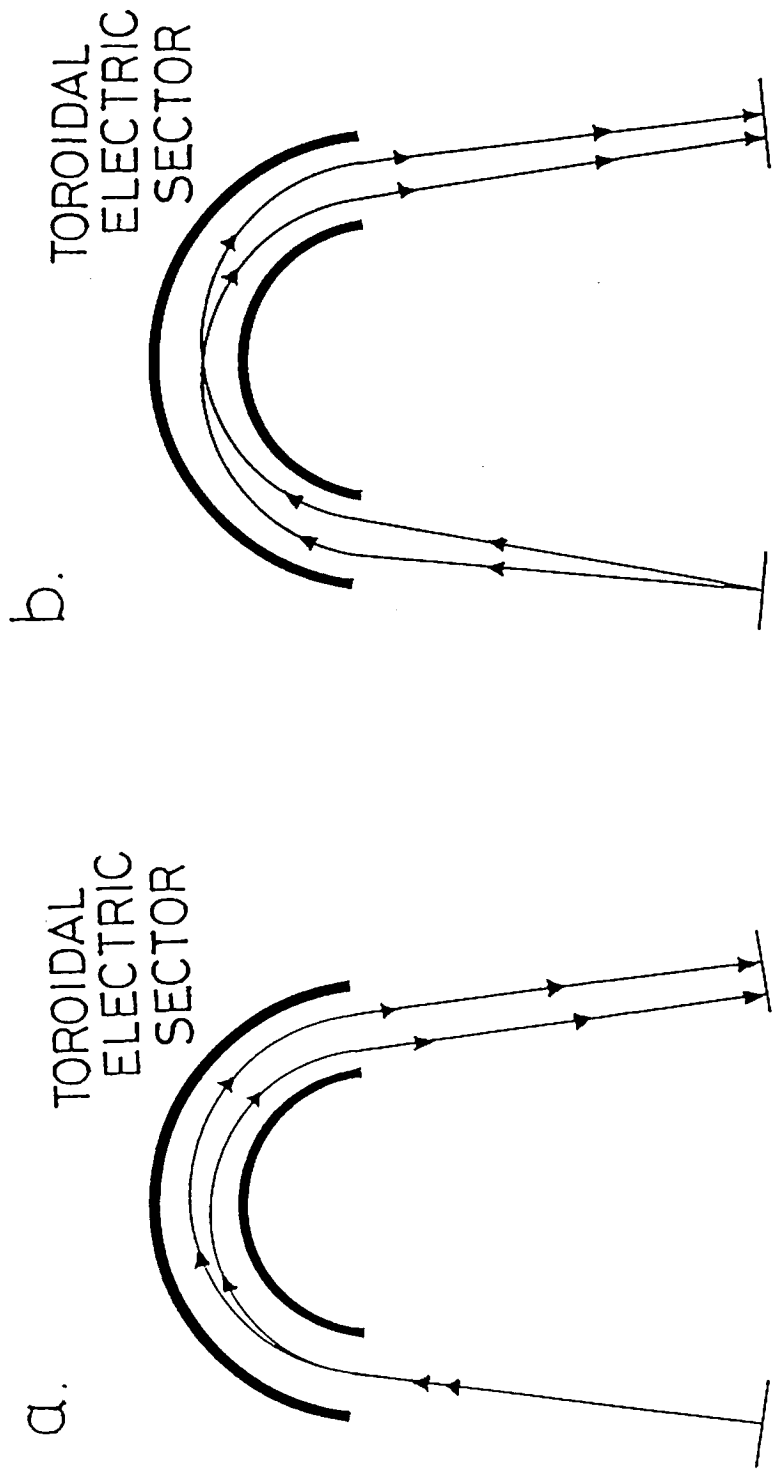Fig. 2 - 1.   The principle of isochronous focusing by a toroidal electric sector.

a) Isochronous focusing with respect to   b) Isochronous focusing with angle
   energy difference.   spread.

sions of the initial elements, as first-order terms, second-order terms and so on.

After achieving the first-order focusing condition in an ion-optical system, the higher-order time aberrations become important. The second-order flight times were obtained by Matsuda et al. [2-2]. In this chapter, the flight times of charged particles moving along arbitrary trajectories in an electric sector of a toroidal field are calculated to a third-order approximation. The second and the third-order time coefficients in the toroidal electric sector are derived using the results of the calculation of the ion trajectory obtained by Matsuo et al. [2-3]. An electric quadrupole lens is also available as an ion-optical device in TOF mass spectrometers. The third-order flight times in the quadrupoles are also calculated.

In the time-of-flight mass spectrometer, the time difference between the flight times of an arbitrary particle and that of the reference particle is important. A path length deviation, l, can be related to the time difference as:

$$l = (T - T_0)v_0 \qquad\qquad (2-4)$$

where T is the flight time of an arbitrary particle, T_0 that of the reference particle and v_0 is the velocity of the reference particle. The concept of path length deviation is convenient for the unified description for ions with any mass. We shall use path length deviations from now on.

For the calculation of the path length deviation of ions, the profiles of the ion trajectories in each ion optical device are necessary. In this thesis, the results of the ion trajectory calculations obtained by previous analyses are used. Therefore, some symbols are not consistent in the thesis. These are: The radius of the toroidal electric sector, a_e, which is expressed as ρ_0 in Section 2-2 and R_0 in Section 2-5. The deflection angle, ϕ_e, is expressed as ω in Section 2-2.

2-2. Third-order flight times in a toroidal condenser

In a toroidal electric sector, the optic axis is chosen as a circular arc of radius ρ_0, which is assumed to be at zero potential. The optic axis is the trajectory of the reference particle of charge e_0, mass m_0 and kinetic energy U_0 with velocity $v_0 = (2U_0/m_0)^{1/2}$. A cylindrical coordinate system $(\rho_0 + x, \omega, y)$ is used as shown in Fig. 2-2. The optic axis is given by a circle ($x=0$, $y=0$). The trajectory of an arbitrary particle of charge e, mass $m = m_0(1+\gamma)e/e_0$ and kinetic energy (at zero potential) $U = U_0(1+\delta)e/e_0$ is described by the coordinates $x(\omega)$ and $y(\omega)$ as functions of ω. γ and δ are the relative mass and energy deviations, respectively.

In a toroidal electric sector, the path length deviation defined in Eq. 2-4 is given by:

$$l = \int_0^s \frac{v_0}{v} \, ds - \rho_0 \omega \qquad (2-5)$$

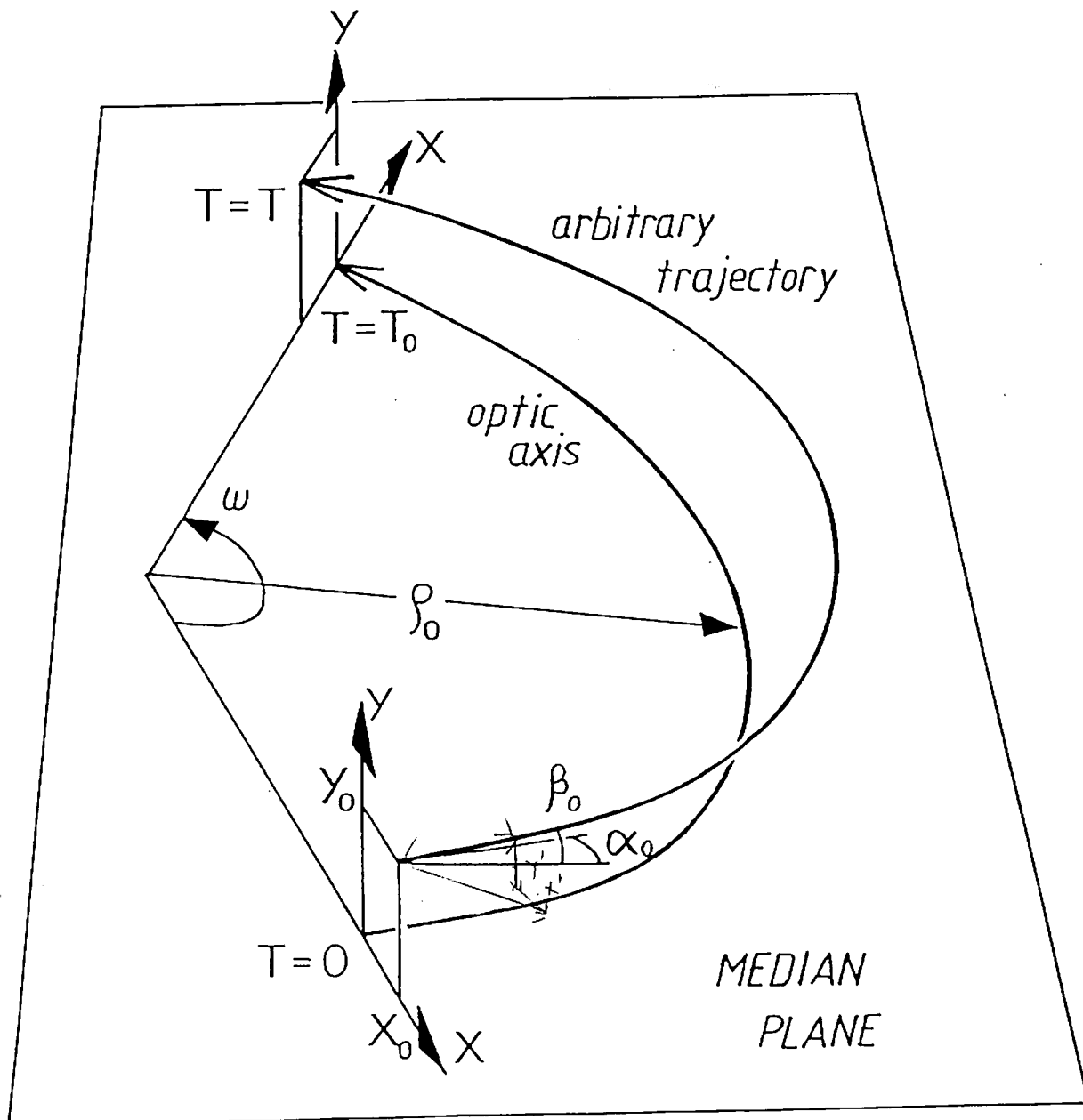In the cylindrical coordinates, the differential element of the

Fig. 2 - 2.   Definition of the coordinate system in a toroidal
electric sector.

path length is given from the algebraic relation:

$$ds = \left[x'^2 + (\rho_0 + x)^2 + y'^2 \right]^{1/2} d\omega \qquad (2\text{-}6)$$

where a prime denotes $d/d\omega$. The relationships between the in-
clination angles of the ion trajectory from the optic axis,
$\alpha(\omega)$ and $\beta(\omega)$, and the derivatives of the spatial coordinates,
$x'(\omega)$ and $y'(\omega)$, are $\tan\alpha = x'/(\rho_0 + x)$ and $\tan\beta = y'/(\rho_0 + x)$,
respectively. Therefore, the line element, ds, is expressed
as:

$$ds = \left[\rho_0 + x \right]\left[1 + \tan^2\alpha + \tan^2\beta \right]^{1/2} d\omega \qquad (2\text{-}7)$$

The velocity, v, of an arbitrary particle in an electric field
is calculated from the energy conservation equation as:

$$
\begin{aligned}
v &= \left[\frac{2(U - e\phi)}{m} \right]^{1/2} \\
&= \left[\frac{2U_0}{m_0} \right]^{1/2} \left[\frac{U/e - \phi}{U_0/e_0} \right]^{1/2} \left[\frac{m/e}{m_0/e_0} \right]^{-1/2} \\
&= v_0 \left[1 + \delta - \frac{2\phi}{\chi_e} \right]^{1/2} \left[1 + \gamma \right]^{-1/2}
\end{aligned}
$$

$$(2\text{-}8)$$

where χ_e is the electric rigidity of an electric field defined
as $\chi_e = 2U_0/e_0$. And $\phi(x,y)$ is an electric potential of the
toroidal field which is assumed as $\phi(0,0)=0$ along the optic
axis. The electric potential should satisfy the Laplace
equation, $\Delta\phi(x,y)=0$. The mirror symmetric condition, $\phi(x,y)=$

-15-

Φ(x,-y), with respect to the median plane should also be applied to the the electric potential, because the structure of the toroidal condenser is mirror symmetric. The electric potential of the toroidal electric field can be expressed as a power series expansion around the optic axis. The expression of the potential was obtained by Wollnik et al. [2-4] as:

$$\phi(x, y) = \chi_c \left[\frac{x}{\rho_0} + \frac{a_{20}}{2} \frac{x^2}{\rho_0^2} - \frac{1}{2}(1 + a_{20}) \frac{y^2}{\rho_0^2} + \frac{a_{30}}{6} \frac{x^3}{\rho_0^3} + \frac{1}{2}(1 - a_{20} - a_{30}) \frac{xy^2}{\rho_0^3} + \cdots \right]$$

(2-9)

where a_{20} and a_{30} are the field indices of the toroidal electric field, respectively. They are determined by the shape of the electrodes of the toroidal condenser. Note that here, the so-called toroidal factor of the electric sector, c, is given by the equation $c=-1-a_{20}$.

The path length deviation defined in Eq. 2-5 of an arbitrary particle is expressed as a function of x(ω), tanα(ω), y(ω), β(ω), γ and δ, which are assumed to be first-order small quantities. Therefore, we may express the path length deviation as a power series expansion of them. Introducing Eqs. 2-7,8,9 to Eq. 2-5 and expanding up to the third order, the obtained expression is:

$$I = \int_0^\omega d\omega \left[2x + \frac{\rho_0}{2}\gamma - \frac{\rho_0}{2}\delta + \frac{f_1}{\rho_0}x^2 + x\gamma - 2x\delta + \frac{\rho_0}{2}\alpha^2 - \frac{\rho_0}{8}\gamma^2 \right.$$

$$- \frac{\rho_0}{4}\gamma\delta + \frac{3\rho_0}{8}\delta^2 + \frac{f_2}{\rho_0}y^2 + \frac{\rho_0}{2}\beta^2 + \frac{f_3}{\rho_0^2}x^3 + \frac{2+k_x^2}{4\rho_0}x^2\gamma$$

$$- \frac{12+3k_x^2}{4\rho_0}x^2\delta + x\alpha^2 - \frac{1}{4}x\gamma^2 - x\gamma\delta + \frac{9}{4}x\delta^2 + \frac{f_4}{\rho_0^2}xy^2 + x\beta^2$$

$$+ \frac{\rho_0}{4}\alpha^2\gamma - \frac{\rho_0}{4}\alpha^2\delta + \frac{\rho_0}{16}\gamma^3 + \frac{\rho_0}{16}\gamma^2\delta + \frac{3\rho_0}{16}\gamma\delta^2 + \frac{k_y^2}{4\rho_0}\gamma y^2$$

$$\left. + \frac{\rho_0}{4}\gamma\beta^2 - \frac{5\rho_0}{16}\delta^3 - \frac{3k_y^2}{4\rho_0}\delta y^2 - \frac{\rho_0}{4}\delta\beta^2 \right]$$

$$(2\text{-}10)$$

where f_1, f_2, f_3, f_4, k_x and k_y are constants related to the field indices, a_{20} and a_{30}, as defined in Table 2-1.

TABLE 2-1.
Abbreviations used in this section.

Symbol	Meaning
f_1	$\frac{1}{2}(5 + a_{20})$
f_2	$-\frac{1}{2}(1 + a_{20})$
f_3	$4 + 2a_{20} + \frac{1}{6}a_{30}$
f_4	$-\frac{1}{2}(3 + 5a_{20} + a_{30})$
k_x	$\sqrt{3 + a_{20}}$
k_y	$\sqrt{-1 - a_{20}}$
s_x	$\sin k_x\omega$
c_x	$\cos k_x\omega$
s_y	$\sin k_y\omega$
c_y	$\cos k_y\omega$

The spatial deviation $x(\omega)$, $y(\omega)$ and inclination angles $\alpha(\omega)$ and $\beta(\omega)$ in Eq. 2-10 are functions of ω, and an explicit form of them is necessary to calculate the path length deviation. The deviations and inclination angles of the ion trajectory can be obtained by solving the trajectory equations of the toroidal

condenser. The third-order deviation x(ω), the second-order deviation y(ω), and the second-order inclination angles α(ω) and β(ω) in Ref. 2-3 are expressed as follows:

$$x = c_x x_0 + \frac{\rho_0 s_x}{k_x}(\tan \alpha_0) + \frac{\rho_0(1-c_x)}{k_x^2}\delta$$

$$+ \sum_m mH(xx|m)x_0^2 + \sum_m mH(x\alpha|m)x_0\alpha_0 + \sum_m mH(x\delta|m)x_0\delta$$

$$+ \sum_m mH(\alpha\alpha|m)\alpha_0^2 + \sum_m mH(\alpha\delta|m)\alpha_0\delta + \sum_m mH(\delta\delta|m)\delta^2$$

$$+ \sum_m mH(yy|m)y_0^2 + \sum_m mH(y\beta|m)y_0\beta_0 + \sum_m mH(\beta\beta|m)\beta_0^2$$

$$+ \sum_m mH(xxx|m)x_0^3 + \sum_m mH(xx\alpha|m)x_0^2\alpha_0 + \sum_m mH(xx\delta|m)x_0^2\delta$$

$$+ \sum_m mH(x\alpha\alpha|m)x_0\alpha_0^2 + \sum_m mH(x\alpha\delta|m)x_0\alpha_0\delta + \sum_m mH(x\delta\delta|m)x_0\delta^2$$

$$+ \sum_m mH(xyy|m)x_0y_0^2 + \sum_m mH(xy\beta|m)x_0y_0\beta_0 + \sum_m mH(x\beta\beta|m)x_0\beta_0^2$$

$$+ \sum_m mH(\alpha\alpha\alpha|m)\alpha_0^3 + \sum_m mH(\alpha\alpha\delta|m)\alpha_0^2\delta + \sum_m mH(\alpha\delta\delta|m)\alpha_0\delta^2$$

$$+ \sum_m mH(\alpha yy|m)\alpha_0 y^2 + \sum_m mH(\alpha y\beta|m)\alpha_0 y_0\beta_0 + \sum_m mH(\alpha\beta\beta|m)\alpha_0\beta_0^2$$

$$+ \sum_m mH(\delta\delta\delta|m)\delta^3 + \sum_m mH(\delta yy|m)\delta y_0^2 + \sum_m mH(\delta y\beta|m)\delta y_0\beta_0$$

$$+ \sum_m mH(\delta\beta\beta|m)\delta\beta_0^2$$

$$\tan \alpha = -\frac{k_x s_x}{\rho_0}x_0 + c_x(\tan \alpha_0) + \frac{s_x}{k_x}\delta$$

$$+ \sum_m mH'(xx|m)x_0^2 + \sum_m mH'(x\alpha|m)x_0\alpha_0 + \sum_m mH'(x\delta|m)x_0\delta$$

$$+ \sum_m mH'(\alpha\alpha|m)\alpha_0^2 + \sum_m mH'(\alpha\delta|m)\alpha_0\delta + \sum_m mH'(\delta\delta|m)\delta^2$$

$$+ \sum_m mH'(yy|m)y_0^2 + \sum_m mH'(y\beta|m)y_0\beta_0 + \sum_m mH'(\beta\beta|m)\beta_0^2$$

$$y = c_y y_0 + \frac{\rho_0 s_y}{k_y}\beta_0$$

$$+ \sum_m mH(yx|m)y_0 x_0 + \sum_m mH(y\alpha|m)y_0\alpha_0 + \sum_m mH(y\delta|m)y_0\delta$$

$$+ \sum_m mH(\beta x|m)\beta_0 x_0 + \sum_m mH(\beta\alpha|m)\beta_0\alpha_0 + \sum_m mH(\beta\delta|m)\beta_0\delta$$

$$\beta = -\frac{k_y s_y}{\rho_0} y_0 + c_y \beta_0$$
$$+ \sum_m mH'(yx|m) y_0 x_0 + \sum_m mH'(y\alpha|m) y_0 \alpha_0 + \sum_m mH'(y\delta|m) y_0 \delta$$
$$+ \sum_m mH'(\beta x|m) \beta_0 x_0 + \sum_m mH'(\beta\alpha|m) \beta_0 \alpha_0 + \sum_m mH'(\beta\delta|m) \beta_0 \delta$$

$$(2-11)$$

where k_x, k_y, s_x, c_x, s_y and c_y are defined in Table 2-1. The elements of the H-matrix, $H(xx|m)$, $H'(xx|m)$, $H(xxx|m)$, etc., have been defined in Eqs. (19a,b), (22a,b) and (26) of Ref. 2-3, respectively. The symbol m represents one of the following functions,

$(1, s_x, c_x, \omega, s_x s_x, s_x c_x, s_x \omega, c_x \omega, s_y s_y, s_y c_y, s_x s_x s_x,$
$s_x s_x c_x, s_x s_x \omega, s_x c_x \omega, s_x \omega \omega, c_x \omega \omega, s_x s_y s_y, s_x s_y c_y, c_x s_y s_y,$
$c_x s_y c_y, s_y s_y \omega, s_y c_y \omega, s_y, c_y, s_x s_y, s_x c_y, c_x s_y, c_x c_y)$.

Introducing Eqs. 2-11 into Eq. 2-10 and performing the integration with respect to ω, we obtain the path length deviation in the toroidal electric sector to a third-order approximation. The final expression of the path length deviation, ℓ, is expressed as a power series expansion of a initial conditions, x_0, $\tan\alpha_0$, y_0, β_0, γ and δ.

$$l = (l|x)x_0 + (l|\alpha)(\tan \alpha_0) + (l|\gamma)\gamma + (l|\delta)\delta$$
$$+ (l|xx)x_0^2 + (l|x\alpha)x_0\alpha_0 + (l|x\gamma)x_0\gamma + (l|x\delta)x_0\delta + (l|\alpha\alpha)\alpha_0^2$$
$$+ (l|\alpha\gamma)\alpha_0\gamma + (l|\alpha\delta)\alpha_0\delta + (l|\gamma\gamma)\gamma^2 + (l|\gamma\delta)\gamma\delta + (l|\delta\delta)\delta^2$$
$$+ (l|yy)y_0^2 + (l|y\beta)y_0\beta_0 + (l|\beta\beta)\beta_0^2$$
$$+ (l|xxx)x_0^3 + (l|xx\alpha)x_0^2\alpha_0 + (l|xx\gamma)x_0^2\gamma + (l|xx\delta)x_0^2\delta$$
$$+ (l|x\alpha\alpha)x_0\alpha_0^2 + (l|x\alpha\gamma)x_0\alpha_0\gamma + (l|x\alpha\delta)x_0\alpha_0\delta + (l|x\gamma\gamma)x_0\gamma^2$$
$$+ (l|x\gamma\delta)x_0\gamma\delta + (l|x\delta\delta)x_0\delta^2 + (l|xyy)x_0y_0^2 + (l|xy\beta)x_0y_0\beta_0$$
$$+ (l|x\beta\beta)x_0\beta_0^2 + (l|\alpha\alpha\alpha)\alpha_0^3 + (l|\alpha\alpha\gamma)\alpha_0^2\gamma + (l|\alpha\alpha\delta)\alpha_0^2\delta$$
$$+ (l|\alpha\gamma\gamma)\alpha_0\gamma^2 + (l|\alpha\gamma\delta)\alpha_0\gamma\delta + (l|\alpha\delta\delta)\alpha_0\delta^2 + (l|\alpha yy)\alpha_0 y_0^2$$
$$+ (l|\alpha y\beta)\alpha y_0\beta_0 + (l|\alpha\beta\beta)\alpha_0\beta_0^2 + (l|\gamma\gamma\gamma)\gamma^3 + (l|\gamma\gamma\delta)\gamma^2\delta$$
$$+ (l|\gamma\delta\delta)\gamma\delta^2 + (l|\gamma yy)\gamma y_0^2 + (l|\gamma y\beta)\gamma y_0\beta_0 + (l|\gamma\beta\beta)\gamma\beta_0^2$$
$$+ (l|\delta\delta\delta)\delta^3 + (l|\delta yy)\delta y_0^2 + (l|\delta y\beta)\delta y_0\beta_0 + (l|\delta\beta\beta)\delta\beta_0^2$$

$$(2-12)$$

To calculate the explicit form of these coefficients, one has to achieve the integrations, $\int_0^\omega m \, d\omega$. The results are denoted by F(m) and are given in Appendix 1. Then the coefficients are given by:

$$(l|x) = 2F(c_x)$$

$$(l|\alpha) = F(s_x)\left[\frac{2\rho_0}{k_x}\right]$$

$$(l|\gamma) = F(1)\left[\frac{\rho_0}{2}\right]$$

$$(l|\delta) = F(1)\left[\frac{2\rho_0}{k_x^2} - \frac{\rho_0}{2}\right] + F(c_x)\left[\frac{-2\rho_0}{k_x^2}\right]$$

$$(l|xx) = F(1)\left[2H(xx|1) + \frac{f_1}{\rho_0}\right] + F(c_x)[2H(xx|c_x)]$$
$$+ F(s_x s_x)\left[2H(xx|s_x s_x) - \frac{f_1}{\rho_0} + \frac{k_x^2}{2\rho_0}\right]$$

$$(l|x\alpha) = F(s_x)[2H(x\alpha|s_x)] + F(s_x c_x)\left[2H(x\alpha|s_x c_x) + 2\frac{f_1}{k_x} - k_x\right]$$

$$(l|x\gamma) = F(c_x)$$

$$(l \mid x\delta) = F(1)\left[2H(x\delta \mid 1) - \frac{2f_1}{k_x^2}\right] + F(c_x)\left[2H(x\delta \mid c_x) + \frac{2f_1}{k_x^2} - 2\right]$$

$$+ F(s_x s_x)\left[2H(x\delta \mid s_x s_x) + \frac{2f_1}{k_x^2} - 1\right] + F(s_x \omega)[2H(x\delta \mid s_x \omega)]$$

$$(l \mid \alpha\alpha) = F(1)\left[2H(\alpha\alpha \mid 1) + \frac{\rho_0}{2}\right] + F(c_x)[2H(\alpha\alpha \mid c_x)]$$

$$+ F(s_x s_x)\left[2H(\alpha\alpha \mid s_x s_x) + \frac{f_1 \rho_0}{k_x^2} - \frac{\rho_0}{2}\right]$$

$$(l \mid \alpha\gamma) = F(s_x)\left[\frac{\rho_0}{k_x}\right]$$

$$(l \mid \alpha\delta) = F(s_x)\left[2H(\alpha\delta \mid s_x) + \frac{2f_1 \rho_0}{k_x^3} - \frac{2\rho_0}{k_x}\right] + F(s_x c_x)\left[2H(\alpha\delta \mid s_x c_x)\right.$$

$$\left. - \frac{2f_1 \rho_0}{k_x^3} + \frac{\rho_0}{k_x}\right] + F(c_x \omega)[2H(\alpha\delta \mid c_x \omega)]$$

$$(l \mid \gamma\gamma) = F(1)\left[\frac{-\rho_0}{8}\right]$$

$$(l \mid \gamma\delta) = F(1)\left[\frac{\rho_0}{k_x^2} - \frac{\rho_0}{4}\right] + F(c_x)\left[\frac{-\rho_0}{k_x^2}\right]$$

$$(l \mid \delta\delta) = F(1)\left[2H(\delta\delta \mid 1) + \frac{2f_1 \rho_0}{k_x^4} - \frac{2\rho_0}{k_x^2} + \frac{3\rho_0}{8}\right]$$

$$+ F(c_x)\left[2H(\delta\delta \mid c_x) - \frac{2f_1 \rho_0}{k_x^4} + \frac{2\rho_0}{k_x^2}\right]$$

$$+ F(s_x s_x)\left[2H(\delta\delta \mid s_x s_x) - \frac{f_1 \rho_0}{k_x^4} + \frac{\rho_0}{2k_x^2}\right] + F(s_x \omega)[2H(\delta\delta \mid s_x \omega)]$$

$$(l \mid yy) = F(1)\left[2H(yy \mid 1) + \frac{f_2}{\rho_0}\right] + F(c_x)[2H(yy \mid c_x)]$$

$$+ F(s_y s_y)[2H(yy \mid s_y s_y)]$$

$$(l \mid y\beta) = F(s_x)[2H(y\beta \mid s_x)] + F(s_y c_y)[2H(y\beta \mid s_y c_y)]$$

$$(l \mid \beta\beta) = F(1)\left[2H(\beta\beta \mid 1) + \frac{\rho_0}{2}\right] + F(c_x)[2H(\beta\beta \mid c_x)]$$

$$+ F(s_y s_y)[2H(\beta\beta \mid s_y s_y)]$$

$$(l \mid xxx) = F(1)\left[2H(xxx \mid 1) + \left(\frac{2f_1}{\rho_0}\right)H(xx \mid c_x)\right] + F(c_x)\left[2H(xxx \mid c_x)\right.$$

$$\left. + \left(\frac{2f_1}{\rho_0}\right)H(xx \mid 1) + \frac{f_3}{\rho_0^2}\right] +$$

$$+ F(s_x s_x)\left[2H(xxx|s_x s_x) - \left(\frac{2f_1}{\rho_0}\right)H(xx|c_x) - k_x H'(xx|s_x)\right]$$

$$+ F(s_x \omega)[2H(xxx|s_x \omega)]$$

$$+ F(s_x s_x c_x)\left[2H(xxx|s_x s_x c_x) + \left(\frac{2f_1}{\rho_0}\right)H(xx|s_x s_x)\right.$$

$$\left. - k_x H'(xx|s_x c_x) - \frac{f_3}{\rho_0^2} + \frac{k_x^2}{\rho_0^2}\right]$$

$$(l|xx\alpha) = F(s_x)\left[2H(xx\alpha|s_x) + \left(\frac{2f_1}{k_x}\right)H(xx|1) + \left(\frac{2f_1}{\rho_0}\right)H(x\alpha|s_x c_x)\right.$$

$$\left. + \rho_0 H'(xx|s_x c_x) - k_x H'(x\alpha|1) + \frac{3f_3}{k_x \rho_0} - \frac{2k_x}{\rho_0}\right]$$

$$+ F(s_x c_x)\left[2H(xx\alpha|s_x c_x) + \left(\frac{2f_1}{k_x}\right)H(xx|c_x) + \left(\frac{2f_1}{\rho_0}\right)H(x\alpha|s_x)\right.$$

$$\left. + \rho_0 H'(xx|s_x) - k_x H'(x\alpha|c_x)\right] + F(c_x \omega)[2H(xx\alpha|c_x \omega)]$$

$$+ F(s_x s_x s_x)\left[2H(xx\alpha|s_x s_x s_x) + \left(\frac{2f_1}{k_x}\right)H(xx|s_x s_x)\right.$$

$$- \left(\frac{2f_1}{\rho_0}\right)H(x\alpha|s_x c_x)$$

$$\left. - \rho_0 H'(xx|s_x c_x) - k_x H'(x\alpha|s_x s_x) - \frac{3f_3}{k_x \rho_0} + \frac{3k_x}{\rho_0}\right]$$

$$(l|xx\gamma) = F(1)\left[H(xx|1) + \frac{1}{2\rho_0} + \frac{k_x^2}{4\rho_0}\right] + F(c_x)[H(xx|c_x)]$$

$$+ F(s_x s_x)\left[H(xx|s_x s_x) - \frac{1}{2\rho_0}\right]$$

$$(l|xx\delta) = F(1)\left[2H(xx\delta|1) + \left(\frac{2f_1}{k_x^2} - 2\right)H(xx|1) - \left(\frac{2f_1}{k_x^2}\right)H(xx|c_x)\right.$$

$$\left. + \left(\frac{2f_1}{\rho_0}\right)H(x\delta|c_x) + \frac{3f_3}{k_x^2 \rho_0} - \frac{3}{\rho_0} - \frac{3k_x^2}{4\rho_0}\right]$$

$$+ F(c_x)\left[2H(xx\delta|c_x) + \left(\frac{2f_1}{k_x^2} - 2\right)H(xx|c_x)\right.$$

$$\left. - \left(\frac{2f_1}{k_x^2}\right)H(xx|1) + \left(\frac{2f_1}{\rho_0}\right)H(x\delta|1) - \frac{3f_3}{k_x^2 \rho_0}\right]$$

$$+ F(s_x s_x)\left[2H(xx\delta|s_x s_x) + \left(\frac{2f_1}{k_x^2} - 2\right)H(xx|s_x s_x)\right.$$

$$+\left(\frac{2f_1}{k_x^2}\right)H(xx|c_x)-\left(\frac{2f_1}{\rho_0}\right)H(x\delta|c_x)$$

$$+\left(\frac{\rho_0}{k_x}\right)H'(xx|s_x)-k_xH'(x\delta|s_x)-\frac{3f_3}{k_x^2\rho_0}+\frac{4}{\rho_0}+\frac{k_x^2}{2\rho_0}\Bigg]$$

$$+F(s_x\omega)[2H(xx\delta|s_x\omega)]+F(s_xs_xc_x)\Bigg[2H(xx\delta|s_xs_xc_x)$$

$$-\left(\frac{2f_1}{k_x^2}\right)H(xx|s_xs_x)+\left(\frac{2f_1}{\rho_0}\right)H(x\delta|s_xs_x)+\left(\frac{\rho_0}{k_x}\right)H'(xx|s_xc_x)$$

$$-k_xH'(x\delta|s_xc_x)+\frac{3f_3}{k_x^2\rho_0}-\frac{3}{\rho_0}\Bigg]+F(s_xc_x\omega)\Bigg[2H(xx\delta|s_xc_x\omega)$$

$$+\left(\frac{2f_1}{\rho_0}\right)H(x\delta|s_x\omega)-k_xH'(x\delta|c_x\omega)\Bigg]$$

$$(l|x\alpha\alpha)=F(1)\Bigg[2H(x\alpha\alpha|1)+\left(\frac{2f_1}{\rho_0}\right)H(\alpha\alpha|c_x)+\rho_0H'(x\alpha|c_x)\Bigg]$$

$$+F(c_x)\Bigg[2H(x\alpha\alpha|c_x)+\left(\frac{2f_1}{\rho_0}\right)H(\alpha\alpha|1)+\rho_0H'(x\alpha|1)+1\Bigg]$$

$$+F(s_xs_x)\Bigg[2H(x\alpha\alpha|s_xs_x)+\left(\frac{2f_1}{k_x}\right)H(x\alpha|s_x)-\left(\frac{2f_1}{\rho_0}\right)H(\alpha\alpha|c_x)$$

$$-\rho_0H'(x\alpha|c_x)-k_xH'(\alpha\alpha|s_x)\Bigg]+F(s_x\omega)[2H(x\alpha\alpha|s_x\omega)]$$

$$+F(s_xs_xc_x)\Bigg[2H(x\alpha\alpha|s_xs_xc_x)+\left(\frac{2f_1}{k_x}\right)H(x\alpha|s_xc_x)$$

$$+\left(\frac{2f_1}{\rho_0}\right)H(\alpha\alpha|s_xs_x)$$

$$+\rho_0H'(x\alpha|s_xs_x)-k_xH'(\alpha\alpha|s_xc_x)+\frac{3f_3}{k_x^2}-3\Bigg]$$

$$(l|x\alpha\gamma)=F(s_x)\big[H(x\alpha|s_x)\big]+F(s_xc_x)\Bigg[H(x\alpha|s_xc_x)+\frac{1}{k_x}\Bigg]$$

$$(l|x\alpha\delta) = F(s_x)\left[2H(x\alpha\delta|s_x) + \left(\frac{2f_1}{k_x^2} - 2\right)H(x\alpha|s_x) - \left(\frac{2f_1}{k_x^2}\right)H(x\alpha|s_xc_x)\right.$$

$$+ \left(\frac{2f_1}{k_x}\right)H(x\delta|1) + \left(\frac{2f_1}{\rho_0}\right)H(\alpha\delta|s_xc_x) + \left(\frac{\rho_0}{k_x}\right)H'(x\alpha|1)$$

$$\left. + \rho_0 H'(x\delta|s_xc_x) - k_x H'(\alpha\delta|1) - \frac{6f_3}{k_x^3} + \frac{4}{k_x}\right]$$

$$+ F(\omega)\left[2H(x\alpha\delta|\omega) + \left(\frac{2f_1}{\rho_0}\right)H(\alpha\delta|c_x\omega) + \rho_0 H'(x\delta|c_x\omega)\right]$$

$$+ F(s_xc_x)\left[2H(x\alpha\delta|s_xc_x) + \left(\frac{2f_1}{k_x^2} - 2\right)H(x\alpha|s_xc_x)\right.$$

$$- \left(\frac{2f_1}{k_x^2}\right)H(x\alpha|s_x) + \left(\frac{2f_1}{k_x}\right)H(x\delta|c_x) + \left(\frac{2f_1}{\rho_0}\right)H(\alpha\delta|s_x)$$

$$+ \left(\frac{\rho_0}{k_x}\right)H'(x\alpha|c_x) + \rho_0 H'(x\delta|s_x) - k_x H'(\alpha\delta|c_x)$$

$$\left. + \frac{6f_3}{k_x^3} - \frac{8}{k_x} - k_x\right] + F(c_x\omega)\left[2H(x\alpha\delta|c_x\omega)\right]$$

$$+ F(s_xs_xs_x)\left[2H(x\alpha\delta|s_xs_xs_x) + \left(\frac{2f_1}{k_x^2}\right)H(x\alpha|s_xc_x)\right.$$

$$+ \left(\frac{2f_1}{k_x}\right)H(x\delta|s_xs_x) - \left(\frac{2f_1}{\rho_0}\right)H(\alpha\delta|s_xc_x) + \left(\frac{\rho_0}{k_x}\right)H'(x\alpha|s_xs_x)$$

$$\left. - \rho_0 H'(x\delta|s_xc_x) - k_x H'(\alpha\delta|s_xs_x) + \frac{6f_3}{k_x^3} - \frac{6}{k_x}\right]$$

$$+ F(s_xs_x\omega)\left[2H(x\alpha\delta|s_xs_x\omega) + \left(\frac{2f_1}{k_x}\right)H(x\delta|s_x\omega)\right.$$

$$\left. - \left(\frac{2f_1}{\rho_0}\right)H(\alpha\delta|c_x\omega) - \rho_0 H'(x\delta|c_x\omega) - k_x H'(\alpha\delta|s_x\omega)\right]$$

$$(l|x\gamma\gamma) = \frac{-F(c_x)}{4}$$

$$(l|x\gamma\delta) = F(1)\left[H(x\delta|1) - \frac{1}{k_x^2} - \frac{1}{2}\right] + F(c_x)\left[H(x\delta|c_x) + \frac{1}{k_x^2} - \frac{1}{2}\right]$$

$$+ F(s_xs_x)\left[H(x\delta|s_xs_x) + \frac{1}{k_x^2}\right] + F(s_x\omega)\left[H(x\delta|s_x\omega)\right]$$

$$(I \mid x\delta\delta) = F(1)\left[2H(x\delta\delta \mid 1) + \left(\frac{2f_1}{k_x^2} - 2 \right) H(x\delta \mid 1) - \left(\frac{2f_1}{k_x^2} \right) H(x\delta \mid c_x) \right.$$

$$\left. + \left(\frac{2f_1}{\rho_0} \right) H(\delta\delta \mid c_x) - \frac{6f_3}{k_x^4} + \frac{6}{k_x^2} + \frac{3}{2} \right]$$

$$+ F(c_x)\left[2H(x\delta\delta \mid c_x) + \left(\frac{2f_1}{k_x^2} - 2 \right) H(x\delta \mid c_x) - \left(\frac{2f_1}{k_x^2} \right) H(x\delta \mid 1) \right.$$

$$\left. + \left(\frac{2f_1}{\rho_0} \right) H(\delta\delta \mid 1) + \frac{6f_3}{k_x^4} - \frac{6}{k_x^2} + \frac{3}{4} \right]$$

$$+ F(s_x s_x)\left[2H(x\delta\delta \mid s_x s_x) + \left(\frac{2f_1}{k_x^2} - 2 \right) H(x\delta \mid s_x s_x) \right.$$

$$+ \left(\frac{2f_1}{k_x^2} \right) H(x\delta \mid c_x)$$

$$- \left(\frac{2f_1}{\rho_0} \right) H(\delta\delta \mid c_x) + \left(\frac{\rho_0}{k_x} \right) H'(x\delta \mid s_x) - k_x H'(\delta\delta \mid s_x)$$

$$\left. + \frac{6f_3}{k_x^4} - \frac{8}{k_x^2} - 1 \right]$$

$$+ F(s_x \omega)\left[2H(x\delta\delta \mid s_x \omega) + \left(\frac{2f_1}{k_x^2} - 2 \right) H(x\delta \mid s_x \omega) \right] +$$

$$+ F(s_x s_x c_x)\left[2H(x\delta\delta \mid s_x s_x c_x) - \left(\frac{2f_1}{k_x^2} \right) H(x\delta \mid s_x s_x) \right.$$

$$+ \left(\frac{2f_1}{\rho_0} \right) H(\delta\delta \mid s_x s_x) + \left(\frac{\rho_0}{k_x} \right) H'(x\delta \mid s_x c_x)$$

$$\left. - k_x H'(\delta\delta \mid s_x c_x) - \frac{3f_3}{k_x^4} + \frac{3}{k_x^2} \right] + F(s_x c_x \omega)\left[2H(x\delta\delta \mid s_x c_x \omega) \right.$$

$$- \left(\frac{2f_1}{k_x^2} \right) H(x\delta \mid s_x \omega) + \left(\frac{2f_1}{\rho_0} \right) H(\delta\delta \mid s_x \omega) + \left(\frac{\rho_0}{k_x} \right) H'(x\delta \mid c_x \omega)$$

$$\left. - k_x H'(\delta\delta \mid c_x \omega) \right] + F(c_x \omega \omega)\left[2H(x\delta\delta \mid c_x \omega \omega) \right]$$

$$(l \mid xyy) = F(1)\left[2H(xyy \mid 1) + \left(\frac{2f_1}{\rho_0}\right)H(yy \mid c_x) + \left(\frac{2f_2}{\rho_0}\right)H(yx \mid c_y)\right]$$

$$+ F(c_x)\left[2H(xyy \mid c_x) + \left(\frac{2f_1}{\rho_0}\right)H(yy \mid 1)\right.$$

$$\left. + \left(\frac{2f_2}{\rho_0}\right)H(yx \mid c_x c_y) + \frac{f_4}{\rho_0^2}\right]$$

$$+ F(s_x s_x)\left[2H(xyy \mid s_x s_x) - \left(\frac{2f_1}{\rho_0}\right)H(yy \mid c_x) - k_x H'(yy \mid s_x)\right]$$

$$+ F(s_x \omega)[2H(xyy \mid s_x \omega)] + F(s_y s_y)\left[2H(xyy \mid s_y s_y)\right.$$

$$\left. - \left(\frac{2f_2}{\rho_0}\right)H(yx \mid c_y) - k_y H'(yx \mid s_y)\right]$$

$$+ F(s_x s_y c_y)\left[2H(xyy \mid s_x s_y c_y) + \left(\frac{2f_2}{\rho_0}\right)H(yx \mid s_x s_y)\right.$$

$$\left. - k_x H'(yy \mid s_y c_y) - k_y H'(yx \mid s_x c_y)\right]$$

$$+ F(c_x s_y s_y)\left[2H(xyy \mid c_x s_y s_y) + \left(\frac{2f_1}{\rho_0}\right)H(yy \mid s_y s_y)\right.$$

$$- \left(\frac{2f_2}{\rho_0}\right)H(yx \mid c_x c_y)$$

$$\left. - k_y H'(yx \mid c_x s_y) - \frac{f_4}{\rho_0^2} + \frac{k_y^2}{\rho_0^2}\right]$$

$$(l \mid xy\beta) = F(s_x)\left[2H(xy\beta \mid s_x) + \left(\frac{2f_2}{\rho_0}\right)H(\beta x \mid s_x c_y) - k_x H'(y\beta \mid 1)\right.$$

$$\left. + \rho_0 H'(yx \mid s_x c_y)\right]$$

$$+ F(s_x c_x)\left[2H(xy\beta \mid s_x c_x) + \left(\frac{2f_1}{\rho_0}\right)H(y\beta \mid s_x) - k_x H'(y\beta \mid c_x)\right]$$

$$+ F(c_x \omega)[2H(xy\beta \mid c_x \omega)]$$

$$+ F(s_y c_y)\left[2H(xy\beta \mid s_y c_y) + \left(\frac{2f_2}{k_y}\right)H(yx \mid c_y) + \left(\frac{2f_2}{\rho_0}\right)H(\beta x \mid s_y)\right.$$

$$\left. + \rho_0 H'(yx \mid s_y) - k_y H'(\beta x \mid c_y)\right]$$

$$+ F(s_x s_y s_y)\left[2H(xy\beta \mid s_x s_y s_y) + \left(\frac{2f_2}{k_y}\right) H(yx \mid s_x s_y)\right.$$

$$- \left(\frac{2f_2}{\rho_0}\right) H(\beta x \mid s_x c_y)$$

$$\left. - k_x H'(y\beta \mid s_y s_y) - \rho_0 H'(yx \mid s_x c_y) - k_y H'(\beta x \mid s_x s_y)\right]$$

$$+ F(c_x s_y c_y)\left[2H(xy\beta \mid c_x s_y c_y) + \left(\frac{2f_1}{\rho_0}\right) H(y\beta \mid s_y c_y)\right.$$

$$+ \left(\frac{2f_2}{k_y}\right) H(yx \mid c_x c_y)$$

$$+ \left(\frac{2f_2}{\rho_0}\right) H(\beta x \mid c_x s_y) + \rho_0 H'(yx \mid c_x s_y) - k_y H'(\beta x \mid c_x c_y)$$

$$\left. + \frac{2f_4}{k_y \rho_0} - \frac{2k_y}{\rho_0}\right]$$

$$(l \mid x\beta\beta) = F(1)\left[2H(x\beta\beta \mid 1) + \left(\frac{2f_1}{\rho_0}\right) H(\beta\beta \mid c_x) + \rho_0 H'(\beta x \mid c_y)\right]$$

$$+ F(c_x)\left[2H(x\beta\beta \mid c_x) + \left(\frac{2f_1}{\rho_0}\right) H(\beta\beta \mid 1) + \rho_0 H'(\beta x \mid c_x c_y) + 1\right]$$

$$+ F(s_x s_x)\left[2H(x\beta\beta \mid s_x s_x) - \left(\frac{2f_1}{\rho_0}\right) H(\beta\beta \mid c_x) - k_x H'(\beta\beta \mid s_x)\right]$$

$$+ F(s_x \omega)\left[2H(x\beta\beta \mid s_x \omega)\right]$$

$$+ F(s_y s_y)\left[2H(x\beta\beta \mid s_y s_y) + \left(\frac{2f_2}{k_y}\right) H(\beta x \mid s_y) - \rho_0 H'(\beta x \mid c_y)\right]$$

$$+ F(s_x s_y c_y)\left[2H(x\beta\beta \mid s_x s_y c_y) + \left(\frac{2f_2}{k_y}\right) H(\beta x \mid s_x c_y)\right.$$

$$\left. - k_x H'(\beta\beta \mid s_y c_y) + \rho_0 H'(\beta x \mid s_x s_y)\right]$$

$$+ F(c_x s_y s_y)\left[2H(x\beta\beta \mid c_x s_y s_y) + \left(\frac{2f_1}{\rho_0}\right) H(\beta\beta \mid s_y s_y)\right.$$

$$\left. + \left(\frac{2f_2}{k_y}\right) H(\beta x \mid c_x s_y) - \rho_0 H'(\beta x \mid c_x c_y) + \frac{f_4}{k_y^2} - 1\right]$$

$$(l \mid \alpha\alpha\alpha) = F(s_x)\left[2H(\alpha\alpha\alpha \mid s_x) + \left(\frac{2f_1}{k_x}\right)H(\alpha\alpha \mid 1) + \rho_0 H'(\alpha\alpha \mid s_x c_x) + \frac{\rho_0}{k_x}\right]$$

$$+ F(s_x c_x)\left[2H(\alpha\alpha\alpha \mid s_x c_x) + \left(\frac{2f_1}{k_x}\right)H(\alpha\alpha \mid c_x) + \rho_0 H'(\alpha\alpha \mid s_x)\right]$$

$$+ F(c_x \omega)\left[2H(\alpha\alpha\alpha \mid c_x \omega)\right]$$

$$+ F(s_x s_x s_x)\left[2H(\alpha\alpha\alpha \mid s_x s_x s_x) + \left(\frac{2f_1}{k_x}\right)H(\alpha\alpha \mid s_x s_x)\right.$$

$$\left. - \rho_0 H'(\alpha\alpha \mid s_x c_x) + \frac{f_3 \rho_0}{k_x^3} - \frac{\rho_0}{k_x}\right]$$

$$(l \mid \alpha\alpha\gamma) = F(1)\left[H(\alpha\alpha \mid 1) + \frac{\rho_0}{4}\right] + F(c_x)\left[H(\alpha\alpha \mid c_x)\right]$$

$$+ F(s_x s_x)\left[H(\alpha\alpha \mid s_x s_x) + \frac{\rho_0}{2k_x^2}\right]$$

$$(l \mid \alpha\alpha\delta) = F(1)\left[2H(\alpha\alpha\delta \mid 1) + \left(\frac{2f_1}{k_x^2} - 2\right)H(\alpha\alpha \mid 1) - \left(\frac{2f_1}{k_x^2}\right)H(\alpha\alpha \mid c_x)\right.$$

$$\left. + \rho_0 H'(\alpha\delta \mid c_x) + \frac{\rho_0}{k_x^2} - \frac{\rho_0}{4}\right]$$

$$+ F(c_x)\left[2H(\alpha\alpha\delta \mid c_x) + \left(\frac{2f_1}{k_x^2} - 2\right)H(\alpha\alpha \mid c_x)\right.$$

$$\left. - \left(\frac{2f_1}{k_x^2}\right)H(\alpha\alpha \mid 1) + \rho_0 H'(\alpha\delta \mid 1) - \frac{\rho_0}{k_x^2}\right]$$

$$+ F(s_x s_x)\left[2H(\alpha\alpha\delta \mid s_x s_x) + \left(\frac{2f_1}{k_x^2} - 2\right)H(\alpha\alpha \mid s_x s_x)\right.$$

$$+ \left(\frac{2f_1}{k_x^2}\right)H(\alpha\alpha \mid c_x)$$

$$+ \left(\frac{2f_1}{k_x}\right)H(\alpha\delta \mid s_x) + \left(\frac{\rho_0}{k_x}\right)H'(\alpha\alpha \mid s_x) - \rho_0 H'(\alpha\delta \mid c_x)$$

$$\left. + \frac{3f_3 \rho_0}{k_x^4} - \frac{4\rho_0}{k_x^2} - \frac{\rho_0}{2}\right] + F(s_x \omega)\left[2H(\alpha\alpha\delta \mid s_x \omega)\right]$$

$$+ F(s_x s_x c_x)\left[2H(\alpha\alpha\delta \mid s_x s_x c_x) - \left(\frac{2f_1}{k_x^2}\right)H(\alpha\alpha \mid s_x s_x)\right.$$

$$+ \left(\frac{2f_1}{k_x}\right)H(\alpha\delta \mid s_x c_x) + \left(\frac{\rho_0}{k_x}\right)H'(\alpha\alpha \mid s_x c_x) + \rho_0 H'(\alpha\delta \mid s_x s_x)$$

$$\left. - \frac{3f_3 \rho_0}{k_x^4} + \frac{3\rho_0}{k_x^2}\right] + F(s_x c_x \omega)\left[2H(\alpha\alpha\delta \mid s_x c_x \omega)\right.$$

$$\left. + \left(\frac{2f_1}{k_x}\right)H(\alpha\delta \mid c_x \omega) + \rho_0 H'(\alpha\delta \mid s_x \omega)\right]$$

$$(l\,|\,\alpha\gamma\gamma) = F(s_x)\left[\frac{-\rho_0}{4k_x}\right]$$

$$(l\,|\,\alpha\gamma\delta) = F(s_x)\left[H(\alpha\delta\,|\,s_x) + \frac{\rho_0}{k_x^3} - \frac{\rho_0}{2k_x}\right] + F(s_x c_x)\left[H(\alpha\delta\,|\,s_x c_x) - \frac{\rho_0}{k_x^3}\right]$$

$$+ F(c_x\omega)\left[H(\alpha\delta\,|\,c_x\omega)\right]$$

$$(l\,|\,\alpha\delta\delta) = F(s_x)\left[2H(\alpha\delta\delta\,|\,s_x) + \left(\frac{2f_1}{k_x^2} - 2\right)H(\alpha\delta\,|\,s_x) - \left(\frac{2f_1}{k_x^2}\right)H(\alpha\delta\,|\,s_x c_x)\right.$$

$$+ \left(\frac{2f_1}{k_x}\right)H(\delta\delta\,|\,1) + \left(\frac{\rho_0}{k_x}\right)H'(\alpha\delta\,|\,1) + \rho_0 H'(\delta\delta\,|\,s_x c_x)$$

$$\left. + \frac{6f_3\rho_0}{k_x^5} - \frac{8\rho_0}{k_x^3} + \frac{3\rho_0}{4k_x}\right]$$

$$+ F(\omega)\left[2H(\alpha\delta\delta\,|\,\omega) - \left(\frac{2f_1}{k_x^2}\right)H(\alpha\delta\,|\,c_x\omega) + \rho_0 H'(\delta\delta\,|\,c_x\omega)\right]$$

$$+ F(s_x c_x)\left[2H(\alpha\delta\delta\,|\,s_x c_x) + \left(\frac{2f_1}{k_x^2} - 2\right)H(\alpha\delta\,|\,s_x c_x)\right.$$

$$- \left(\frac{2f_1}{k_x^2}\right)H(\alpha\delta\,|\,s_x) + \left(\frac{2f_1}{k_x}\right)H(\delta\delta\,|\,c_x) + \left(\frac{\rho_0}{k_x}\right)H'(\alpha\delta\,|\,c_x)$$

$$\left. + \rho_0 H'(\delta\delta\,|\,s_x) - \frac{6f_3\rho_0}{k_x^5} + \frac{8\rho_0}{k_x^3} + \frac{\rho_0}{k_x}\right]$$

$$+ F(c_x\omega)\left[2H(\alpha\delta\delta\,|\,c_x\omega) + \left(\frac{2f_1}{k_x^2} - 2\right)H(\alpha\delta\,|\,c_x\omega)\right]$$

$$+ F(s_x s_x s_x)\left[2H(\alpha\delta\delta\,|\,s_x s_x s_x) + \left(\frac{2f_1}{k_x^2}\right)H(\alpha\delta\,|\,s_x c_x)\right.$$

$$+ \left(\frac{2f_1}{k_x}\right)H(\delta\delta\,|\,s_x s_x) + \left(\frac{\rho_0}{k_x}\right)H'(\alpha\delta\,|\,s_x s_x) - \rho_0 H'(\delta\delta\,|\,s_x c_x)$$

$$\left. - \frac{3f_3\rho_0}{k_x^5} + \frac{3\rho_0}{k_x^3}\right] + F(s_x s_x\omega)\left[2H(\alpha\delta\delta\,|\,s_x s_x\omega)\right.$$

$$+ \left(\frac{2f_1}{k_x^2}\right)H(\alpha\delta\,|\,c_x\omega) + \left(\frac{2f_1}{k_x}\right)H(\delta\delta\,|\,s_x\omega)$$

$$\left. + \left(\frac{\rho_0}{k_x}\right)H'(\alpha\delta\,|\,s_x\omega) - \rho_0 H'(\delta\delta\,|\,c_x\omega)\right] + F(s_x\omega\omega)\left[2H(\alpha\delta\delta\,|\,s_x\omega\omega)\right]$$

$$(I \mid \alpha yy) = F(s_x)\left[2H(\alpha yy \mid s_x) + \left(\frac{2f_1}{k_x}\right)H(yy \mid 1) + \left(\frac{2f_2}{\rho_0}\right)H(y\alpha \mid s_x c_y)\right.$$

$$\left. + \frac{f_4}{k_x \rho_0}\right] + F(s_x c_x)\left[2H(\alpha yy \mid s_x c_x)\right.$$

$$\left. + \left(\frac{2f_1}{k_x}\right)H(yy \mid c_x) + \rho_0 H'(yy \mid s_x)\right] + F(c_x \omega)[2H(\alpha yy \mid c_x \omega)]$$

$$+ F(s_y c_y)\left[2H(\alpha yy \mid s_y c_y) + \left(\frac{2f_2}{\rho_0}\right)H(y\alpha \mid s_y) - k_y H'(y\alpha \mid c_y)\right]$$

$$+ F(s_x s_y s_y)\left[2H(\alpha yy \mid s_x s_y s_y) + \left(\frac{2f_1}{k_x}\right)H(yy \mid s_y s_y)\right.$$

$$\left. - \left(\frac{2f_2}{\rho_0}\right)H(y\alpha \mid s_x c_y) - k_y H'(y\alpha \mid s_x s_y) - \frac{f_4}{k_x \rho_0} + \frac{k_y^2}{k_x \rho_0}\right]$$

$$+ F(c_x s_y c_y)\left[2H(\alpha yy \mid c_x s_y c_y) + \left(\frac{2f_2}{\rho_0}\right)H(y\alpha \mid c_x s_y)\right.$$

$$\left. + \rho_0 H'(yy \mid s_y c_y) - k_y H'(y\alpha \mid c_x c_y)\right]$$

$$(I \mid \alpha y\beta) = F(1)\left[2H(\alpha y\beta \mid 1) + \left(\frac{2f_2}{\rho_0}\right)H(\beta\alpha \mid c_y) + \rho_0 H'(y\beta \mid c_x)\right.$$

$$\left. + \rho_0 H'(y\alpha \mid c_y)\right] + F(c_x)\left[2H(\alpha y\beta \mid c_x)\right.$$

$$\left. + \left(\frac{2f_2}{\rho_0}\right)H(\beta\alpha \mid c_x c_y) + \rho_0 H'(y\beta \mid 1) + \rho_0 H'(y\alpha \mid c_x c_y)\right]$$

$$+ F(s_x s_x)\left[2H(\alpha y\beta \mid s_x s_x) + \left(\frac{2f_1}{k_x}\right)H(y\beta \mid s_x) - \rho_0 H'(y\beta \mid c_x)\right]$$

$$+ F(s_x \omega)[2H(\alpha y\beta \mid s_x \omega)]$$

$$+ F(s_y s_y)\left[2H(\alpha y\beta \mid s_y s_y) + \left(\frac{2f_2}{k_y}\right)H(y\alpha \mid s_y) - \left(\frac{2f_2}{\rho_0}\right)H(\beta\alpha \mid c_y)\right.$$

$$\left. - \rho_0 H'(y\alpha \mid c_y) - k_y H'(\beta\alpha \mid s_y)\right] +$$

$$+ F(s_x s_y c_y)\left[2H(\alpha y\beta \mid s_x s_y c_y) + \left(\frac{2f_1}{k_x}\right)H(y\beta \mid s_y c_y)\right.$$

$$\left. + \left(\frac{2f_2}{k_y}\right)H(y\alpha \mid s_x c_y) + \left(\frac{2f_2}{\rho_0}\right)H(\beta\alpha \mid s_x s_y)\right.$$

$$+ \rho_0 H'(y\alpha | s_x s_y) - k_y H'(\beta\alpha | s_x c_y) + \frac{2f_4}{k_x k_y} - \frac{2k_y}{k_x}\Bigg]$$

$$+ F(c_x s_y s_y)\Bigg[2H(\alpha y\beta | c_x s_y s_y) + \left(\frac{2f_2}{k_y}\right)H(y\alpha | c_x s_y)$$

$$- \left(\frac{2f_2}{\rho_0}\right)H(\beta\alpha | c_x c_y)$$

$$+ \rho_0 H'(y\beta | s_y s_y) - \rho_0 H'(y\alpha | c_x c_y) - k_y H'(\beta\alpha | c_x s_y)\Bigg]$$

$$(l | \alpha\beta\beta) = F(s_x)\Bigg[2H(\alpha\beta\beta | s_x) + \left(\frac{2f_1}{k_x}\right)H(\beta\beta | 1) + \rho_0 H'(\beta\alpha | s_x c_y) + \frac{\rho_0}{k_x}\Bigg]$$

$$+ F(s_x c_x)\Bigg[2H(\alpha\beta\beta | s_x c_x) + \left(\frac{2f_1}{k_x}\right)H(\beta\beta | c_x) + \rho_0 H'(\beta\beta | s_x)\Bigg]$$

$$+ F(c_x \omega)[2H(\alpha\beta\beta | c_x \omega)]$$

$$+ F(s_y c_y)\Bigg[2H(\alpha\beta\beta | s_y c_y) + \left(\frac{2f_2}{k_y}\right)H(\beta\alpha | c_y) + \rho_0 H'(\beta\alpha | s_y)\Bigg]$$

$$+ F(s_x s_y s_y)\Bigg[2H(\alpha\beta\beta | s_x s_y s_y) + \left(\frac{2f_1}{k_x}\right)H(\beta\beta | s_y s_y)$$

$$+ \left(\frac{2f_2}{k_y}\right)H(\beta\alpha | s_x s_y) - \rho_0 H'(\beta\alpha | s_x c_y) + \frac{f_4 \rho_0}{k_x k_y^2} - \frac{\rho_0}{k_x}\Bigg]$$

$$+ F(c_x s_y c_y)\Bigg[2H(\alpha\beta\beta | c_x s_y c_y) + \left(\frac{2f_2}{k_y}\right)H(\beta\alpha | c_x c_y)$$

$$+ \rho_0 H'(\beta\beta | s_y c_y) + \rho_0 H'(\beta\alpha | c_x s_y)\Bigg]$$

$$(l | \gamma\gamma\gamma) = F(1)\left[\frac{\rho_0}{16}\right]$$

$$(l | \gamma\gamma\delta) = F(1)\left[\frac{-\rho_0}{4k_x^2} + \frac{\rho_0}{16}\right] + F(c_x)\left[\frac{\rho_0}{4k_x^2}\right]$$

$$(l | \gamma\delta\delta) = F(1)\left[H(\delta\delta | 1) + \frac{\rho_0}{k_x^4} - \frac{\rho_0}{2k_x^2} + \frac{3\rho_0}{16}\right]$$

$$+ F(c_x)\left[H(\delta\delta | c_x) - \frac{\rho_0}{k_x^4} + \frac{\rho_0}{2k_x^2}\right]$$

$$+ F(s_x s_x)\left[H(\delta\delta | s_x s_x) - \frac{\rho_0}{2k_x^4}\right] + F(s_x \omega)[H(\delta\delta | s_x \omega)]$$

$$(l\,|\,\gamma yy) = F(1)\left[H(yy\,|\,1) + \frac{k_y^2}{4\rho_0}\right] + F(c_x)\left[H(yy\,|\,c_x)\right]$$

$$+ F(s_y s_y)\left[H(yy\,|\,s_y s_y)\right]$$

$$(l\,|\,\gamma y\beta) = F(s_x)\left[H(y\beta\,|\,s_x)\right] + F(s_y c_y)\left[H(y\beta\,|\,s_y c_y)\right]$$

$$(l\,|\,\gamma\beta\beta) = F(1)\left[H(\beta\beta\,|\,1) + \frac{\rho_0}{4}\right] + F(c_x)\left[H(\beta\beta\,|\,c_x)\right]$$

$$+ F(s_y s_y)\left[H(\beta\beta\,|\,s_y s_y)\right]$$

$$(l\,|\,\delta\delta\delta) = F(1)\left[2H(\delta\delta\delta\,|\,1) + \left(\frac{2f_1}{k_x^2} - 2\right)H(\delta\delta\,|\,1) - \left(\frac{2f_1}{k_x^2}\right)H(\delta\delta\,|\,c_x)\right.$$

$$\left. + \frac{4f_3\rho_0}{k_x^6} - \frac{6\rho_0}{k_x^4} + \frac{3\rho_0}{4k_x^2} - \frac{5\rho_0}{16}\right]$$

$$+ F(c_x)\left[2H(\delta\delta\delta\,|\,c_x) + \left(\frac{2f_1}{k_x^2} - 2\right)H(\delta\delta\,|\,c_x) - \left(\frac{2f_1}{k_x^2}\right)H(\delta\delta\,|\,1)\right.$$

$$\left. - \frac{4f_3\rho_0}{k_x^6} + \frac{6\rho_0}{k_x^4} - \frac{3\rho_0}{4k_x^2}\right]$$

$$+ F(s_x s_x)\left[2H(\delta\delta\delta\,|\,s_x s_x) + \left(\frac{2f_1}{k_x^2} - 2\right)H(\delta\delta\,|\,s_x s_x)\right.$$

$$\left. + \left(\frac{2f_1}{k_x^2}\right)H(\delta\delta\,|\,c_x) + \left(\frac{\rho_0}{k_x}\right)H'(\delta\delta\,|\,s_x) - \frac{3f_3\rho_0}{k_x^6} + \frac{4\rho_0}{k_x^4} + \frac{\rho_0}{2k_x^2}\right]$$

$$+ F(s_x\omega)\left[2H(\delta\delta\delta\,|\,s_x\omega) + \left(\frac{2f_1}{k_x^2} - 2\right)H(\delta\delta\,|\,s_x\omega)\right]$$

$$+ F(s_x s_x c_x)\left[2H(\delta\delta\delta\,|\,s_x s_x c_x) - \left(\frac{2f_1}{k_x^2}\right)H(\delta\delta\,|\,s_x s_x)\right.$$

$$\left. + \left(\frac{\rho_0}{k_x}\right)H'(\delta\delta\,|\,s_x c_x) + \frac{f_3\rho_0}{k_x^6} - \frac{\rho_0}{k_x^4}\right]$$

$$+ F(s_x c_x\omega)\left[2H(\delta\delta\delta\,|\,s_x c_x\omega) - \left(\frac{2f_1}{k_x^2}\right)H(\delta\delta\,|\,s_x\omega)\right.$$

$$\left. + \left(\frac{\rho_0}{k_x}\right)H'(\delta\delta\,|\,c_x\omega)\right] + F(c_x\omega\omega)\left[2H(\delta\delta\delta\,|\,c_x\omega\omega)\right]$$

$$
\begin{aligned}
(l\,|\,\delta yy) = F(1)&\left[2H(\delta yy\,|\,1) + \left(\frac{2f_1}{k_x^2} - 2\right)H(yy\,|\,1) - \left(\frac{2f_1}{k_x^2}\right)H(yy\,|\,c_x)\right. \\
&\left. + \left(\frac{2f_2}{\rho_0}\right)H(y\delta\,|\,c_y) + \frac{f_4}{k_x^2\rho_0} - \frac{3k_y^2}{4\rho_0}\right] \\[4pt]
+ F(c_x)&\left[2H(\delta yy\,|\,c_x) + \left(\frac{2f_1}{k_x^2} - 2\right)H(yy\,|\,c_x) - \left(\frac{2f_1}{k_x^2}\right)H(yy\,|\,1)\right. \\
&\left. + \left(\frac{2f_2}{\rho_0}\right)H(y\delta\,|\,c_xc_y) - \frac{f_4}{k_x^2\rho_0}\right] \\[4pt]
+ F(s_xs_x)&\left[2H(\delta yy\,|\,s_xs_x) + \left(\frac{2f_1}{k_x^2}\right)H(yy\,|\,c_x) + \left(\frac{\rho_0}{k_x}\right)H'(yy\,|\,s_x)\right] \\[4pt]
+ F(s_x\omega)&\left[2H(\delta yy\,|\,s_x\omega)\right] \\[4pt]
+ F(s_ys_y)&\left[2H(\delta yy\,|\,s_ys_y) + \left(\frac{2f_1}{k_x^2} - 2\right)H(yy\,|\,s_ys_y)\right. \\
&\left. - \left(\frac{2f_2}{\rho_0}\right)H(y\delta\,|\,c_y) - k_yH'(y\delta\,|\,s_y) - \frac{f_4}{k_x^2\rho_0} + \frac{k_y^2}{k_x^2\rho_0} + \frac{k_y^2}{2\rho_0}\right] \\[4pt]
+ F(s_xs_yc_y)&\left[2H(\delta yy\,|\,s_xs_yc_y) + \left(\frac{2f_2}{\rho_0}\right)H(y\delta\,|\,s_xs_y)\right. \\
&\left. + \left(\frac{\rho_0}{k_x}\right)H'(yy\,|\,s_yc_y) - k_yH'(y\delta\,|\,s_xc_y)\right] + \\[4pt]
+ F(c_xs_ys_y)&\left[2H(\delta yy\,|\,c_xs_ys_y) - \left(\frac{2f_1}{k_x^2}\right)H(yy\,|\,s_ys_y)\right. \\
&\left. - \left(\frac{2f_2}{\rho_0}\right)H(y\delta\,|\,c_xc_y) - k_yH'(y\delta\,|\,c_xs_y) + \frac{f_4}{k_x^2\rho_0} - \frac{k_y^2}{k_x^2\rho_0}\right] \\[4pt]
+ F(s_yc_y\omega)&\left[2H(\delta yy\,|\,s_yc_y\omega) + \left(\frac{2f_2}{\rho_0}\right)H(y\delta\,|\,s_y\omega)\right. \\
&\left. - k_yH'(y\delta\,|\,c_y\omega)\right]
\end{aligned}
$$

$$(I|\delta y\beta) = F(s_x)\left[2H(\delta y\beta|s_x) + \left(\frac{2f_1}{k_x^2} - 2\right)H(y\beta|s_x) + \left(\frac{2f_2}{\rho_0}\right)H(\beta\delta|s_x c_y)\right.$$

$$\left. + \left(\frac{\rho_0}{k_x}\right)H'(y\beta|1) + \rho_0 H'(y\delta|s_x c_y)\right]$$

$$+ F(\omega)\left[2H(\delta y\beta|\omega) + \left(\frac{2f_2}{\rho_0}\right)H(\beta\delta|c_y\omega) + \rho_0 H'(y\delta|c_y\omega)\right]$$

$$+ F(s_x c_x)\left[2H(\delta y\beta|s_x c_x) - \left(\frac{2f_1}{k_x^2}\right)H(y\beta|s_x) + \left(\frac{\rho_0}{k_x}\right)H'(y\beta|c_x)\right]$$

$$+ F(c_x\omega)[2H(\delta y\beta|c_x\omega)] + F(s_y c_y)\left[2H(\delta y\beta|s_y c_y)\right.$$

$$+ \left(\frac{2f_1}{k_x^2} - 2\right)H(y\beta|s_y c_y) + \left(\frac{2f_2}{k_y}\right)H(y\delta|c_y)$$

$$+ \left(\frac{2f_2}{\rho_0}\right)H(\beta\delta|s_y) + \rho_0 H'(y\delta|s_y) - k_y H'(\beta\delta|c_y)$$

$$\left. + \frac{2f_4}{k_x^2 k_y} - \frac{2k_y}{k_x^2} - k_y\right] + F(s_x s_y s_y)\left[2H(\delta y\beta|s_x s_y s_y)\right.$$

$$+ \left(\frac{\rho_0}{k_x}\right)H'(y\beta|s_y s_y) + \left(\frac{2f_2}{k_y}\right)H(y\delta|s_x s_y)$$

$$\left. - \left(\frac{2f_2}{\rho_0}\right)H(\beta\delta|s_x c_y) - \rho_0 H'(y\delta|s_x c_y) - k_y H'(\beta\delta|s_x s_y)\right] +$$

$$+ F(c_x s_y c_y)\left[2H(\delta y\beta|c_x s_y c_y) - \left(\frac{2f_1}{k_x^2}\right)H(y\beta|s_y c_y)\right.$$

$$+ \left(\frac{2f_2}{k_y}\right)H(y\delta|c_x c_y) + \left(\frac{2f_2}{\rho_0}\right)H(\beta\delta|c_x s_y)$$

$$\left. + \rho_0 H'(y\delta|c_x s_y) - k_y H'(\beta\delta|c_x c_y) - \frac{2f_4}{k_x^2 k_y} + \frac{2k_y}{k_x^2}\right]$$

$$+ F(s_y s_y\omega)\left[2H(\delta y\beta|s_y s_y\omega) + \left(\frac{2f_2}{k_y}\right)H(y\delta|s_y\omega)\right.$$

$$\left. - \left(\frac{2f_2}{\rho_0}\right)H(\beta\delta|c_y\omega) - \rho_0 H'(y\delta|c_y\omega) - k_y H'(\beta\delta|s_y\omega)\right]$$

$$(I \mid \delta\beta\beta) = F(1)\left[2H(\delta\beta\beta \mid 1) + \left(\frac{2f_1}{k_x^2} - 2\right)H(\beta\beta \mid 1) - \left(\frac{2f_1}{k_x^2}\right)H(\beta\beta \mid c_x)\right.$$

$$\left. + \rho_0 H'(\beta\delta \mid c_y) + \frac{\rho_0}{k_x^2} - \frac{\rho_0}{4}\right]$$

$$+ F(c_x)\left[2H(\delta\beta\beta \mid c_x) + \left(\frac{2f_1}{k_x^2} - 2\right)H(\beta\beta \mid c_x)\right.$$

$$\left. - \left(\frac{2f_1}{k_x^2}\right)H(\beta\beta \mid 1) + \rho_0 H'(\beta\delta \mid c_x c_y) - \frac{\rho_0}{k_x^2}\right]$$

$$+ F(s_x s_x)\left[2H(\delta\beta\beta \mid s_x s_x) + \left(\frac{2f_1}{k_x^2}\right)H(\beta\beta \mid c_x)\right.$$

$$\left. + \left(\frac{\rho_0}{k_x}\right)H'(\beta\beta \mid s_x)\right] + F(s_x \omega)[2H(\delta\beta\beta \mid s_x \omega)]$$

$$+ F(s_y s_y)\left[2H(\delta\beta\beta \mid s_y s_y) + \left(\frac{2f_1}{k_x^2} - 2\right)H(\beta\beta \mid s_y s_y)\right.$$

$$\left. + \left(\frac{2f_2}{k_y}\right)H(\beta\delta \mid s_y) - \rho_0 H'(\beta\delta \mid c_y) + \frac{f_4 \rho_0}{k_x^2 k_y^2} - \frac{\rho_0}{k_x^2} - \frac{\rho_0}{2}\right]$$

$$+ F(s_x s_y c_y)\left[2H(\delta\beta\beta \mid s_x s_y c_y) + \left(\frac{2f_2}{k_y}\right)H(\beta\delta \mid s_x c_y) + \right.$$

$$\left. + \left(\frac{\rho_0}{k_x}\right)H'(\beta\beta \mid s_y c_y) + \rho_0 H'(\beta\delta \mid s_x s_y)\right]$$

$$+ F(c_x s_y s_y)\left[2H(\delta\beta\beta \mid c_x s_y s_y) - \left(\frac{2f_1}{k_x^2}\right)H(\beta\beta \mid s_y s_y)\right.$$

$$\left. + \left(\frac{2f_2}{k_y}\right)H(\beta\delta \mid c_x s_y) - \rho_0 H'(\beta\delta \mid c_x c_y) - \frac{f_4 \rho_0}{k_x^2 k_y^2} + \frac{\rho_0}{k_x^2}\right]$$

$$+ F(s_y c_y \omega)\left[2H(\delta\beta\beta \mid s_y c_y \omega) + \left(\frac{2f_2}{k_y}\right)H(\beta\delta \mid c_y \omega)\right.$$

$$\left. + \rho_0 H'(\beta\delta \mid s_y \omega)\right]$$

2-3. Third-order flight times in an electric quadrupole lens

In an electric quadrupole lens, the cartesian coordinate system (x, y, z) is used. The x-axis is perpendicular to the principal trajectory of the quadrupole lens in the median plane. The y-axis is perpendicular to the median plane, and the z-axis is tangent to the principal trajectory. The electric potential $\Phi(x,y)$ in the electric quadrupole lens is given as:

$$\phi(x,y) = \frac{\chi_e}{2} k^2 (x^2 - y^2) \tag{2-14}$$

where χ_e is the electric rigidity defined in Eq. 2-8, and k^2 is the gradient of the field strength divided by the electric rigidity. The third-order ion trajectory in electric quadrupoles was obtained by Smith [2-5] and Fujita et al. [2-6].

The path length deviation of the quadrupole lens, with effective length L, is calculated by the equation:

$$l = \int_0^s \frac{v_0}{v} ds - L \tag{2-15}$$

where $ds = (1 + x'^2 + y'^2)^{1/2} dz$. A prime denotes d/dz. The velocity v of an arbitrary particle is given by Eq. 2-8, where the electric potential Φ is given in Eq. 2-14. Introducing the results of the trajectory calculation and the electric potential into Eq. 2-15, the third-order expression of the path length deviation in the quadrupole lens can be derived as a power series similar to Eq. 2-12. The coefficients of a power

series are:

$$(l|x) = 0, \ (l|\alpha) = 0, \ (l|\gamma) = \frac{L}{2}, \ (l|\delta) = -\frac{L}{2},$$

$$(l|xx) = k^2 \frac{L}{2}, \ (l|x\alpha) = 0, \ (l|x\gamma) = 0, \ (l|x\delta) = 0,$$

$$(l|\alpha\alpha) = \frac{L}{2}, \ (l|\alpha\gamma) = 0, \ (l|\alpha\delta) = 0, \ (l|\gamma\gamma) = -\frac{L}{8},$$

$$(l|\gamma\delta) = -\frac{L}{4}, \ (l|\delta\delta) = \frac{3L}{8}, \ (l|yy) = -\frac{k^2 L}{2}, \ (l|y\beta) = 0,$$

$$(l|\beta\beta) = \frac{L}{2}, \ (l|xxx) = 0, \ (l|xx\alpha) = 0, \ (l|xx\gamma) = \frac{k^2 L}{4},$$

$$(l|xx\delta) = -\frac{3k^2 L}{4}, \ (l|x\alpha\alpha) = 0, \ (l|x\alpha\gamma) = 0, \ (l|x\alpha\delta) = 0, \ (l|x\gamma\gamma) = 0,$$

$$(l|x\gamma\delta) = 0, \ (l|x\delta\delta) = 0, \ (l|xyy) = 0, \ (l|xy\beta) = 0,$$

$$(l|x\beta\beta) = 0, \ (l|\alpha\alpha\alpha) = 0, \ (l|\alpha\alpha\gamma) = \frac{L}{4}, \ (l|\alpha\alpha\delta) = -\frac{L}{4}, \ (l|\alpha\gamma\gamma) = 0,$$

$$(l|\alpha\gamma\delta) = 0, \ (l|\alpha\delta\delta) = 0, \ (l|\alpha yy) = 0, \ (l|\alpha y\beta) = 0,$$

$$(l|\alpha\beta\beta) = 0, \ (l|\gamma\gamma\gamma) = \frac{L}{16}, \ (l|\gamma\gamma\delta) = \frac{L}{16}, \ (l|\gamma\delta\delta) = \frac{3L}{16},$$

$$(l|\gamma yy) = -\frac{3k^2 L}{4}, \ (l|\gamma y\beta) = 0, \ (l|\gamma\beta\beta) = \frac{L}{4},$$

$$(l|\delta\delta\delta) = -\frac{5L}{16}, \ (l|\delta yy) = \frac{3k^2 L}{4}, \ (l|\delta y\beta) = 0, \ (l|\delta\beta\beta) = -\frac{L}{4}$$

(2-16)

2-4. Third-order flight times in a drift space

Knowledge of the path length deviation through a drift space is necessary to estimate flight times in the whole system. The path length deviation in the drift space of length L is obtained by the equation:

$$l = \int_0^s \frac{v_0}{v} ds - L$$

(2-17)

The non-vanishing coefficients of the power series of the path length deviation in the drift space are:

$$(l|\gamma) = \frac{L}{2}, (l|\delta) = -\frac{L}{2}, (l|\alpha\alpha) = \frac{L}{2}, (l|\gamma\gamma) = -\frac{L}{8},$$

$$(l|\gamma\delta) = -\frac{L}{4}, (l|\delta\delta) = \frac{3L}{8}, (l|\beta\beta) = \frac{L}{2}, (l|\alpha\alpha\gamma) = \frac{L}{4},$$

$$(l|\alpha\alpha\delta) = -\frac{L}{4}, (l|\gamma\gamma\gamma) = \frac{L}{16}, (l|\gamma\gamma\delta) = \frac{L}{16}, (l|\gamma\delta\delta) = \frac{3L}{16},$$

$$(l|\gamma\beta\beta) = \frac{L}{4}, (l|\delta\delta\delta) = -\frac{5L}{16}, (l|\delta\beta\beta) = -\frac{L}{4}.$$

<div align="right">(2-18)</div>

2-5. <u>Influences of fringing fields on flight time</u>

In previous sections, the flight time of charged particles in a toroidal electric condenser and an electric quadrupole lens were calculated in the third-order approximation. These calculations, however, are only concerned with the idealized main region of the electric fields. When charged particles pass through a real toroidal electric condenser, they have to travel through fringing fields at the entrance and exit of the condenser. The influences of fringing fields on flight times of charged particles can not be neglected in the third-order approximation. The influences of fringing fields of the toroidal condenser on the particle trajectories were calculated by Matsuda in the third-order approximation [2-7]. The results of the calculation, the effects of the fringing-fields were expressed as a small shift and bend of the ion trajectory at the ideal field boundaries of the condenser. In this section, the third-order influences of the fringing-fields on the flight times of the toroidal condenser are calculated by extending the theory of Ref. 2-7. The results are expressed as
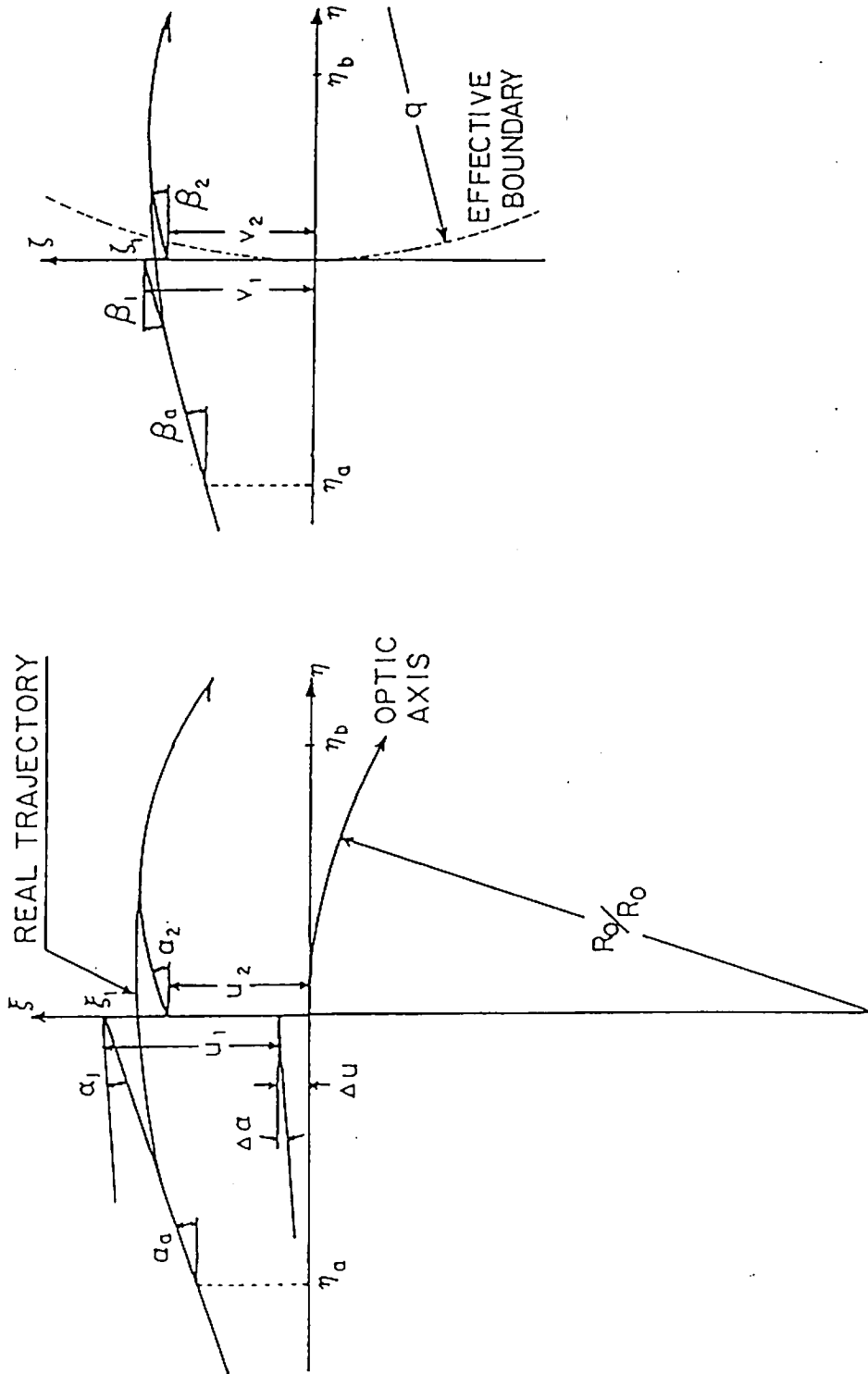
Fig. 2 – 3.   The coordinate system in the entrance fringing field of a toroidal electric sector. The ξ – ζ plane coincides with the ideal field boundary. The optic axis is shown in ξ – η plane. The projections of the ideal and real trajectory are shown in the ξ – η plane and η – ζ plane, respectively.

-39-

a small change of the path length deviation at the ideal field boundaries of the condenser.

Firstly, we consider the effect of the entrance fringing field. Following Ref. 2-7, the rectangular coordinate system (ξ, η, ζ) is used as shown in Fig. 2-3, where the ξ-η plain coincides with the median plane. R_0 is the radius of curvature of the main path in the toroidal electric field. In this figure, the optic axis and real trajectory are given as the results of Ref. 2-7. The ξ-ζ plane coincides with the ideal field boundary. The fringing field is represented by the distribution function of the electric field $E(\eta)$ along η-axis. The function vanishes at the point η_a and gradually increases with η and is equal to E_0 ($= X_e/R_0$) at the point η_b, as shown in Fig. 2-4.
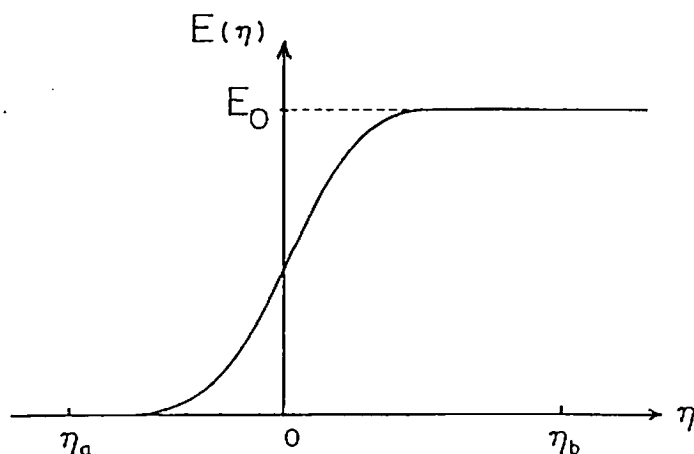
Fig. 2-4. The distribution function $E(\eta)$ of the fringing field along the η-axis.

The length of the fringing field region between η_a and η_b is assumed to be first order small quantity. The curvature of effective field boundary in the η-ζ plane is represented by q and other abbreviations in this section are same as Ref. 2-7. The

small shift and bend of the optic axis, Δu and $\Delta\alpha$, were given in Eqs. (57) and (58) in Ref. 2-7. The transformation at the entrance fringing field of an arbitrary particle between $(u_1, \tan\alpha_1, v_1, \beta_1)$ and $(u_2, \tan\alpha_2, v_2, \beta_2)$ were calculated in Eqs. (60)-(63) of Ref. 2-7.

The path length deviation of the charged particle in travel from η_a to η_b is given as:

$$\ell = \int_{\eta_a}^{\eta_b} \frac{v_0}{v(\eta)} \cdot \frac{ds}{d\eta} \, d\eta - R_0 (\eta_b + \frac{1}{6} k\eta_b^3 - \eta_a) \qquad (2\text{-}19)$$

The differential element, ds, is given as:

$$ds = R_0 (1 + \tan^2\alpha + \tan^2\beta)^{\frac{1}{2}} \, d\eta \qquad (2\text{-}20)$$

The inverse velocity, $1/v(\eta)$, was calculated in Eq. (31) of Ref. 2-7 as:

$$1/v(\eta) = (2U_0/m)^{-\frac{1}{2}} [1 - \frac{1}{2}\delta + (E/E_0)\xi - \frac{1}{6}(E''/E_0)\xi^3 - (k/E_0)\int\int E d\eta d\eta$$

$$+ (k/E_0)\eta\int E d\eta + (E/E_0)\{kI_{1a} - \frac{1}{2}(k+c)\xi^2 - \frac{3}{2}\xi\delta + \frac{1}{2}c\zeta^2\}$$

$$+ (E'/E_0)\{-\frac{1}{2}k\xi^2\eta + \frac{1}{6}\xi^3/q - \frac{1}{2}\xi\zeta^2/q\} - (E''/E_0)\{\frac{1}{2}kI_{1a}\xi^2\}$$

$$+ \frac{3}{2}(E^2/E^2_0)\xi^2 + \frac{3}{8}\delta^2] \qquad (2\text{-}21)$$

The $\xi(\eta)$, $\zeta(\eta)$, $\sin\alpha(\eta)$ and $\sin\beta(\eta)$ are also functions of η in the fringing field region, the explicit expressions for them were given in Eqs. (32)-(35) of Ref. 2-7. The second-order $\xi(\eta)$ and first-order $\zeta(\eta)$, $\sin\alpha(\eta)$, $\sin\beta(\eta)$ are given as:

$$\xi(\eta) = \xi_1 + \alpha_a \eta - (1/E_0) \int\int E d\eta d\eta + \frac{1}{2}\xi_1^2 E/E_0$$

$$\zeta(\eta) = \zeta_1$$

$$\sin\alpha(\eta) = \sin\alpha_a - (1/E_0)\int E d\eta + \frac{1}{2}\xi_1^2 E'/E_0$$

$$\sin\beta(\eta) = \sin\beta_a \qquad\qquad (2\text{-}22)$$

Introducing Eqs. 2-20,21,22 into Eq. 2-19 and performing the integration with respect to η, we obtain the path length deviation of an arbitrary particle from η_a to η_b. The result is given as:

$$
\begin{aligned}
\ell = R_0 \left(\frac{m_0}{m}\right)^{\frac{1}{2}} & [\eta_b - \eta_a - I_{1a}\eta_b + 2kI_2 + \frac{3}{2}I_{3a} + \frac{1}{6}k\eta_b^3 + \xi_1\eta_b \\
& - 2\alpha_a I_{1a} - \frac{1}{2}\delta(\eta_b - \eta_a) + \xi_1^2\{3I_{4a} + \frac{1}{2}(4 - k - c)\eta_b\} \\
& - \frac{3}{2}\xi_1\delta\eta_b + \frac{1}{2}\alpha_a^2(\eta_b - \eta_a) + \frac{3}{8}\delta^2(\eta_b - \eta_a) \\
& + \frac{1}{2}\zeta_1^2(c - k)\eta_b - \frac{1}{2}\beta_a^2(\eta_b - \eta_a) + \frac{1}{6}\xi_1^3/q \\
& + \xi_1^2\alpha_a - \frac{1}{2}\xi_1\zeta_1^2/q] \\
& - R_0(\eta_b + \frac{1}{6}k\eta_b^3 - \eta_a)
\end{aligned}
$$

$$(2\text{-}23)$$

where I_{1a}, I_2, I_{3a} and I_{4a} are definite integrals which depend on the fringing field distribution $E(\eta)$. These were defined by Eqs. (39), (41), (42) and (44) of Ref. 2-7 as:

$$I_{1a} = E_0^{-1} \int_a^b \int E \, d\eta \, d\eta - \frac{1}{2}\eta_b{}^2$$

$$I_2 = E_0^{-1} \int_a^b \eta \left(\int E \, d\eta\right) d\eta - \frac{1}{3}\eta_b{}^3$$

$$I_{3a} = E_0^{-2} \int_a^b \left(\int E \, d\eta\right)^2 d\eta - \frac{1}{3}\eta_b{}^3$$

$$I_{4a} = E_0^{-2} \int_a^b E^2 \, d\eta - \eta_b \qquad\qquad (2\text{-}24)$$

The effect of the fringing field on the flight time should be translated into the transformation at the ideal filed boundary. Therefore, $\eta_a = 0$, $\eta_b = 0$, $k = 1$ and $m = m_0(1+\Upsilon)$ are introduced into Eq. 2-23. The ξ_1, α_a, ζ_1, β_a become u_1, α_1, v_1, β_1 using the transformation of Eq. (59) of Ref. 2-7 as:

$$\xi_1 = u_1 + \Delta u$$

$$\alpha_a = \alpha_1 + \Delta\alpha$$

$$\zeta_1 = v_1$$

$$\beta_a = \beta_1 \qquad\qquad (2\text{-}25)$$

The final expression of the influence of the entrance fringing field on flight time is obtained. It is expressed as the transformation of the path length deviation from ℓ_1 to ℓ_2 at the ideal field boundary.

$$\ell_2 = \ell_1 + \Delta\ell - 2I_{1a}R_0\alpha_1 + 3I_{4a}R_0u_1^2 + \frac{R_0}{6q}u_1^3 + R_0u_1^2\alpha_1 - \frac{R_0}{2q}u_1v_1^2$$

$$\Delta\ell = 2I_2R_0 + \frac{3}{2}I_{3a}R_0$$

$$(2\text{-}26)$$

where $\Delta\ell$ is the path length deviation between the real main path and the optic axis.

The transformation of the trajectory at the exit side of the fringing field, $(u_3, \tan\alpha_3, v_3, \beta_3)$ to $(u_4, \tan\alpha_4, v_4, \beta_4)$ were obtained in Eqs. (66)-(69) of Ref. 2-7. The transformation of the path length deviation of the exit fringing field from ℓ_3 to ℓ_4 at the ideal field boundary can be obtained from Eq. 2-26 by substituting $u_1 = u_4$, $\alpha_1 = -\alpha_4$, $v_1 = v_4$, $\ell_1 = -\ell_4$ and $\ell_2 = -\ell_3$. The result is:

$$\ell_4 = \ell_3 + \Delta\ell + 2I_{1a}R_0\alpha_3 + 3I_{4a}R_0u_3^2 + \frac{R_0}{6q}u_3^3 - R_0u_3^2\alpha_3 - \frac{R_0}{2q}u_3v_3^2$$

$$(2\text{-}27)$$

In an electric quadrupole lens, the influences of the fringing fields on the ion trajectory were calculated by Matsuda et al. [2-8]. From using these results, the effects of the fringing-fields of the quadrupole lens on the flight times can be neglected in a third-order approximation.

2-6. General transfer matrices and computer program

The third-order flight times in the toroidal electric

condenser, the electric quadrupole lens and the drift space are calculated as path length deviations. The results of the calculations are expressed as a power series expansion of the initial conditions of the ion; x_0, $\tan\alpha_0$, y_0, β_0, γ and δ, to a third-order approximation. The coefficients of the power series are given in explicit forms for the quadrupole lens and the drift space. For a toroidal condenser, the explicit forms of the coefficients will be very long and complicated. Therefore, we express them by using the H-matrix and the function F(m). The H-matrix is given by the results of the trajectory calculations for the toroidal condenser in Ref. 2-3. The function F(m) is the result of integrating the respective m function with respect to ω, and an explicit form of F(m) is given in Appendix 1. These expressions are convenient for programming and debugging.

The influences of the fringing fields on flight times are also calculated as the small change of the path length deviation at the ideal field boundaries.

The trajectories and flight times of charged particles can be expressed by a general transfer matrix, which contains one extra row and column for the flight time [2-9]. The transfer matrix of an ion-optical device is obtained by the multiplication of three matrices, for the entrance fringing field, for the ideal main region and for the exit fringing field. The elements of the last row of each transfer matrix are given by the coefficients obtained in previous sections. Flight times in a TOF mass spectrometer, or an ion-optical system, can be

expressed as a total transfer matrix obtained by making the matrix product of the general transfer matrices for respective ion-optical devices. The ion-optical characteristics of the TOF mass spectrometer can be estimated by taking the product of these general transfer matrices. The general transfer matrix for the third-order approximation is shown schematically in Fig. 2-5.

The computer program 'TRIO' was already developed by Matsuo et. al [2-10] for the calculation of the ion trajectory. A new computer program, which calculates the elements of the general transfer matrix numerically, has been constructed by modification of TRIO. The coefficients of the path length deviation of the TOF mass spectrometer can be calculated up to third-order by this program.

Fig. 2-5. General transfer matrix of third-order.

REFERENCES

2-1. J.M.B. Bakker, Int. J. Mass Spectrom. Ion Phys., 6 (1971) 291.

2-2. H. Matsuda, T. Matsuo, D. Ioanoviciu, H. Wollnik and V. Rabbel, Int. J. Mass Spectrom. Ion Phys., 42 (1982) 157.

2-3. T. Matsuo, H. Matsuda and H. Wollnik, Nucl. Instrum. Methods, 103 (1972) 515.

2-4. H. Wollnik, T. Matsuo and H. Matsuda, Nucl. Instrum. Methods, 102 (1972) 13.

2-5. D.L. Smith, Nucl Instrum. Methods, 79 (1970) 144.

2-6. Y. Fujita and H. Matsuda, Nucl. Instrum. Methods, 123 (1975) 495.

2-7. H. Matsuda, Nucl. Instrum. Methods, 91 (1971) 637.

2-8. H. Matsuda and H. Wollnik, Nucl. Instrum. Methods. 103 (1972) 117.

2-9. W.G. Davies, Nucl. Instrum. Methods. 169 (1980) 337.

2-10. T. Matsuo, H. Matsuda, Y. Fujita and H. Wollnik, Mass spectrosc. (Jpn), 24 (1976) 19.

3. ION OPTICS OF TIME-OF-FLIGHT MASS SPECTROMETERS WITH MULTIPLE FOCUSING

3-1. Isochronous and spatial focusing

In a TOF mass spectrometer, the spatial deviations (x_f, y_f), the inclination angles (α_f, β_f) and the path length deviation (ℓ_f) of an ion at a detector are given in a first-order approximation as:

$$x_f = X_x x_0 + X_\alpha \alpha_0 + X_\delta \delta$$

$$\alpha_f = A_x x_0 + A_\alpha \alpha_0 + A_\delta \delta$$

$$y_f = Y_y y_0 + Y_\beta \beta_0$$

$$\beta_f = B_y y_0 + B_\beta \beta_0$$

$$\ell_f = L_x x_0 + L_\alpha \alpha_0 + L_\delta \delta \qquad (3-1)$$

where x_0 and y_0 are the half width and height of a source slit, respectively, α_0 and β_0 are the horizontal and vertical inclination angles at the source slit, respectively, and δ is the relative energy deviation.

Because the flight time of an ion is proportional to the square root of its mass, the mass resolution, $M/\Delta M$, of the TOF system is given by the half of the time resolution of the system.

$$\frac{M}{\Delta M} = \frac{T_f}{2\,\Delta t}$$

$$(3-2)$$

where T_f is the flight time of the ion given in Eq. 2-3.
Δt expresses the resolvable time width, which is given by
$\ell_f/v_0 + t_0 + t_d$, where v_0 is the velocity of a reference ion,
t_0 is the duration of operation of the ion source and t_d is
the time resolution of the detection system. The flight time,
T_f, is given by L_f/v_0, where L_f is the total flight length,
therefore the mass resolving power of the TOF mass spectrometer
can be expressed as:

$$\frac{M}{\Delta M} = \frac{L_f}{2(\ell_f + v_0 t_0 + v_0 t_d)}$$

$$(3-3)$$

The path length deviation, ℓ_f, is given, in the third-order
approximation, as:

$$\ell_f = L_x x_0 + L_\alpha \alpha_0 + L_\delta \delta + L_{\alpha\alpha} \alpha_0^2 + L_{\alpha\delta} \alpha_0 \delta + L_{\delta\delta} \delta^2 + L_{yy} y_0^2$$

$$+ L_{y\beta} y_0 \beta_0 + L_{\beta\beta} \beta_0^2 + L_{\alpha\alpha\alpha} \alpha_0^3 + L_{\alpha\alpha\delta} \alpha_0^2 \delta + L_{\alpha\delta\delta} \alpha_0 \delta^2$$

$$+ L_{\alpha yy} \alpha_0 y_0^2 + L_{\alpha y\beta} \alpha_0 y_0 \beta_0 + L_{\alpha\beta\beta} \alpha_0 \beta_0^2 + L_{\delta\delta\delta} \delta^3 + L_{\delta yy} \delta y_0^2$$

$$+ L_{\delta y\beta} \delta y_0 \beta_0 + L_{\delta\beta\beta} \delta \beta_0^2$$

$$(3-4)$$

where the coefficients can be calculated by the computer
program described in Chapter 2.

A small denominator of Eq. 3-3 is necessary to achieved a
high resolving power in the TOF system. In order to minimize

the path length deviation, the condition of triple isochronous focusing ($L_x=0$, $L_\alpha=0$, $L_\delta=0$) should be met. Furthermore, the higher-order coefficients should be small. Both fast pulse operation of an ion source and precise time measuring are also required for high resolution. A large numerator of Eq. 3-3 also increases the resolving power of the system, therefore a long flight path is also required. From a practical viewpoint, small geometrical size is desirable, therefore, it is preferable to devise a compact configuration with long path length.

In order to increase the ion transmission efficiency of the TOF system, 2-dimensional stigmatic focusing and energy focusing in space are necessary. Triple spatial focusing ($X_\alpha=0$, $Y_\beta=0$, $X_\delta=0$) is also required. The TOF system will have a large acceptance area for an ion beam diverging with a wide solid angle, if the condition of the spatial focusing is achieved.

There are several requirements mentioned above in order to attain high performance in a TOF mass spectrometer. In this chapter, ion optical designs of the TOF systems which have a capacity for high resolution and high transmission are investigated in detail. Other practical improvements in both the ion source and the detection system will be given in a later chapter. The procedure of the investigation of the TOF system is as follows:

At first, the conditions for the first-order focusing were considered in an ion-optical system. All the possible solutions, which satisfy both isochronous focusing and spatial

focusing, were studied. Then, the systems were estimated to a
higher-order property of ion-optical characteristics. The
geometrical configuration were also considered for each system.

The method of transfer matrix analysis is convenient for
the systematic search for multiple focusing systems. The
first-order relations of Eqs. 3-1 are expressed by using the
total transfer matrix [R] of the system as:

$$
\begin{bmatrix} x_f \\ \alpha_f \\ y_f \\ \beta_f \\ \delta \\ \ell_f \end{bmatrix}
=
\begin{bmatrix} & & & R & & \end{bmatrix}
\begin{bmatrix} x_0 \\ \alpha_0 \\ y_0 \\ \beta_0 \\ \delta \\ \ell_0 \end{bmatrix}
$$

where

$$
[R] =
\begin{bmatrix}
X_x & X_\alpha & 0 & 0 & X_\delta & 0 \\
A_x & A_\alpha & 0 & 0 & A_\delta & 0 \\
0 & 0 & Y_y & Y_\beta & 0 & 0 \\
0 & 0 & B_y & B_\beta & 0 & 0 \\
0 & 0 & 0 & 0 & 1 & 0 \\
L_x & L_\alpha & 0 & 0 & L_\delta & 1
\end{bmatrix}
\qquad (3\text{-}5)
$$

The conditions for the triple isochronous and triple spatial
focusing are given respectively as:

$$
L_x = 0, \ L_\alpha = 0, \ L_\delta = 0 \ \text{ and } \ X_\alpha = 0, \ Y_\beta = 0, \ X_\delta = 0 \qquad (3\text{-}6)
$$

Since we usually measure ions which are accelerated by a

constant voltage in the ion source, only ion-optical devices

with electric field are used as actual components in the

analyzer for the TOF system. In order to achieve the

isochronous focusing with energy spread, the spatial dispersive

effect of an analyzer is necessary, thus, the use of an

electric sector is considered.

The system consisting of a single toroidal electric sector

is shown schematically in Fig. 3-1. The first-order coeffi-

cients of the total transfer matrix are the functions of the

lengths of the two drift spaces, D_1 and D_2, and the constants

of the toroidal electric sector (mean radius, a_e; deflection

angle, ϕ_e; field index, c). One of the three parameters of

D_1, D_2 and a_e is a normalization factor of the size of the

system. Therefore, the number of adjustable parameters of the

system with a single toroidal sector is four. On the other

hand, the number of independent equations of six-fold multiple

focusing given in Eqs. 3-6 is five. Consequently, six-fold

focusing can not be achieved simultaneously by using a single

toroidal sector, because the number of parameters of the system

is insufficient for the number of the equations.

3-2. Symmetrical systems consisting of two electric fields

In order to obtain the solution of the six-fold multiple

focusing conditions given in Eqs. 3-6, tandem arrangements of

toroidal electric sectors were considered. The ion-optical

system consisting of two similar electric sectors is schemati-

cally shown in Fig. 3-2. In this case, three drift regions

(length D_1, D_2, D_3) exist. Therefore, the number of parameters

TOROIDAL
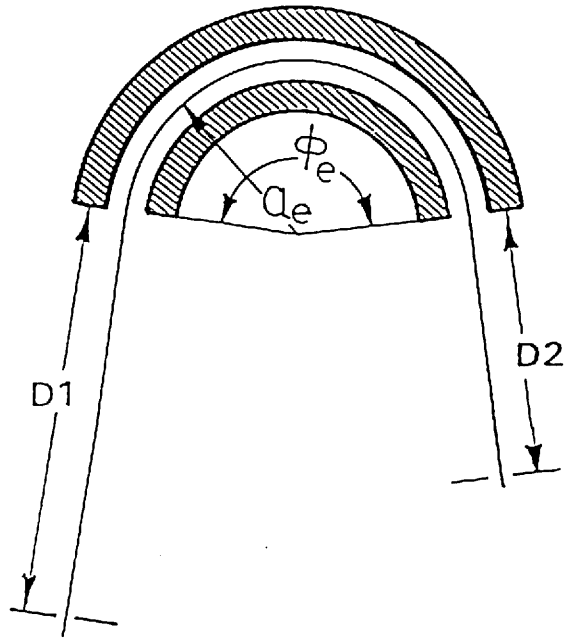ELECTRIC
SECTOR field index C

ϕ_e

a_e

D1

D2

Fig. 3 - 1. Schematic diagram of an ion-optical
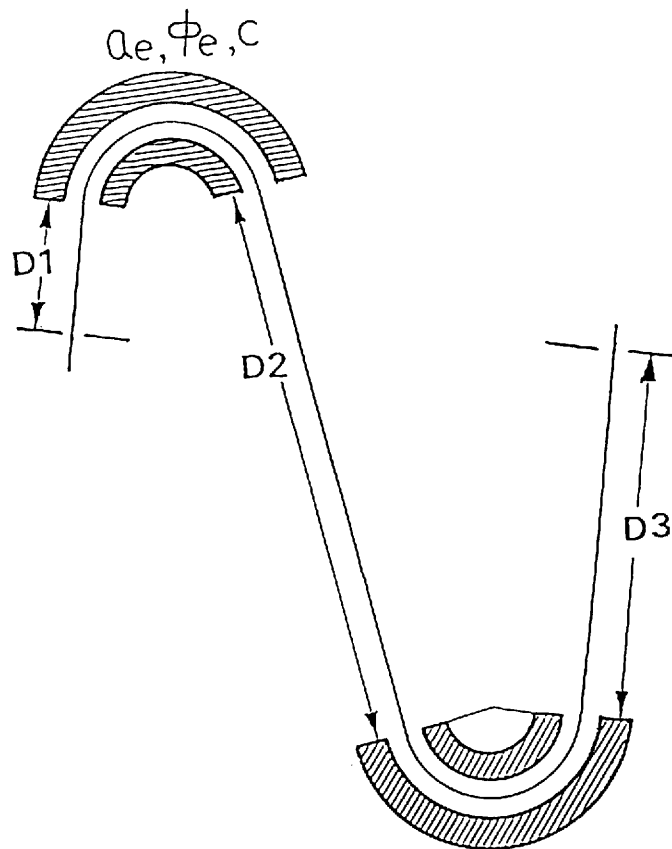system consisting of a single toroidal
electric sector.

Fig. 3 - 2. Schmatic drawing of an ion-optical
system consisting of two similar
toroidal electric sectors.

in the system without the normalization factor is five. This number coincides with that of the independent equations of the conditions of six-fold multiple focusing. This suggests the existence of solutions of the ion-optical design, which satisfy multiple focusing simultaneously.

In the search for the solutions, the consideration of a symmetrical arrangement is very useful. If the symmetrical alignment is utilized, the number of equations to be satisfied is reduced from five to four. Let us consider symmetrical systems consisting of two similar electric sectors as shown in Fig. 3-3. The first half part of the whole system is composed of the first drift region (length D_1), the toroidal electric sector (a_e, ϕ_e, c) and the second drift region (length D_2). As the latter half is a symmetrical figure of the first half, its components are, in order, drift region (D_2), a similar toroidal sector and drift region (D_1). Four different cases shown in Fig. 3-3 (a-d) can be applied to the system consisting of two electric sectors, considering both the direction of the deflection of the two sectors, and an image profile at the intermediate position. We define the systems shown in Figs. 3-3 (a) and (b) as point symmetrical and those shown in Figs. 3-3 (c) and (d) as plane symmetrical. 'Point symmetrical' means that the both figures of the first half and latter half coincide after 180° rotation with respect to the symmetrical point. The 'plane symmetrical' means coincidence after reflection by a mirror on the symmetrical plane. The general transfer matrix, [Q], which expresses the first half of the whole system is considered. The matrix elements of [Q] are
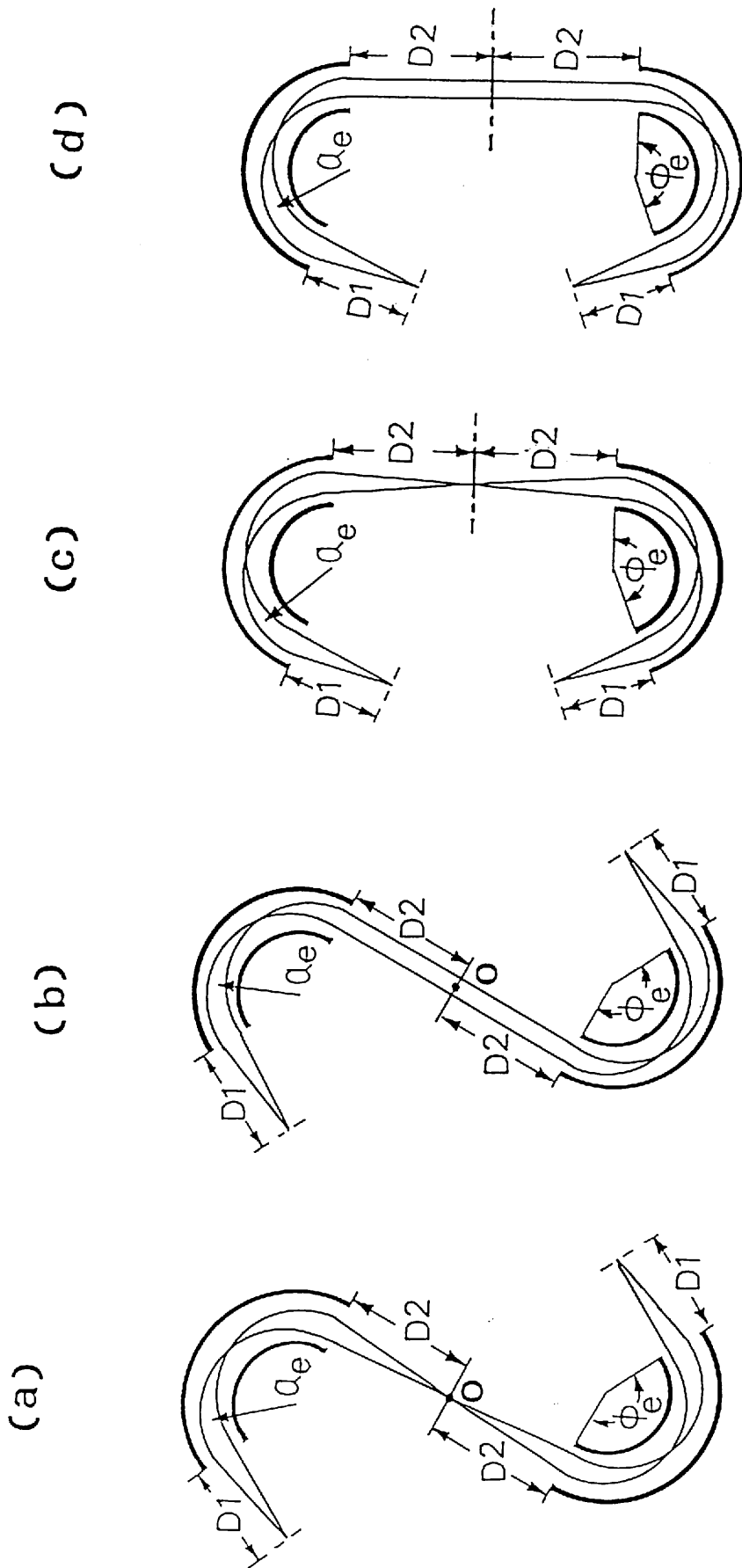
Fig. 3 - 3. Schematic diagrams of the symmetrical systems consisting of two electric sectors.
a) Point symmetrical system with an intermediate image ([Q*]·[Q] system); b) point
symmetrical system without an intermediate image ([Q*]/[Q] system); c) plane symmetrical
system with an intermediate image ([Q']·[Q] system); d) plane symmetrical system
without an intermediate image ([Q']/[Q] system).

defined as:

$$[Q] = \begin{bmatrix} (x|x) & (x|\alpha) & 0 & 0 & (x|\delta) & 0 \\ (\alpha|x) & (\alpha|\alpha) & 0 & 0 & (\alpha|\delta) & 0 \\ 0 & 0 & (y|y) & (y|\beta) & 0 & 0 \\ 0 & 0 & (\beta|y) & (\beta|\beta) & 0 & 0 \\ 0 & 0 & 0 & 0 & 1 & 0 \\ (\ell|x) & (\ell|\alpha) & 0 & 0 & (\ell|\delta) & 1 \end{bmatrix}$$

$$(3-7)$$

We discuss the relationships between the multiple focusing conditions in Eqs. 3-6 and the elements of matrix [Q].

3-2-a. <u>Point-symmetrical system with an intermediate image ([Q*]·[Q] system)</u>

Two similar electric fields are arranged as shown in Fig. 3-3 (a). Here the first half and the latter half are point symmetrical with respect to the intermediate point O. In this case, the existence of an intermediate image at the point O is assumed. The matrices [Q] and [Q*] express the former and the latter half of the whole system, respectively. The total transfer matrix [R] is expressed to be [R]=[Q*]·[Q], where [Q*] is a point-symmetrical matrix of [Q] and the symbol '·' indicates that the system has an intermediate image. It should be noted that the element (x|α) of matrix [Q] is assumed to be zero from the condition of an intermediate image. The elements of the point symmetrical matrix [Q*] are expressed by the elements of matrix [Q]. The relationships between them are given in Appendix 2.

After the multiplication of [Q*]·[Q], the total transfer

matrix [R] is given by the terms of the elements of matrix [Q] as:

$$[R] = \begin{bmatrix}
1 & 0 & 0 & 0 & 2(x|\delta)(\alpha|\alpha) & 0 \\
2(x|x)(\alpha|x) & 1 & 0 & 0 & 2(x|\delta)(\alpha|x) & 0 \\
0 & 0 & 2(y|y)(\beta|\beta)-1 & 2(y|\beta)(\beta|\beta) & 0 & 0 \\
0 & 0 & 2(y|y)(\beta|y) & 2(y|y)(\beta|\beta)-1 & 0 & 0 \\
0 & 0 & 0 & 0 & 1 & 0 \\
2(x|x)(\alpha|x)(l|\alpha) & 2(l|\alpha) & 0 & 0 & \begin{matrix} 2(l|\delta)-2(x|\delta)(\alpha|\alpha)(l|x) \\ +2(x|\delta)(\alpha|x)(l|\alpha) \end{matrix} & 1
\end{bmatrix}$$

$$(3-8)$$

Therefore, the six coefficients are expressed as:

$$X_\alpha = 0$$

$$X_\delta = 2(x|\delta)(\alpha|\alpha)$$

$$Y_\beta = 2(y|\beta)(\beta|\beta)$$

$$L_x = 2(x|x)(\alpha|x)(l|\alpha)$$

$$L_\alpha = 2(l|\alpha)$$

$$L_\delta = 2(l|\delta) - 2(x|\delta)(\alpha|\alpha)(l|x) + 2(x|\delta)(\alpha|x)(l|\alpha)$$

$$(3-9)$$

Applying the multiple focusing conditions given in Eqs. 3-6, one obtains the necessary conditions as:

$$(x|\alpha) = 0$$
$$2(x|\delta)(\alpha|\alpha) = 0$$
$$2(y|\beta)(\beta|\beta) = 0$$
$$2(x|x)(\alpha|x)(l|\alpha) = 0$$
$$2(l|\alpha) = 0$$
$$2(l|\delta) - 2(x|\delta)(\alpha|\alpha)(l|x) + 2(x|\delta)(\alpha|x)(l|\alpha) = 0$$

$$(3-10)$$

On the other hand, the elements of a transfer matrix have always the following relations in any transfer matrix, if the dispersive elements of the matrix are given by mass and energy mode.

$$(x|x)(\alpha|\alpha) - (x|\alpha)(\alpha|x) = 1$$

$$(y|y)(\beta|\beta) - (y|\beta)(\beta|y) = 1$$

$$(l|x) = 2[(x|x)(\alpha|\delta) - (x|\delta)(\alpha|x)]$$

$$(l|\alpha) = 2[(x|\alpha)(\alpha|\delta) - (x|\delta)(\alpha|\alpha)]$$

$$(3-11)$$

In these equations, the first two equations are the representation of the well-known Liouville's theorem. The other two equations, reported by Wollnik et al. [3-1], are obtained by the condition of symplecticity. By introducing Eqs. 3-11 into Eqs. 3-10, one can simplify the requirements for the multiple focusing to give:

$$(x|\alpha) = 0$$
$$(x|\delta) = 0$$
$$(l|\delta) = 0$$
$$(y|\beta)(\beta|\beta) = 0$$

$$(3-12)$$

The elements of matrix [Q] in Eqs. 3-12 are complicated functions of the two drift lengths (D_1, D_2) and the parameters of

the toroidal field (a_e, ϕ_e, c). An exhaustive investigation of the solutions for Eqs. 3-12 was accomplished. Six feasible systems gave all possible solutions, and are given in Table 3-1. In this table, the second and third-order coefficients, which are numerically calculated by using the computer program discussed in Chapter 2, are also given. All parameters are normalized to give an unit length of total path. These systems are shown schematically in Fig. 3-4. The system a-4 is the same as that proposed by Poschenrieder [1-9].

3-2-b. <u>Point-symmetrical system without an intermediate image</u>

<u>([Q*]/[Q] system: parallel at a symmetrical point)</u>

The schematic diagram of this configuration is shown in Fig. 3-3 (b). Similar to the previous case, the first half, [Q], and the latter half, [Q*], are point symmetrical with respect to point O. The total transfer matrix [R] can be written as [R]=[Q*]/[Q], where the symbol '/' indicates that the beam is parallel between the sectors. The matrix [Q] is given by Eq. 3-7, but the element $(\alpha|\alpha)$ is equal to zero instead of $(x|\alpha)=0$ from the condition of the parallel beam. After performing the matrix product of [Q*]/[Q], the total transfer matrix [R] is expressed by the elements of [Q] as:

$$[R] = \begin{bmatrix} -1 & 0 & 0 & 0 & 0 & 0 \\ 2(x|x)(\alpha|x) & -1 & 0 & 0 & 2(x|\delta)(\alpha|x) & 0 \\ 0 & 0 & 2(y|y)(\beta|\beta)-1 & 2(y|\beta)(\beta|\beta) & 0 & 0 \\ 0 & 0 & 2(y|y)(\beta|y) & 2(y|y)(\beta|\beta)-1 & 0 & 0 \\ 0 & 0 & 0 & 0 & 1 & 0 \\ 2(l|x)+2(x|x)(\alpha|x)(l|\alpha) & 0 & 0 & 0 & 2(l|\delta)+2(x|\delta)(\alpha|x)(l|\alpha) & 1 \end{bmatrix}$$

(3-13)

Table 3-1. Six solutions of the multiple focusing TOF systems of case (a) in Fig. 3-3. Aberration coefficients are also given.

|	a - 1	a - 2	a - 3	a - 4	a - 5	a - 6
a_e	0.0717	0.0659	0.0348	0.0326	0.0101	0.0101
ϕ_e	160.9°	164.4°	197.1°	200.9°	290.1°	291.4°
c	0.1156	0.2440	0.9360	0.9849	1.5576	1.5614
D_1	0.1493	0.1555	0.1901	0.1297	0.2243	0.2243
D_2	0.1493	0.1555	0.1904	0.1930	0.2244	0.2243
L_x	0.0000	0.0000	0.0000	0.0000	0.0000	0.0000
L_α	0.0000	0.0000	0.0000	0.0000	0.0000	0.0000
L_δ	0.0000	0.0000	0.0000	0.0000	0.0000	0.0000
$L_{\alpha\alpha}$	−0.35	−0.39	−0.74	−0.79	−3.41	−3.45
$L_{\alpha\delta}$	0.31	0.33	0.49	0.51	1.38	1.40
$L_{\delta\delta}$	0.29	0.33	0.69	0.73	1.94	1.98
L_{yy}	3.01	55.11	18.93	65.09	35.29	120.68
$L_{y\beta}$	0.00	10.75	−0.02	14.85	−0.26	33.86
$L_{\beta\beta}$	0.40	0.73	−0.72	0.74	−2.07	1.90
$L_{\alpha\alpha\alpha}$	36	53	607	765	28626	29190
$L_{\alpha\alpha\delta}$	−49	−70	−606	−741	−17347	−17753
$L_{\alpha\delta\delta}$	22	31	202	240	3509	3605
$L_{\delta\delta\delta}$	−4	−5	−22	−25	−229	−236
$L_{\alpha yy}$	9	−10	−301	−530	30549	175332
$L_{\alpha y\beta}$	5	35	−82	−189	−1597	30148
$L_{\alpha\beta\beta}$	0	3	−14	−18	1628	1587
$L_{\delta yy}$	−10	−150	150	−70	−8232	−49102
$L_{\delta y\beta}$	0	−47	32	13	502	−8529
$L_{\delta\beta\beta}$	1	−3	2	1	−459	−465
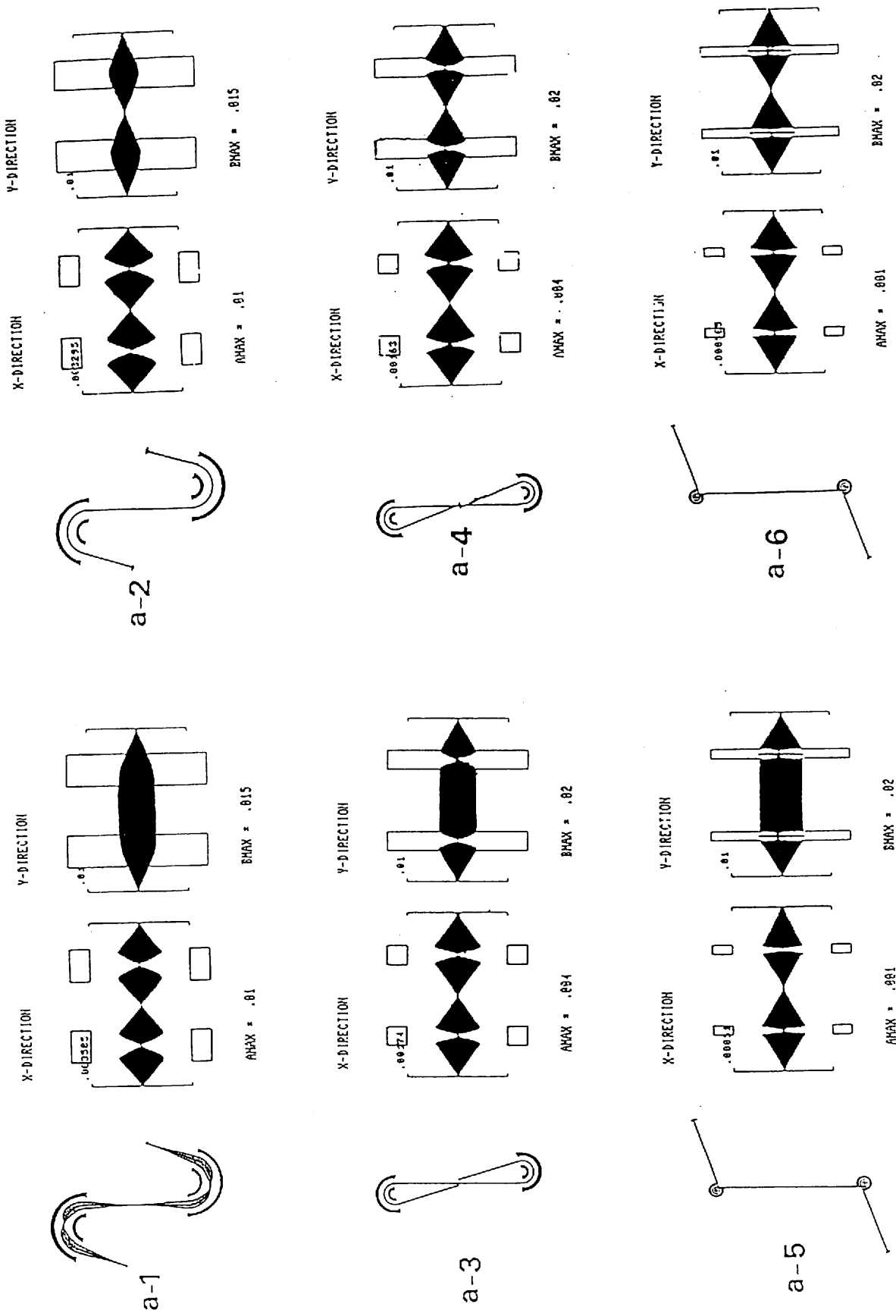
Fig. 3-4. Schematic drawings of the six systems of the case (a). Beam profiles in the systems are also shown.

The necessary conditions for matrix elements of [Q] to obtain multiple (six-fold) focusing can be derived from Eq. 3-13 by using Eqs. 3-11 as:

$$(\alpha|\alpha) = 0$$
$$(x|\delta) = 0$$
$$(l|\delta) = 0$$
$$(y|\beta)(\beta|\beta) = 0 \qquad\qquad (3-14)$$

All feasible systems are shown in Table 3-2. These systems are shown schematically in Fig. 3-5. The system b-2 is the same as that proposed by Poschenrieder.

3-2-c. <u>Plane-symmetrical system with an intermediate image</u>
   <u>([Q']·[Q] system)</u>

The schematic diagram of this configuration is shown in Fig. 3-3 (c). The total transfer matrix [R] can be obtained in the form [R]=[Q']·[Q] where [Q'] is the plane-symmetrical matrix of [Q]. The elements of matrix [Q'] can be expressed by the elements of matrix [Q]. The detailed relationships are also given in the Appendix 2. The matrix [R] is expressed by the elements of [Q] as:

$$[R] = \begin{bmatrix} 1 & 0 & 0 & 0 & 0 & 0 \\ 2(x|x)(\alpha|x) & 1 & 0 & 0 & 2(x|x)(\alpha|\delta) & 0 \\ 0 & 0 & 2(y|y)(\beta|\beta)-1 & 2(y|\beta)(\beta|\beta) & 0 & 0 \\ 0 & 0 & 2(y|y)(\beta|y) & 2(y|y)(\beta|\beta)-1 & 0 & 0 \\ 0 & 0 & 0 & 0 & 1 & 0 \\ 2(l|x)-2(x|x)(\alpha|x)(l|\alpha) & 0 & 0 & 0 & 2(l|\delta)-2(x|x)(\alpha|\delta)(l|\alpha) & 1 \end{bmatrix}$$

$$(3-15)$$

Table 3-2. Six solutions of the multiple focusing TOF mass systems of case (b) in Fig. 3-3. Aberration coefficients are also given.

	b - 1	b - 2	b - 3	b - 4	b - 5	b - 6
a_e	0.0736	0.0679	0.0339	0.0324	0.0101	0.0100
ϕ_e	156.4°	159.9°	196.7°	199.5°	290.1°	291.1°
c	0.1609	0.2758	0.9842	1.017	1.5662	1.5690
D_1	0.0945	0.0989	0.1261	0.1275	0.1490	0.1492
D_2	0.2047	0.2117	0.2575	0.2597	0.2997	0.2999
L_x	0.0000	0.0000	0.0000	0.0000	0.0000	0.0000
L_α	0.0000	0.0000	0.0000	0.0000	0.0000	0.0000
L_δ	0.0000	0.0000	0.0000	0.0000	0.0000	0.0000
$L_{\alpha\alpha}$	0.12	0.13	0.22	0.22	-0.31	-0.27
$L_{\alpha\delta}$	0.00	0.00	0.00	0.00	-0.01	0.01
$L_{\delta\delta}$	0.30	0.34	0.73	0.76	2.00	2.01
L_{yy}	15.26	102.18	35.04	93.17	86.85	208.71
$L_{y\beta}$	-1.56	12.20	3.91	11.65	7.47	29.65
$L_{\beta\beta}$	0.30	0.52	-0.25	0.26	-0.65	0.75
$L_{\alpha\alpha\alpha}$	-1	-1	-6	-1	-582	249
$L_{\alpha\alpha\delta}$	-30	-40	-338	-381	-8283	-8287
$L_{\alpha\delta\delta}$	0	0	-1	0	-21	9
$L_{\delta\delta\delta}$	-5	-6	-27	-30	-242	-258
$L_{\alpha yy}$	-9	-125	239	1150	-86023	-269930
$L_{\alpha y\beta}$	10	29	-55	-21	13926	-14249
$L_{\alpha\beta\beta}$	-1	2	3	-2	-58	-49
$L_{\delta yy}$	-37	-259	104	-621	-47252	-138672
$L_{\delta y\beta}$	-5	-58	13	-25	3495	-9540
$L_{\delta\beta\beta}$	1	-2	-1	-1	-237	-237
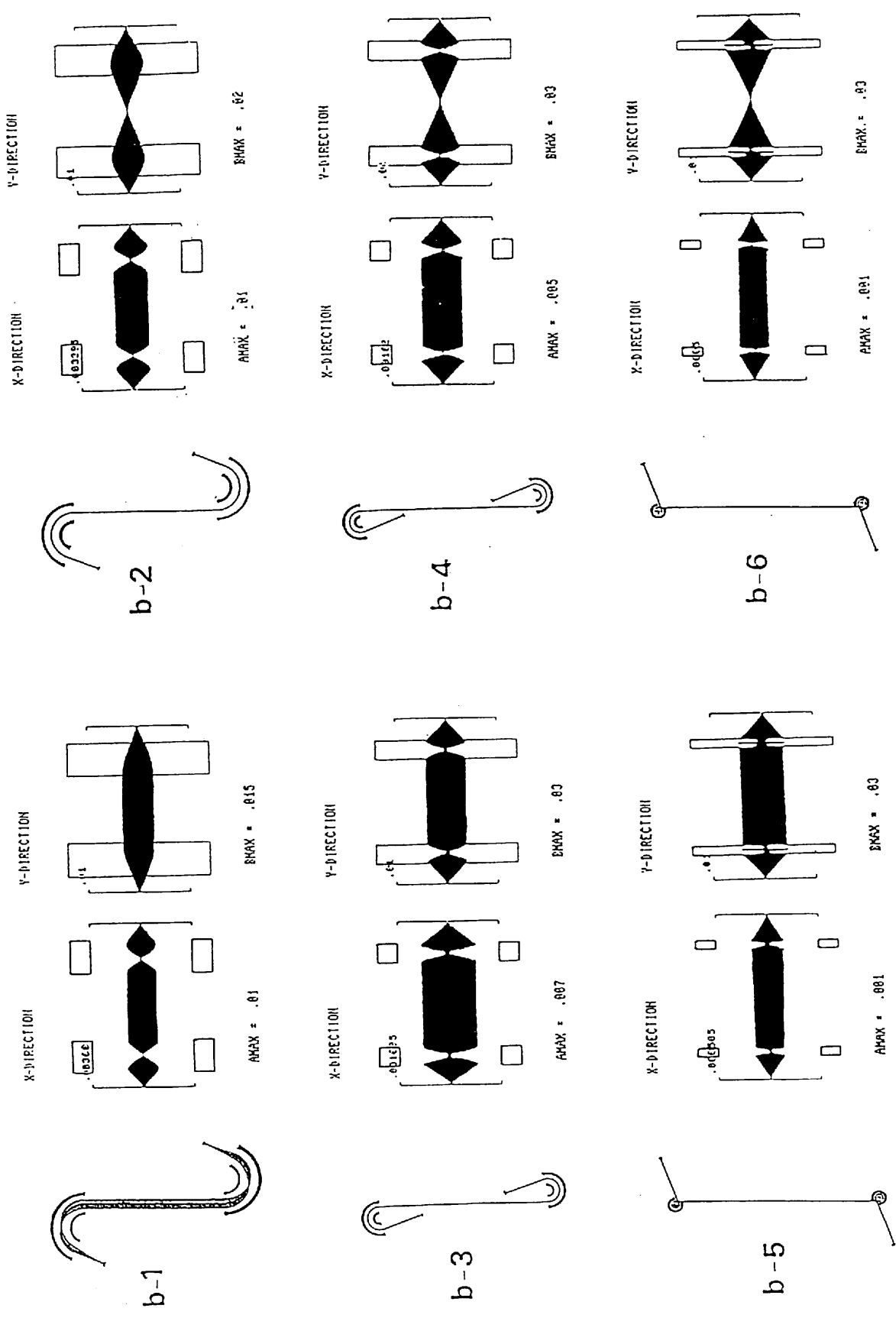
Fig. 3-5. Schematic drawings of the six systems of the case (b).
Beam profiles in the systems are also shown.

The necessary conditions of [Q] for the six-fold focusing are:

$$(x|\alpha) = 0$$
$$(\alpha|\delta) = 0$$
$$(l|\delta) = 0$$
$$(y|\beta)(\beta|\beta) = 0 \qquad\qquad (3\text{-}16)$$

Unfortunately, There is no feasible solution to satisfy Eqs. 3-16 simultaneously.

3-2-d. Plane-symmetrical system without an intermediate image ([Q']/[Q] system: parallel at symmetrical plane)

The schematic diagram of this configuration is shown in Fig. 3-3 (d). The total transfer matrix is written as [R]=[Q']/[Q]. The matrix [R] is given by:

$$[R] = \begin{bmatrix} -1 & 0 & 0 & 0 & 2(x|\alpha)(\alpha|\delta) & 0 \\ 2(x|x)(\alpha|x) & -1 & 0 & 0 & 2(x|x)(\alpha|\delta) & 0 \\ 0 & 0 & 2(y|y)(\beta|\beta)-1 & 2(y|\beta)(\beta|\beta) & 0 & 0 \\ 0 & 0 & 2(y|y)(\beta|y) & 2(y|y)(\beta|\beta)-1 & 0 & 0 \\ 0 & 0 & 0 & 0 & 1 & 0 \\ -2(x|x)(\alpha|x)(l|\alpha) & 2(l|\alpha) & 0 & 0 & \begin{array}{c}2(l|\delta)+2(x|\alpha)(\alpha|\delta)(l|x) \\ -2(x|x)(\alpha|\delta)(l|\alpha)\end{array} & 1 \end{bmatrix}$$

$$(3\text{-}17)$$

The necessary conditions for multiple focusing are:

$$(\alpha|\alpha) = 0$$
$$(\alpha|\delta) = 0$$
$$(l|\delta) = 0$$
$$(y|\beta)(\beta|\beta) = 0 \qquad\qquad (3\text{-}18)$$

Here, no feasible solution was found.

3-3. Symmetrical systems consisting of three electric fields

Consider a system consisting of three similar electric sectors. The total transfer matrix [R] is considered in two cases as [R]=[Q']·[Q] or [Q']/[Q], because only plane-symmetrical systems are allowed for the whole system. A search for the feasible systems which satisfy the multiple (six-fold) focusing produced thirty three examples. The schematic diagram of the TOF systems consisting of three electric sectors are shown in Fig. 3-6 (a,b). The deflection of the second sector is the same direction with those of the first and third sectors in the case (a). Case (b) has an opposite direction of deflection of the second sector to those of the first and third sectors. The deflections of the first and third sectors should coincide by the condition of the symmetrical arrangement of the system. All of the feasible solutions are listed in Table 3-3.

3-4. Doubly symmetrical systems consisting of four electric fields

In this section, the systems consisting of four electric sectors are considered. In this case, much more freedom may be attained in designing a TOF mass spectrometer, even under the restriction of multiple focusing. Therefore, one can expect better ion-optical characteristics of the TOF instrument. In the search for the ion-optical systems, a doubly symmetrical consideration was adopted into the arrangement of four electric sectors in the system. A system with doubly symmetric can be realized in the following way. Since the whole system should have an intermediate image, two cases [Q*]·[Q] and [Q']·[Q] are

(b)

a_e, ϕ_e, c

(a)

a_e, ϕ_e, c
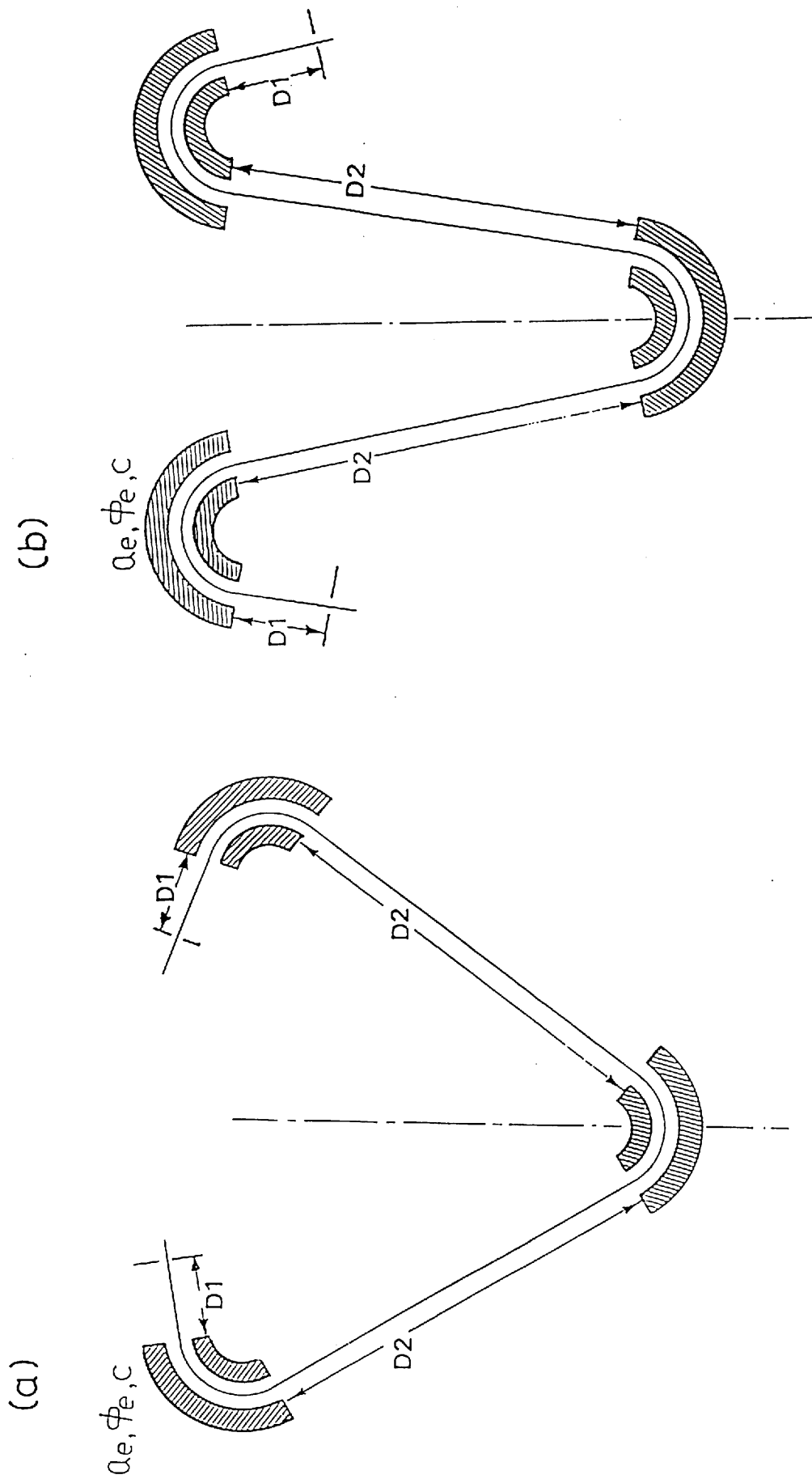
Fig. 3 – 6. Schematic diagrams of symmetrical TOF systems consisting of three similar electric sectors. Both systems are plane symmetrical with respect to the half of the whole system.

Table 3-3. Ion-optical parameters of the multiple focusing
TOF systems consisting of three electric sectors.

	a-1	a-2	a-3	a-4	a-5	a-6
a_e	0.0341	0.0328	0.0320	0.0252	0.0238	0.0232
ϕ_e	274.7°	277.7°	279.9°	300.3°	305.4°	307.7°
c	0.0228	0.0774	0.1129	0.4041	0.4637	0.4897
D_1	0.0849	0.0871	0.0886	0.1007	0.1032	0.1043
D_2	0.1697	0.1743	0.1772	0.2014	0.2064	0.2086

	a-7	a-8	a-9	a-10	a-11	a-12
a_e	0.0637	0.0562	0.0524	0.0255	0.0236	0.0228
ϕ_e	142.0°	147.1°	150.1°	187.5°	192.2°	194.3°
c	0.0823	0.2451	0.3287	0.9824	1.0343	1.0560
D_1	0.0872	0.0945	0.0980	0.1250	0.1272	0.1281
D_2	0.1755	0.1890	0.1960	0.2500	0.2543	0.2561

	a-13	a-14	a-15	a-16	a-17	a-18
a_e	0.0068	0.0068	0.0067	0.1315	0.0875	0.0740
ϕ_e	287.6°	288.9°	289.5°	54.4°	52.5°	52.0°
c	1.5758	1.5795	1.5814	0.4389	0.9709	1.1279
D_1	0.1495	0.1496	0.1497	0.1043	0.1265	0.1331
D_2	0.2990	0.2993	0.2994	0.2085	0.2530	0.2662

Table 3-3 (continued)

	b - 1	b - 2	b - 3	b - 4	b - 5	b - 6
a_e	0.0509	0.0469	0.0447	0.0237	0.0222	0.0215
ϕ_e	152.7°	156.3°	158.4°	192.2°	196.4°	198.2°
c	0.0608	0.1880	0.2560	0.9316	0.9840	1.0062
D_1	0.0987	0.1027	0.1049	0.1268	0.1286	0.1294
D_2	0.1975	0.2053	0.2097	0.2537	0.2573	0.2588

	b - 7	b - 8	b - 9	b -10	b - 11	b - 12
a_e	0.0068	0.0067	0.0066	0.0373	0.0355	0.0344
ϕ_e	288.8°	290.1°	290.7°	264.5°	268.4°	271.0°
c	1.5623	1.5663	1.5682	0.0260	0.0876	0.1279
D_1	0.1496	0.1497	0.1498	0.0806	0.0835	0.0853
D_2	0.2992	0.2995	0.2996	0.1612	0.1669	0.1705

	b - 13	b - 14	b - 15
a_e	0.0265	0.0250	0.0243
ϕ_e	293.8°	299.6°	302.2°
c	0.4245	0.4869	0.5139
D_1	0.0986	0.1014	0.1026
D_2	0.1972	0.2027	0.2051

allowed for the total transfer matrix, [R]. The half part

of whole system expressed by [Q] may be divided

into two parts by the consideration of the symmetrical

arrangement. If we express the transfer matrix of first half

part of [Q] as [P], four different types: [P*]·[P], [P*]/[P],

[P']·[P] and [P']/[P], are possible for the matrix [Q].

Therefore, eight possible combinations can be considered for

the doubly symmetrical system with four electric sectors.

Here, the investigation of the system [R]=[Q*]·[Q] with

[Q]=[P*]/[P] is described. The schematic arrangement is shown

in Fig. 3-7. The first half part, having the first and second

electric sectors, and latter half, having the third and fourth

sectors are point symmetrical arrangement with respect to the

center of the whole system. The whole system is a point sym-

metrical figure with 180° rotation with respect to the center

point. At the center, an intermediate image exists, because

the beam is focused. In between the first and second sectors,

the beam is not focused. The alignment of the first and second

sectors is also point symmetrical, so the deflection of the two

sectors is in opposite direction. In this case, the total

transfer matrix [R] can be obtained by the multiplication of the

four matrices as: [R]=[P*]/[P]·[P*]/[P].

From the results of the multiplication, [R] can be

expressed by using the elements of matrix [P], which expresses

the first quarter of the whole system with one sector, as:

TOROIDAL
ELECTRIC
SECTOR
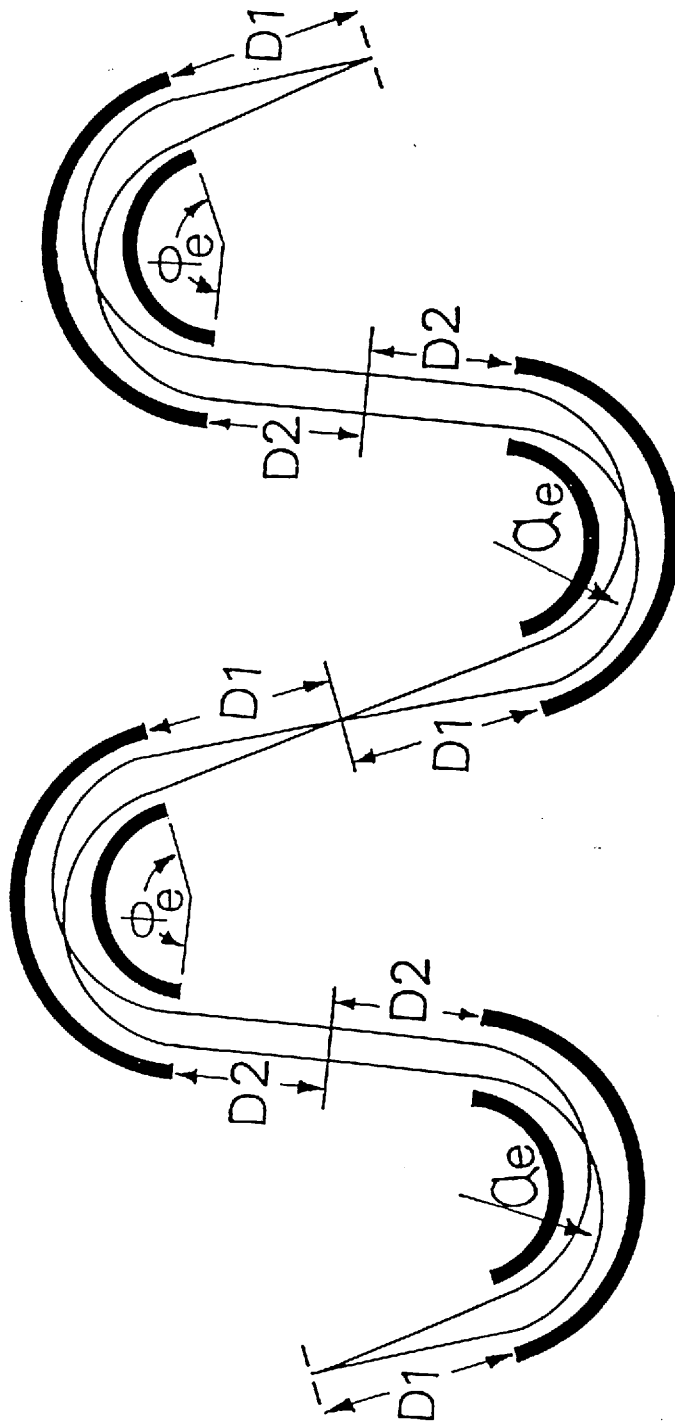
Fig. 3-7. Schematic drawing of doubly symmetrical system consisting of four similar electric sectors. The arrangement of the system is $[R]=[Q*]\cdot[Q]$ with $[Q]=[P*]/[P]$.

$$[R] = \begin{bmatrix}
1 & 0 & 0 & 0 & 0 & 0 \\
-4(x|x)(\alpha|x) & 1 & 0 & 0 & 0 & 0 \\
0 & 0 & 8(y|y)(y|\beta)(\beta|y)(\beta|\beta)+1 & 4(y|\beta)(\beta|\beta)[2(y|y)(\beta|\beta)-1] & 0 & 0 \\
0 & 0 & 4(y|y)(\beta|y)[2(y|y)(\beta|\beta)-1] & 8(y|y)(y|\beta)(\beta|y)(\beta|\beta)+1 & 0 & 0 \\
0 & 0 & 0 & 0 & 1 & 0 \\
0 & 0 & 0 & 0 & 4(l|\delta)+4(x|\delta)(\alpha|x)(l|\alpha) & 1
\end{bmatrix}$$

$$(3-19)$$

The six elements of the matrix [R] are:

$$X_\alpha = 0$$

$$X_\delta = 0$$

$$Y_\beta = 4(y|\beta)(\beta|\beta)[2(y|y)(\beta|\beta)-1]$$

$$L_x = 0$$

$$L_\alpha = 0$$

$$L_\delta = 4(l|\delta) + 4(x|\delta)(\alpha|x)(l|\alpha)$$

$$(3-20)$$

The four coefficients of matrix [R], namely X_α, X_δ, L_x and L_α, are eliminated by the doubly symmetrical condition. From the requirements of multiple focusing, the necessary conditions for the matrix elements of [P] can be obtained by using Eqs. 3-11 as:

$$(\alpha|\alpha) = 0$$
$$(l|\delta) - 2(x|\delta)(\alpha|\delta) = 0$$
$$(y|\beta)(\beta|\beta)[2(y|y)(\beta|\beta)-1] = 0 \qquad (3-21)$$

It should be noted that the necessary conditions are relaxed compared with the previous case, by introducing the doubly symmetrical condition. A search was made for the solutions of Eqs. 3-21. A special arrangement of four toroidal sectors for a TOF mass spectrometer, which satisfies multiple focusing conditions is possible, if the appropriate condition of the

toroidal electric sector is fulfilled. The relationship of the deflection angle, ϕ_e, and the field index, c, of the toroidal sector is shown in Fig. 3-8 by the solid lines. In this figure, the numbers attached to the lines indicate the number of focusing nodes in the y-direction. The drift lengths, D_1 and D_2, are determined by Eqs. 3-21 for each case.

3-5. <u>Higher-order characteristics of doubly symmetrical systems</u>

The previous sections showed that many solutions exist which satisfy the condition of multiple isochronous and spatial focusing in the first-order approximation. In order to find better TOF systems among these solutions, the higher-order characteristics must be considered. The geometrical configuration of the TOF system is also important from a practical viewpoint. In order to compare the higher-order characteristics of the different types of doubly symmetrical TOF systems, five representative cases, A-E, as shown in Fig. 3-8, were chosen. The second and third-order coefficients of A-E were calculated, where the value of the second-order field index of the toroidal electric field, c_2, was chosen to be -c. The results are given in Table 3-4. As can be seen from this table, case D has smaller absolute value of higher-order coefficients than any of the others. The schematic drawings of the systems A-E are shown in Fig. 3-9. In this figure, the systems are normalized to have equal flight length. As can be seen from this figure, case D has the smallest configuration. Therefore, the TOF systems near case D was examined in more detail.
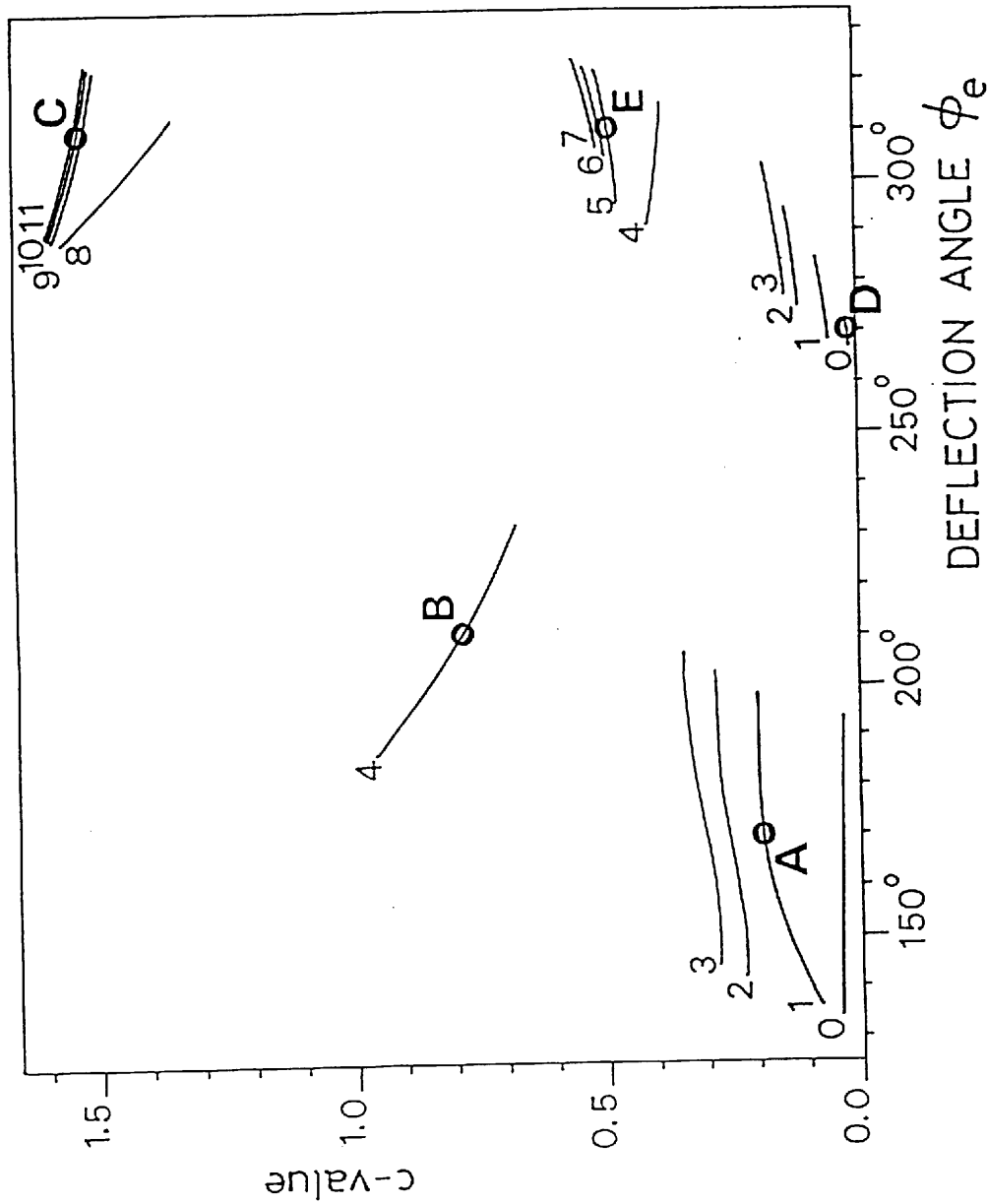
Fig. 3-8.   Relationship between c-value and ϕ_e of the toroidal sector, which is necessary to achieve the multiple focusing in a doubly symmetrical system. All sets of c and ϕ_e on the solid line give feasible TOF systems. The numbers attached to the lines indicate the number of focusing nodes in the y-direction.

Table 3-4. Ion-optical parameters and aberration coefficients for five representative cases: A, B, C, D and E in Fig. 3-8. Case D' has minimized higher-order aberrations.

	A	B	C	D	D'	E
a_e	0.0384	0.0269	0.0101	0.0292	0.0290	0.0214
ϕ_e	170.0°	210.0°	310.0°	270.0°	269.0°	310.0°
c	0.1863	0.7848	1.5121	0.0151	0.0150	0.4743
D_1	0.0266	0.0210	0.0228	0.0637	0.0689	0.0470
D_2	0.1094	0.1304	0.17626	0.0486	0.0452	0.0870
L_x	0.0000	0.0000	0.0000	0.0000	0.0000	0.0000
L_α	0.0000	0.0000	0.0000	0.0000	0.0000	0.0000
L_δ	0.0000	0.0000	0.0000	0.0000	0.0000	0.0000
$L_{\alpha\alpha}$	0.35	0.69	2.25	0.95	0.97	1.33
$L_{\alpha\delta}$	0.81	4.33	29.63	0.73	0.60	3.01
$L_{\delta\delta}$	0.69	7.10	98.07	0.48	0.42	2.56
L_{yy}	239.30	-38.40	-128865.70	2.89	0.01	-1469.80
$L_{y\beta}$	-14.87	0.00	-0.06	0.00	0.00	67.45
$L_{\beta\beta}$	0.39	17.90	-0.95	0.24	0.00	-1.34
$L_{\alpha\alpha\alpha}$	-8	-27	-460	-47	-51	-116
$L_{\alpha\alpha\delta}$	-45	-262	-9169	-58	-54	-340
$L_{\alpha\delta\delta}$	-61	-822	-60514	-26	-19	-374
$L_{\delta\delta\delta}$	-47	-1173	-155088	-5	-3	-162
$L_{\alpha yy}$	483	-5899	-5962517	-6	-7	60577
$L_{\alpha y\beta}$	31	-782	2219	2	0	2522
$L_{\alpha\beta\beta}$	-4	27	37	0	0	-45
$L_{\delta yy}$	613	-18264	-36743426	-5	-6	35202
$L_{\delta y\beta}$	-70	1881	-37695	1	0	956
$L_{\delta\beta\beta}$	-1	-106	228	0	0	35
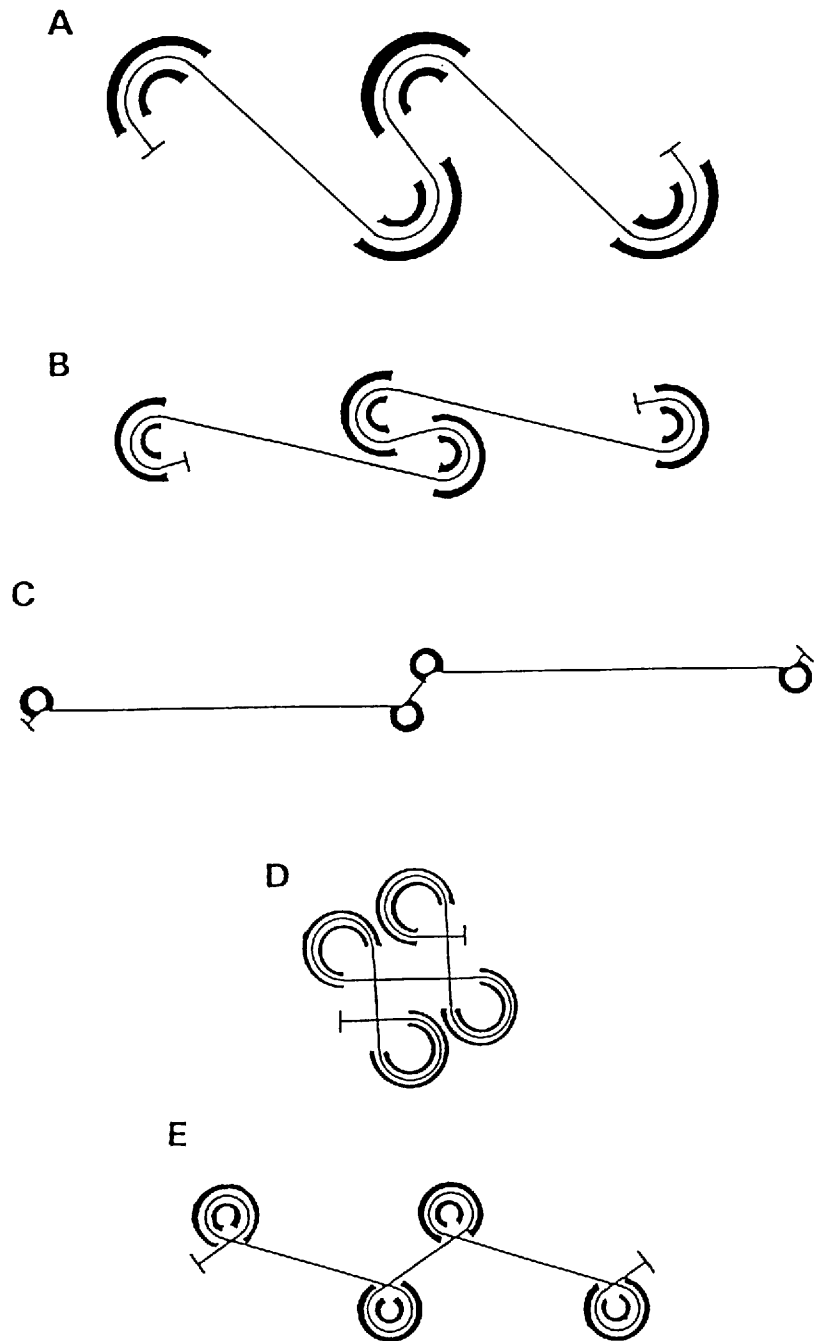
Fig. 3 - 9.   Schematic drawings of the five examples of
              an ion-optical system with four electric
              sectors in Table 3 - 4.   All systems are
              normalized to have equal total path length.

The behavior of the higher-order coefficients was investigated by varying the deflection angle, ϕ_e. The results are shown in Fig. 3-10. The variation of the second-order coefficients is not critical. Any systems with toroidal electric sectors whose deflection angles are between 267° and 271° may be chosen. It was found that the influence of the field index, c_2, on some second-order coefficients was significant, as shown in Fig. 3-11. The value 0.002 of c_2 was the best in the case of ϕ_e=269°. The higher-order coefficients of the system with c_2=0.002 are also given in Table 3-4 as D'. The schematic diagram of the TOF system with ϕ_e=269° is shown in Fig. 3-12. In this case, the area of whole system is in a circle of $0.24L_f$ diameter, where L_f is the total flight length. Therefore, a very compact TOF mass spectrometer can be realized using this design.

3-6. <u>Summary</u>

We have considered the ion optics for multiple (six-fold) focusing TOF mass spectrometers from the viewpoint of a symmetrical arrangement of the toroidal electric sectors. Twelve suitable systems consisting of two electric sectors were found. The systems a-1 and b-1 given in Table 3-1 and 3-2 are satisfactory in the higher-order character. We have also investigated the doubly symmetrical systems consisting of four electric sectors, and many solutions have been found. The system of case D' in Table 3-4 shown in Fig. 3-12 is excellent in both higher-order and geometric characteristics.
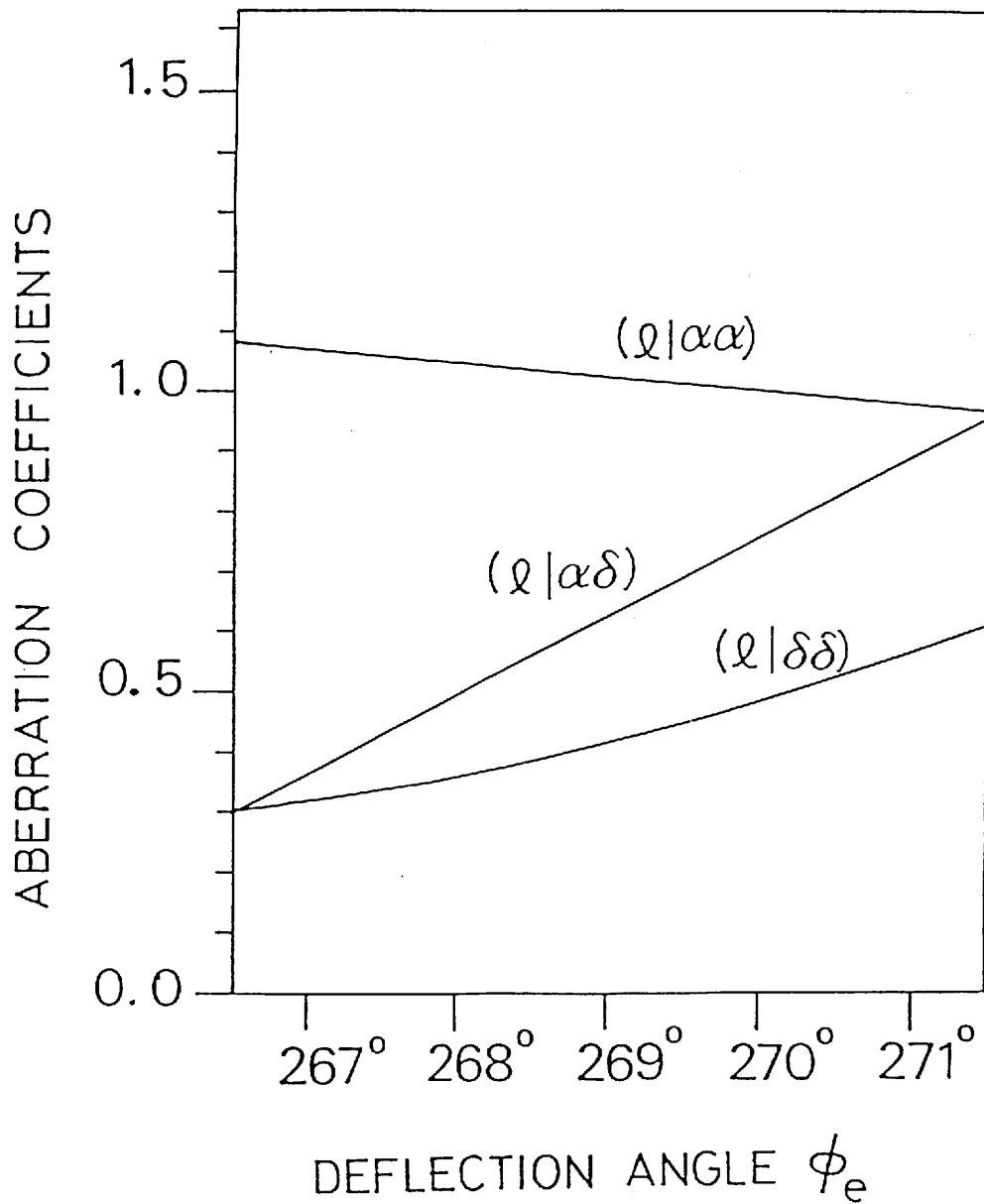
Fig. 3 - 10. Variation of second-order aberration coefficients of the four sector system near case D with deflection angle ϕ_e (267°-271°). All system satisfy the multiple focusing conditions.
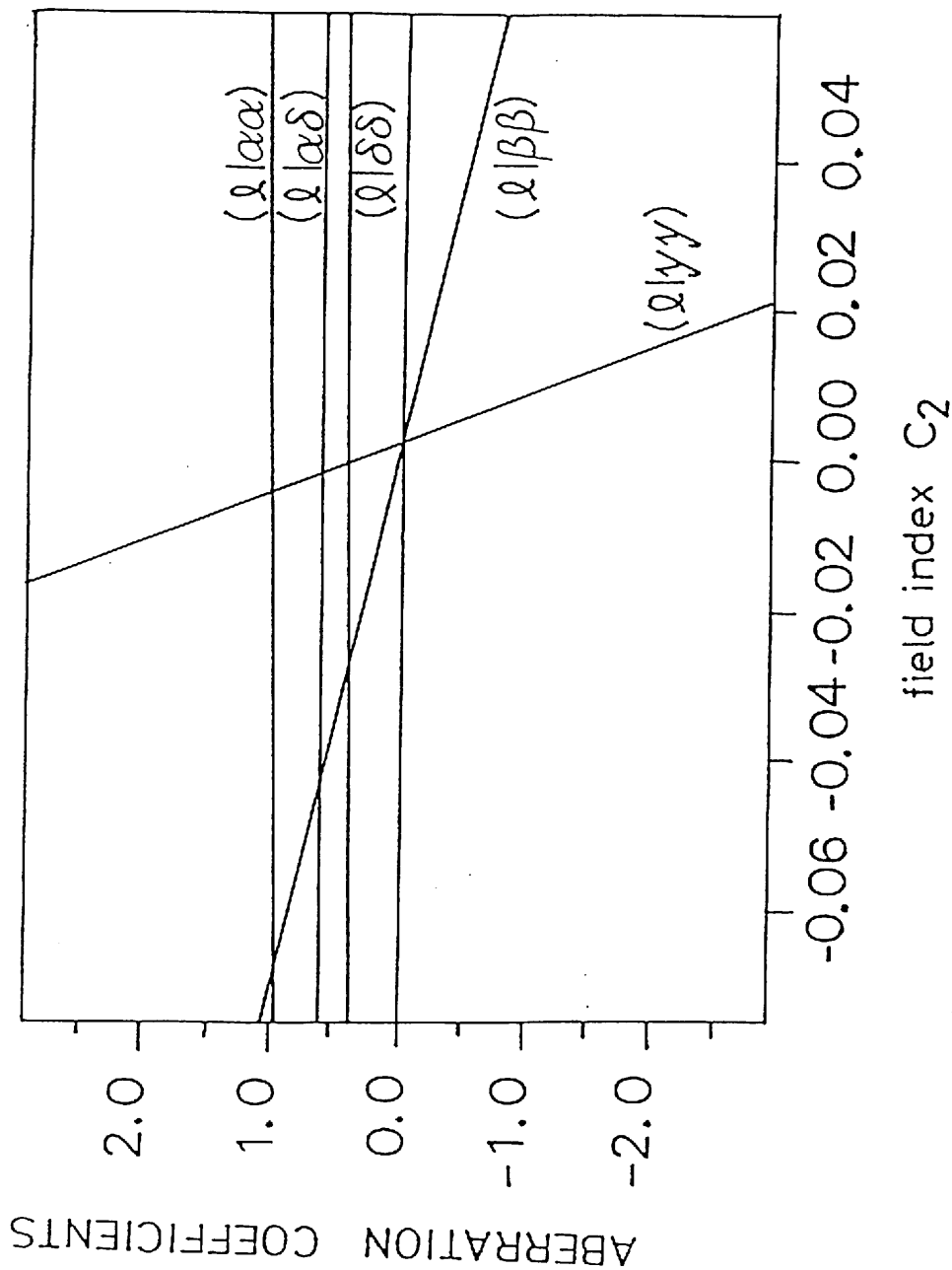
Fig. 3-11. Variation of second-order aberration coefficients with field index c_2 for the system with $\phi_e = 269°$.

field index C_2

ABERRATION COEFFICIENTS

$(\ell|\alpha\alpha)$
$(\ell|\alpha\delta)$
$(\ell|\delta\delta)$
$(\ell|\beta\beta)$
$(\ell|\gamma\gamma)$

DETECTOR
SLIT

TOROIDAL
ELECTRIC
FIELD

$2 \cdot D_2$

a_e

ϕ_e

D_1

ϕ_e

SOURCE
SLIT

$\phi_e = 269.0°$

$c = 0.015$

$C_2 = 0.002$

$D_1 = 2.38 a_e$

$D_2 = 1.56 a_e$
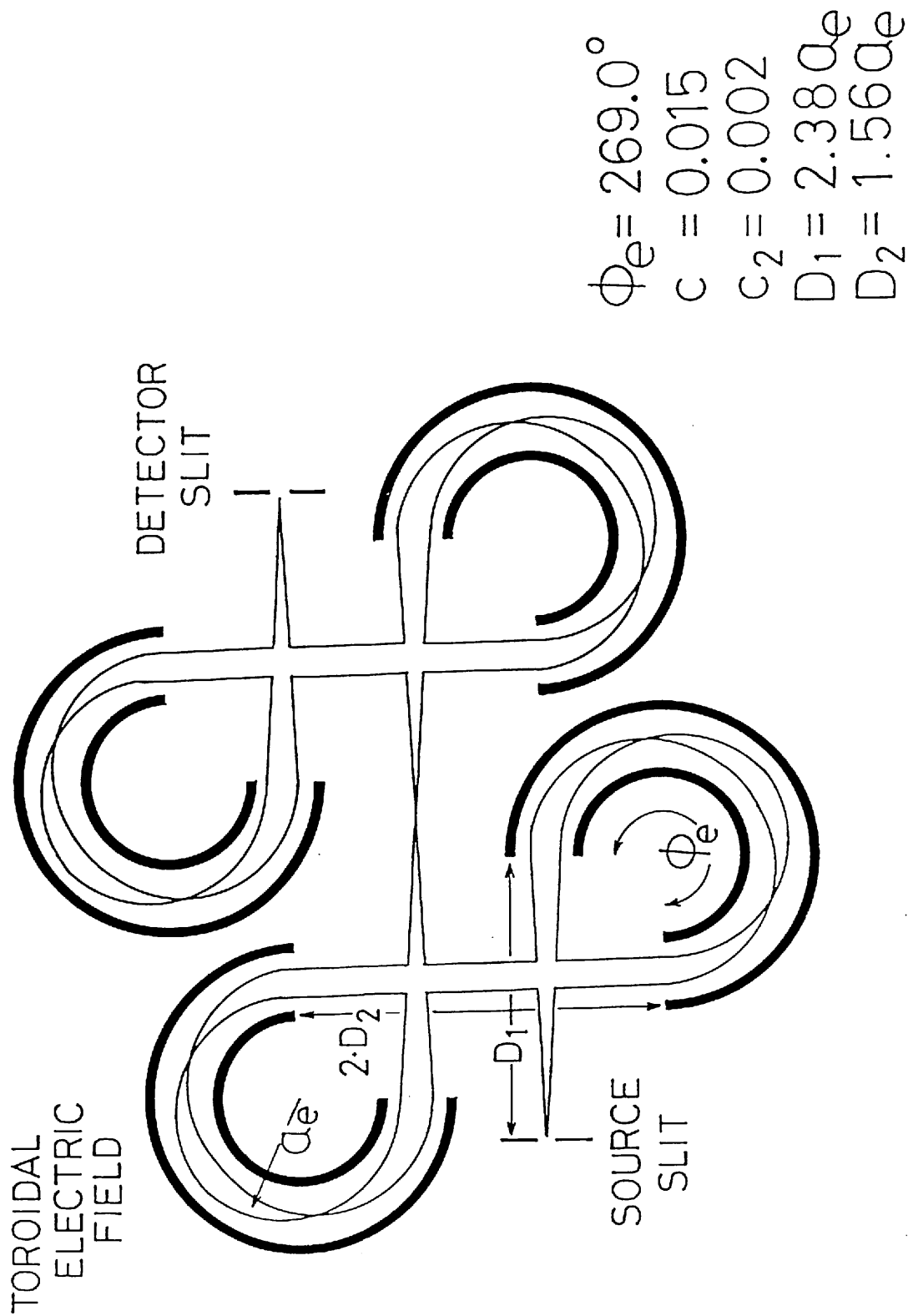
Fig. 3 – 12. Schematic drawing of the doubly symmetrical TOF system with $\phi_e = 269°$.

REFERENCE

3-1. H. Wollnik and T. Matsuo, Int. J. Mass Spectrom. Ion
     Phys., <u>37</u> (1981) 209.

4. CONSTRUCTION OF THE NEW TIME-OF-FLIGHT MASS SPECTROMETER

4-1. Introduction

In the previous chapter, the ion optics of TOF mass spectrometers consisting of electric sectors was studied. In the search for a high performance TOF system, symmetrical arrangements of toroidal electric sectors were introduced. The consideration of symmetrical alignment into the system can reduce the difficulty of an exhaustive inquiry. As the results of the investigation show, many ion-optical designs of TOF mass spectrometers which satisfy the triple isochronous and triple spatial focusing were found. These TOF systems can be theoretically expected to exhibit both high resolution and high transmission. The ion-optical system for an excellent TOF mass spectrometer which consists four toroidal electric sectors with 269° deflection was proposed. The four sector system has good characteristics of both ion optical consideration of the higher-order coefficients, and practical size of the geometrical figure, as well as the multiple focusing conditions. In order to confirm the theoretical prediction, a TOF mass spectrometer which has 1.7m flight path length was constructed. The ion optical characteristics of the system were examined experimentally. The technical data of the construction are reported in this chapter.

4-2. Whole assembly

We adopted the mean radius of toroidal fields, a_e, to be

5cm. From the multiple focusing conditions, two drift lengths are determined to be $D_1 = 11.9$cm and $D_2 = 7.8$cm. The total flight path length is 1.727m, while the diameter of the vacuum chamber is only 41cm. The physical parameters and the aberration coefficients of the system are given as D' in Table 3-4. A schematic diagram of the whole apparatus is shown in Fig. 4-1. The four electric condensers were fixed by screws on the base plate of the circular vacuum chamber (41cm diameter, 13cm height). The vacuum chamber was evacuated through a 10cm diameter hole at the center of the base by a 4 inch oil diffusion pump. The vacuum in the system was maintained at 1×10^{-6} Torr. Aluminum beam guides were attached along all ion paths of the drift regions in order to eliminate the effect of any stray electric field from the condenser electrodes. The guides were grounded and their aperture was 10mm×20mm. A commercial 16-stage Be/Cu secondary-electron-multiplier was used as the ion detector, and was shielded in order to eliminate stray electrons or ions. A photograph of the inner part of the apparatus is shown in Fig. 4-2.

4-3. Toroidal electric field

In the proposed TOF mass spectrometer, the toroidal electric field ($c=0.015$, $c_2=0.002$) is required from the ion-optical design. This time, the toroidal field was produced using a cylindrical condenser terminated with Matsuda plates, which was proposed by Matsuda [4-1] to change the focus of the electric sector. The cross-sectional view of the electrodes of the condenser and Matsuda plates is shown in Fig. 4-3. This
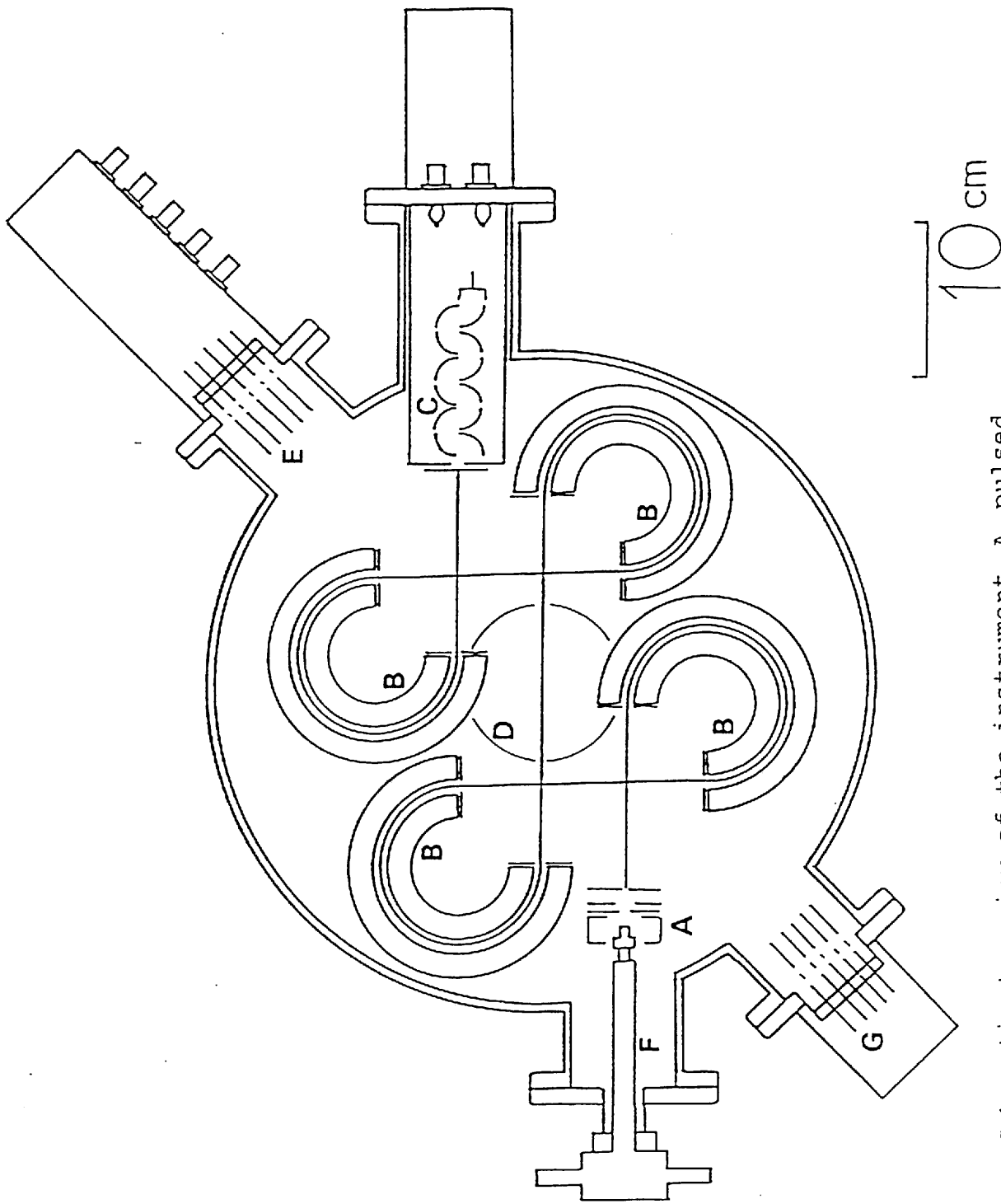
Fig. 4-1. Schematic top view of the instrument. A, pulsed ion source; B, cylindrical condensers with Matsuda plates; C, ion detector; D, vacuum chamber pumping port; E, inlet of electric power for condenser electrodes; F, sample probe for SIMS analysis; G, inlet of electric power for ion source.
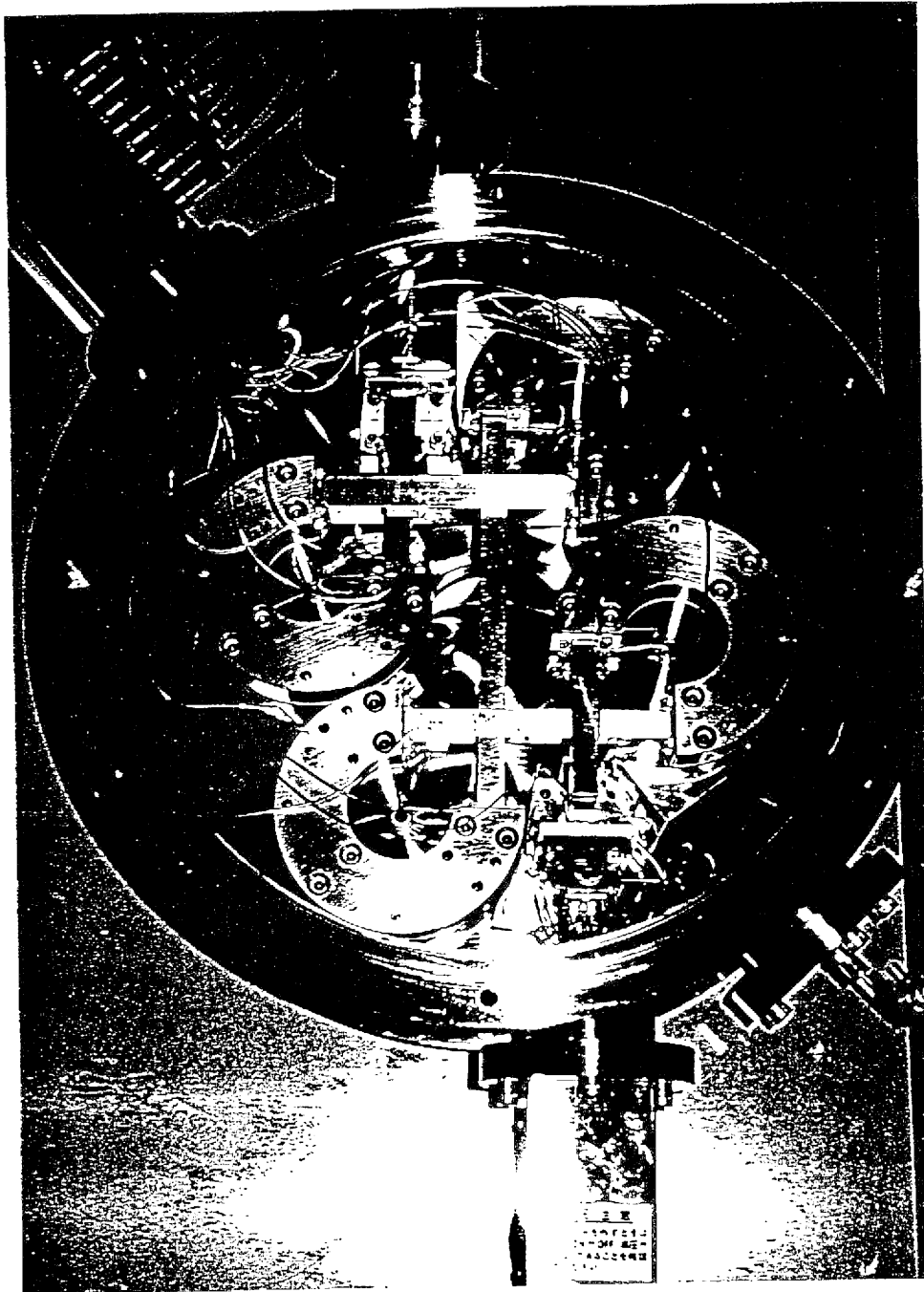
Fig. 4-2. A photograph of the inner part of the vacuum chamber.
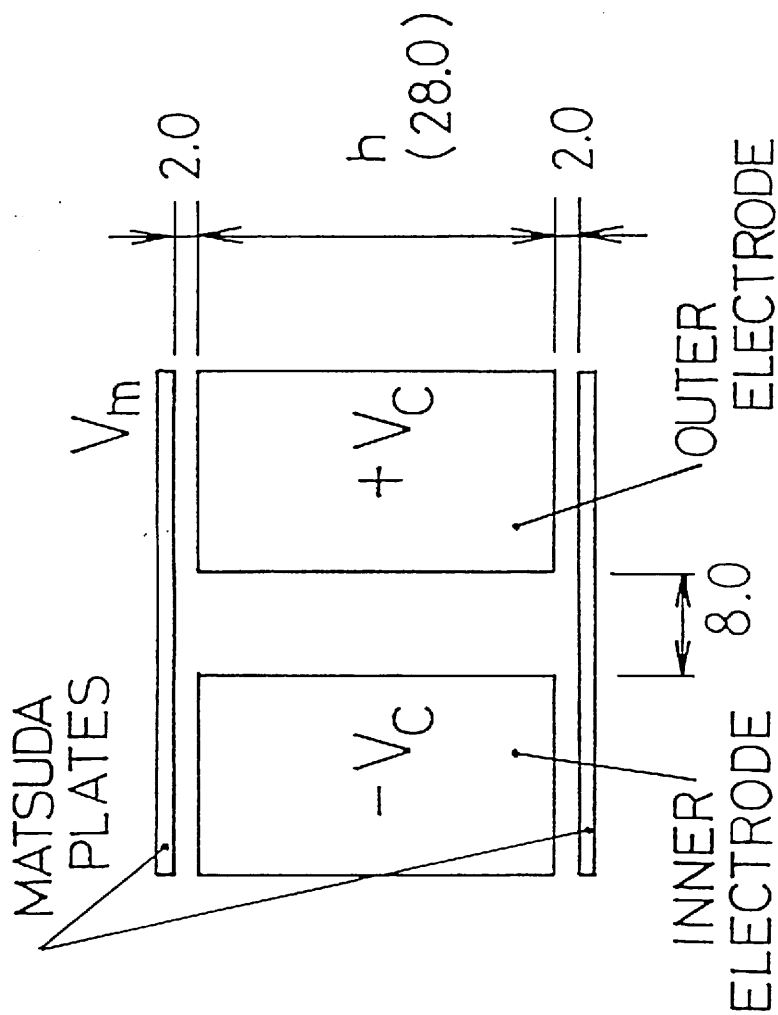
Fig. 4 - 3. Cross-sectional view of the cylindrical electrodes and Matsuda plates. V_m, Voltage applied to the Matsuda plates; V_c, voltage applied to the cylindrical electrodes; h, height of the cylinders.

configuration has two merits compared to the usually used toroidal condenser:

1.) The focal length of the electric sector can be easily changed by varying the applied voltage to the Matsuda plates, because the value of the field index, c, is adjusted electrically.

2.) The shape of the toroidal condenser is so complicated, the surface of the electrodes are special curve in three dimensional space. Therefore, a special machine, for instance numerically controlled, is needed to produce the electrode. However, the cylindrical condenser has a simple shape, and can be easily manufactured on an ordinary lathe.

In order to determine the dimensions of the electrodes, an electric field produced with the condenser and Matsuda plates was calculated by a computer simulation program reported by Matsuda et al. [4-2]. The field indices, c and c_2, of the toroidal field can be adjusted by changing the potential, V_m, applied to the Matsuda plates and the height, h, of the condenser electrodes. In the calculation, a mean radius of 5cm and a gap distance of 8mm were assumed in the cylindrical condenser. The relationship between V_m and h, which gave c=0.015 and c_2=0.002, was obtained and this is shown in Fig. 4-4. From this figure it was determined that h=28mm and V_m=0.13V_c, where V_c was the potential of outer electrode of the condenser. In the case of an acceleration voltage of 3kV, ±480V and 62V should be applied to the electrodes of the
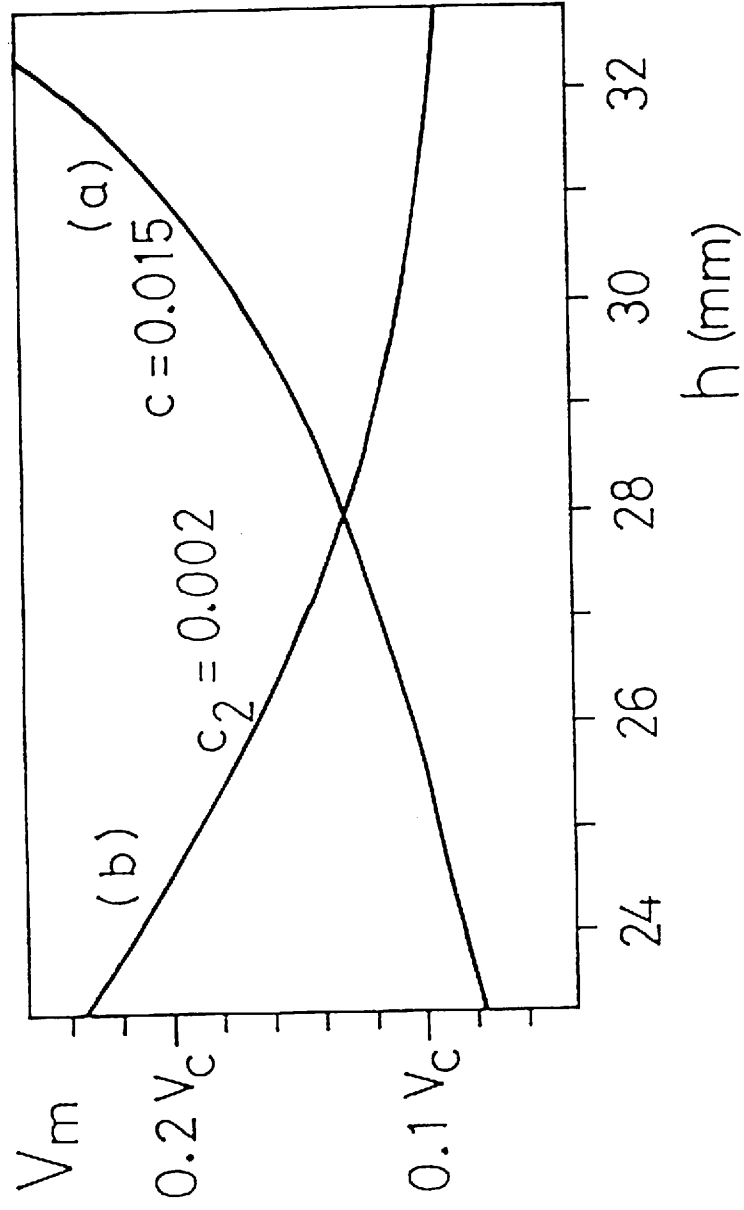
Fig. 4 – 4. Relationship between the height of condenser electrodes, h, and the voltage applied to Matsuda plates, V_m, for (a) $c=0.015$ and (b) $c_2=0.002$. The h and V_m are determined to be 28 mm and 0.13 V_c, respectively.

cylindrical condenser and Matsuda plates, respectively. At the
fringes of the condenser, Herzog shields were placed, so that
the ideal field boundaries can coincide with the front faces of
the cylindrical electrodes. The distance between the shield
and the electrode was 1mm and the aperture of the shield was
5.8mm×20mm.

4-4. Time measuring system

The precise measurement of the flight times of an ions is
needed for high resolution TOF mass spectrometry. The fast
electric circuits were developed in the field of the experimen-
tal research of nuclear physics. This advanced technological
apparatus is introduced into our TOF mass spectrometer.

A schematic diagram of the time measuring circuits is
shown in Fig. 4-5. An oscillator triggers a delay generator
which suitably adjusts the timing for the 'start' signal. The
oscillator also provides a trigger pulse for the pulse gener-
ator of the ion source. The produced ion is immediately ex-
tracted by the constant potential on the drawing-out plate from
the ion source. After traveling in the analyzer, the ion is
detected by the secondary-electron-multiplier and a pre-
amplifier. The output signal is sent to a fast amplifier and
then to a constant-fraction discriminator. The output of the
discriminator acts a 'stop' signal. The time interval between
'start' and 'stop' signals is converted into an analog output
by a time-to-pulse-height converter. The output is digitized
and is accumulated in a multi-channel analyzer. The TOF mass
spectra are analyzed by a small computer and are stored on
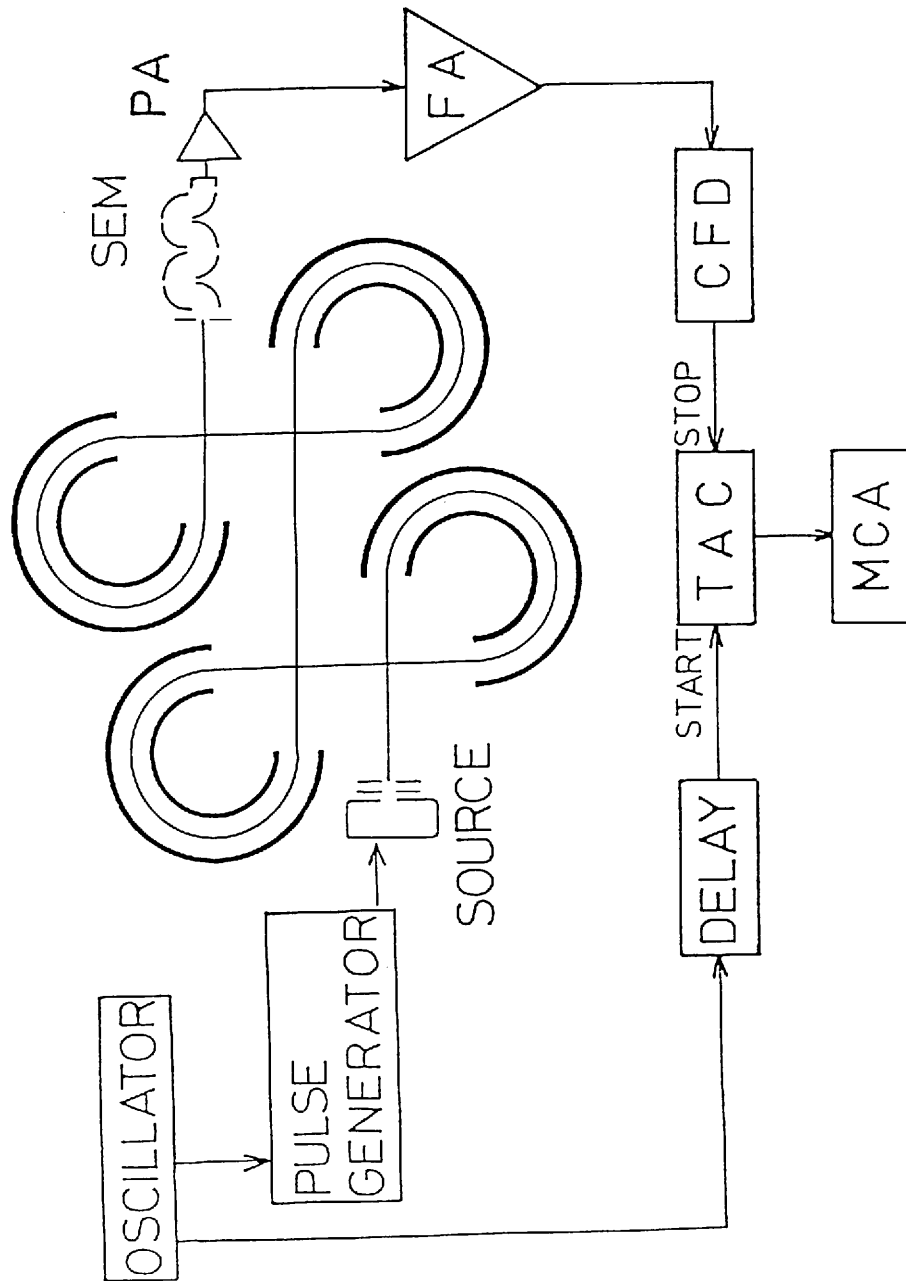
Fig. 4 – 5. Block diagram of the pulse operation and time measuring system, SEM, secondary-electron-multiplier; PA, pre-amplifier; FA, fast amplifier; CFD, constant-fraction discriminator; TAC, time-to-pulse-height converter; MCA, multi-channel analyzer.

floppy disks.

4-5. <u>Ion sources</u>

In a TOF mass spectrometer, pulsed operation of the ion source is indispensable. The time period of the operation is significant in the resolution of TOF mass spectra.

Two types of ion sources were used in this TOF mass spectrometer. Firstly, an electron impact type (EI) ion source was used for the preliminary experiments. In this source, a gaseous sample in the ionization chamber is ionized by a electron beam. The energy of the electron is typically around 70eV. The pulse operation of EI ion source is shown schematically in Fig. 4-6. The grid electrode, which is located between the filament and the ionization chamber, is usually kept at a negative bias for stopping the invasion of the electron beam. The pulse generator, which is floating at a potential near the acceleration voltage, is operated by the trigger pulse from the oscillator through a photo coupler. The pulse generator provides a short positive pulse to the grid electrode. The sample gas is thus ionized in short duration by the pulsed electron beam.

Fig. 4-7 shows, schematically, the second ion source used, that for secondary ion mass spectrometry (SIMS) of large molecules. In the secondary ion source, a primary ion beam with a few keV energy collides with sample species, the sample is thus ionized. In our TOF mass spectrometer, the primary ion beam is injected from the upper part of the analyzer chamber. Now two spherical condensers are introduced into the primary ion gun.
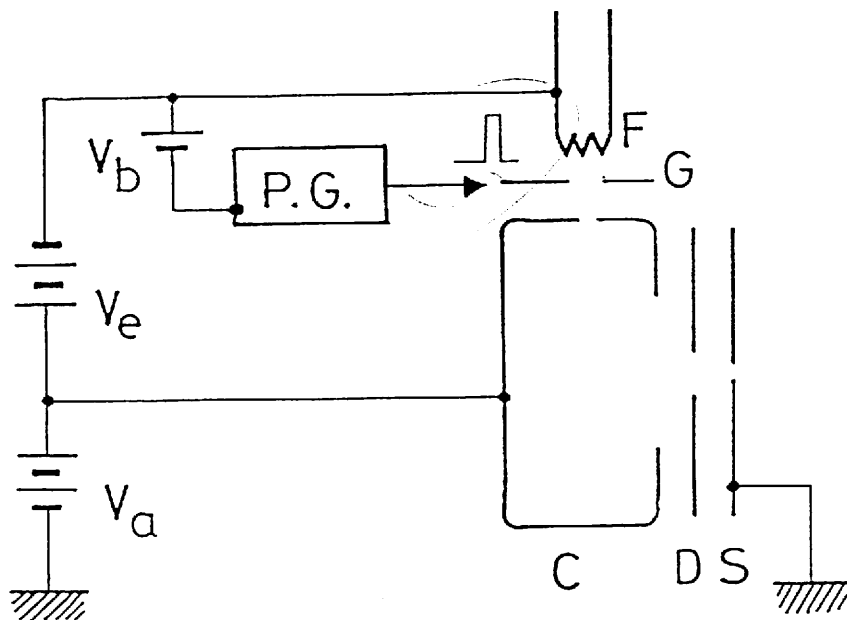
Fig. 4 - 6. Schematic diagram of the pulse operation
of the electron impact type ion source.
P.G., Pulse generator; F, filament; G, grid
electrode; C, ionization chamber; D, drawing-
out plate; S, source slit; V_a, acceleration
valtage of ions; V_b, bias voltage for grid
electrode; V_e, electron energy.
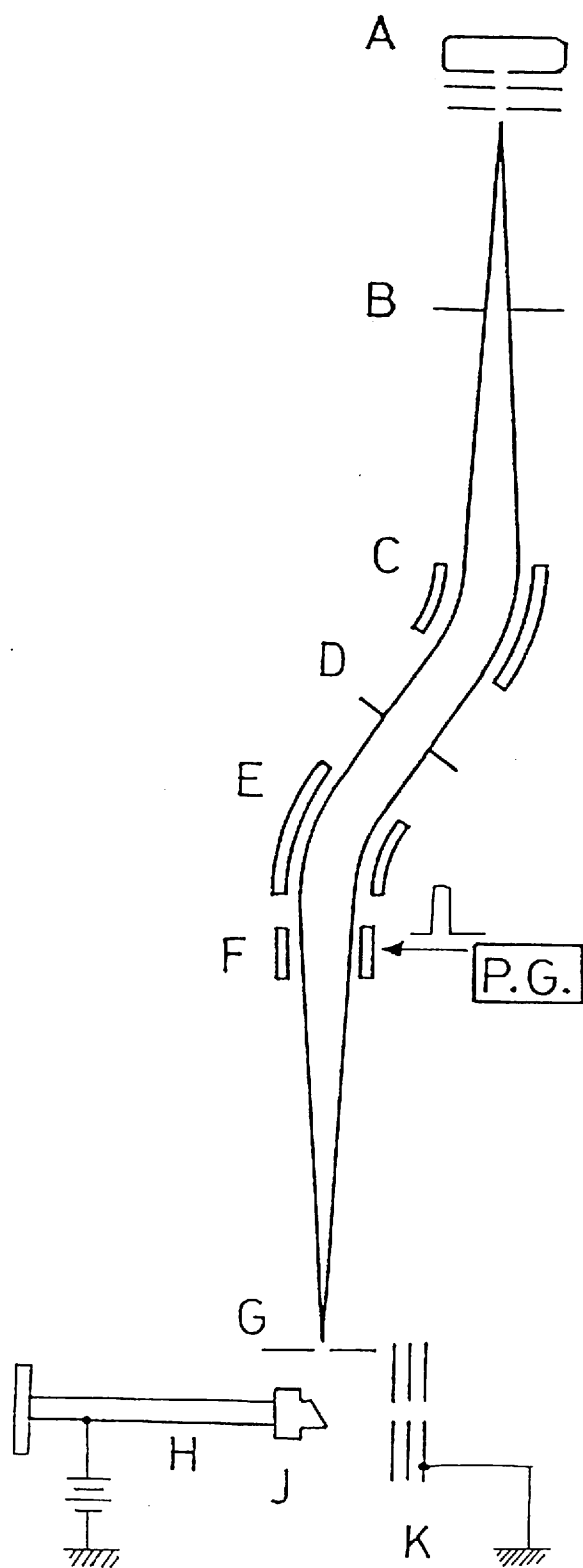
Fig. 4 - 7.   Schematic drawing of the primary ion gun and
pulse operation of the secondary ion source
for SIMS analysis. A, primary ion source;
B and D, collimating slits; C and E, spherical
condensers; F, deflection plates; G, defining
slit; H, sample probe; J, sample tip; K,
secondary ion source; P.G., pulse generator.

The ion beam is focused at the defining slit located near the sample tip by the spherical condensers. It is swept rapidly by a voltage pulse of the pulse generator applied to the deflection plate. Therefore, the primary ion beam can pass through the defining slit for only a short period, and attack the sample tip. The angle of incidence of the primary beam and that of ion extraction are 60° and 30°, respectively. The neutral atoms which cause the background interference in the TOF spectra are eliminated by the condensers in the primary beam. The vacuum chamber of the primary ion gun is 15cm diameter and 30cm height. The chamber is evacuated by a 6 inch oil diffusion pump with a liquid nitrogen trap. The sample probe was also attached to the analyzer chamber. A differentially pumped vacuum lock was used for the sample probe in order to avoid violation of the vacuum during sample exchange. A photograph of the TOF mass spectrometer with the primary ion source is shown in Fig. 4-8.
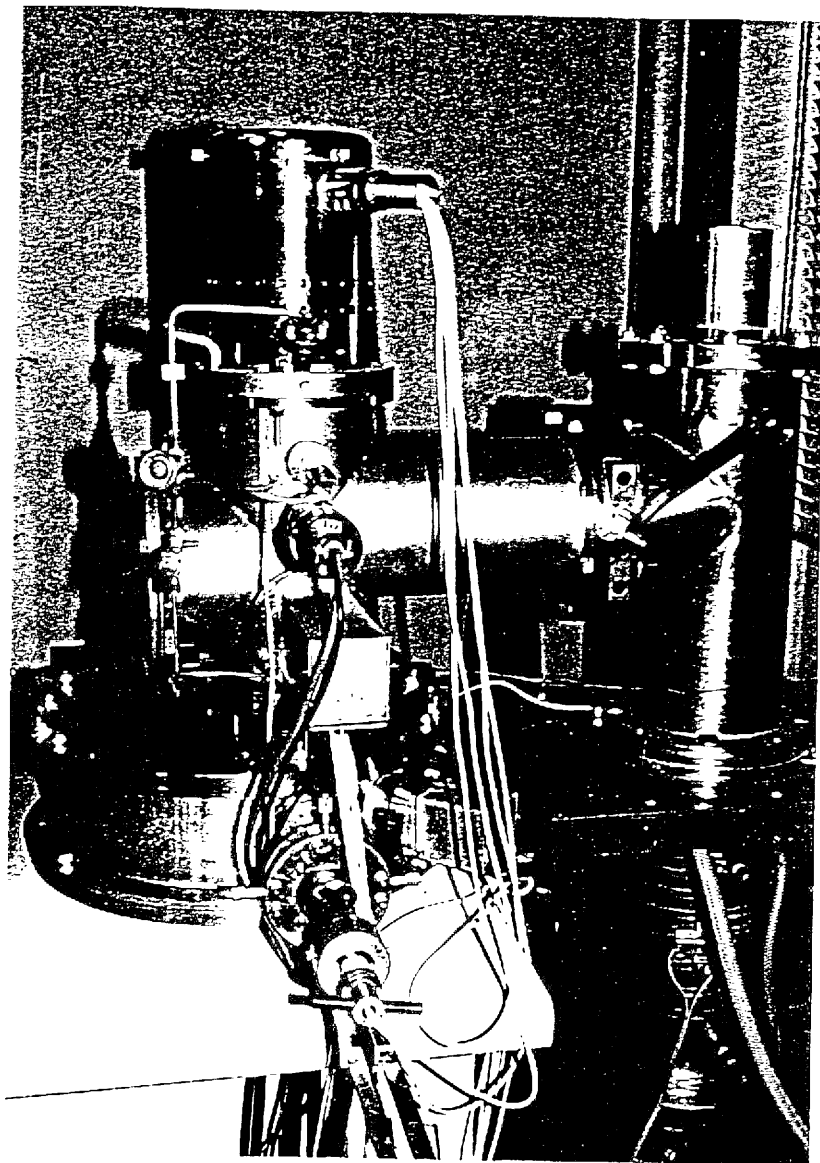
Fig. 4-8. A photograph of the profile of the TOF mass
spectrometer with primary ion gun for SIMS.

REFERENCES

4-1. H. Matsuda, Rev. Sci. Instrum., 32 (1961) 850.

4-2. H. Matsuda and Y. Fujita, Int. J. Mass Spectrom. Ion Phys., 16 (1975) 395.

5. PERFORMANCE AND RESULT

5-1. Mass resolution of the new TOF mass spectrometer

The mass resolving power, $M/\Delta M$, of TOF mass spectrometer is theoretically studied in Chapter 3, and is given in Eqs. 3-2 and 3-3 rewriting:

$$\frac{M}{\Delta M} = \frac{T_f}{2\Delta t}$$

$$= \frac{L_f}{2(\ell_f + v_0 t_0 + v_0 t_d)} \qquad (5-1)$$

Three terms in the denominator of Eq. 5-1 should therefore be kept small to obtain high resolution in the system. These are:

1.) ℓ_f, the path length deviation of the system;
2.) t_0, the duration of the pulse operation of the ion source;
3.) t_d, the time resolution of the detection system.

In order to minimize the path length deviation, ℓ_f, four toroidal electric sectors are introduced into the analyzing region, such that triple isochronous focusing is theoretically achieved. Ions with different energies and different initial conditions can be coincidentally focused at the detector.

Considering the duration of the pulse operation of the ion source, we can estimate it by three functions:

1.) The pulse time of the electron (or primary ion) beam used for ionization.

2.) The reaction time during ionization.

3.) The time consumed by ion extraction, T_{ext}.

The time duration of the electron (or primary ion) beam is restricted by the time width of the pulse generator. The pulse width was around 15ns (full width at half maximum, FWHM) in the case of the pulse generator used for the EI ion source, and about 5ns in the case of the pulse generator used for the primary ion gun for SIMS.

The reaction time during ionization is considered to be less than 1ns.

The ion extraction time, T_{ext}, which is the time used for the movement of a stationary ion at birth to the drawing-out plate, is estimated as:

$$T_{ext} = 144 \times d_{ext} \left(\frac{M}{Z V_{ext}} \right)^{\frac{1}{2}} \quad (ns)$$

(5-2)

where d_{ext} (mm) is the distance between the ionizing point and the drawing-out plate, V_{ext} (volt) is the potential difference between the voltage of the ionization chamber and that of the drawing-out plate, M (dalton) and Z (e) are mass and charge of an ion, respectively. From this equation, in the case of $d_{ext}=5mm$, the relationships between the extraction voltage, V_{ext} and extraction time, T_{ext}, for a nitrogen ion (M/Z=28) are calculated in Table 5-1. In a real ion source, a spatial deviation of the ionizing position exists. Furthermore, a

spread of the initial kinetic energy distribution caused by the ionization process also exists. These cause a time deviation in the ion extraction time, so the ion peak is already broad at the entrance slit of the analyzer, before the flight through the system.

Table 5-1.
Variation of the ion extraction time, T_{ext}, calculated from in Eq. 5-2, for nitorogen ion (M/Z=28) with extraction voltage, V_{ext}, where the length of the extraction region, d_{ext}, is 5mm.

V_{ext} (volt)	T_{ext} (ns)
10	1200
20	850
50	540
100	380
200	270
300	220
500	170
1000	120

The variation of the time width of the mass peaks in the TOF mass spectra was measured by using an EI ion source, changing the extraction voltage, V_{ext}. The time widths (FWHM) of the nitrogen ion peak (M/Z=28) in TOF mass spectra are plotted vs. V_{ext} in Fig. 5-1 . From interpolation of this figure, the peak width decreases in proportion to $1/\sqrt{V_{ext}}$, thus, high voltage extraction can reduce the time difference at ion extraction. However, in the case of the EI source, the ionization was strongly inhibited for the high extraction voltage larger
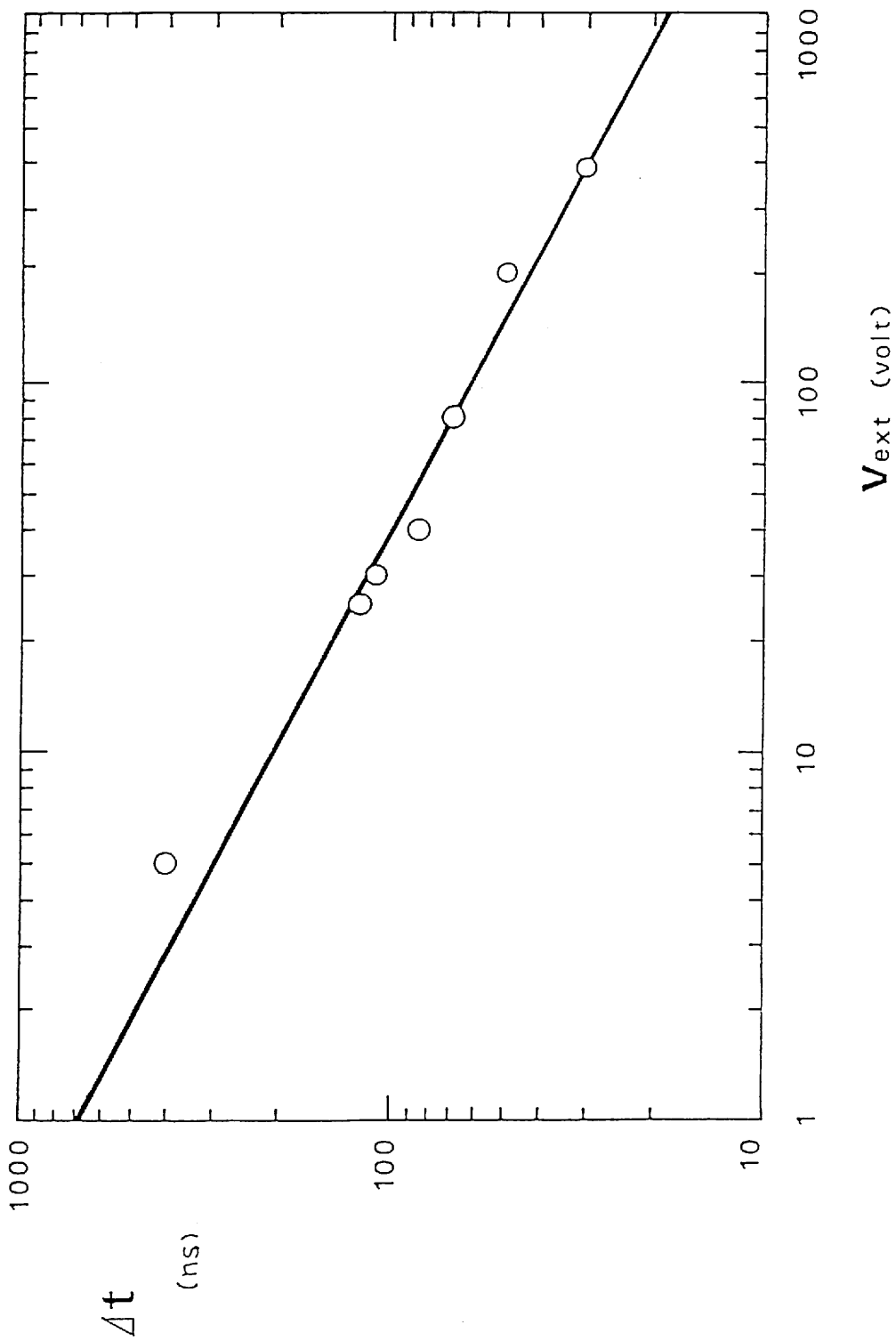
Fig. 5 – 1. Variation of the time width of nitrogen ion peak in TOF mass spectra with the extraction voltage.

than 300V. The reason is that a high voltage generates a strong electric field in the ionization chamber which has a detrimental effect on the electron beam. From Fig. 5-1, the deviation of the ion extraction time is estimated to be about 10% of T_{ext}.

Next, the time resolution in the measuring system, t_d, is considered. Adjustment of the gain and shaping of the amplifier, and the threshold level of the discriminator, can be possible to restrict the time resolution in the detection system to 2ns. The resolution of the time-to-pulse-height converter (TAC) is 0.01% of the measuring time range, and the full range of it can be changed to up to 800μs. Therefore, the resolution is 10ns in the case of a time range of 100μs, and is 100ps in the range of 1μs. On the other hand, the A-D converter of the multi-channel analyzer (MCA) must digitize the output of the TAC to 2048 channels. Therefore, the time channel width of MCA is 50ns for 100μs TAC range and 500ps for 1μs range.

When the precise investigation of a specific range of a TOF spectrum is required, a suitable delay for the start signal of the TAC is used. A precise delay generator, which is capable of producing dozens of micro-seconds delay, is also available as a standard nuclear circuit. The time resolution of such a delay generator is about 1ns. Consequently, the time

resolution in the time measuring system in the measurements of around 100μs, is considered to be less than 5ns when the delay generator is used.

An example of the TOF mass spectrum of xenon using the EI ion source is shown in Fig. 5-2. Experimental conditions were as follows: acceleration voltage, 3kV; filament current, 4.5A; electron energy, 78eV; peak electron current, 300μA; frequency of oscillator, 20kHz; effective pulse width (FWHM), 15ns; ion extraction voltage, 280V; TAC time range, 4μs; start delay, 25μs; time channel width, 1.7ns; accumulation time, 100s: In the TOF mass spectrum, the isotopes of xenon can be clearly seen with good S/N ratio. The flight time of xenon 132 was 26.07μs, and a peak width (FWHM) of 18ns was obtained for this isotope. This value corresponds to a mass resolution of 730.

The value for the path length deviation must be estimated to give a full appraisal of the system. We take a TOF mass spectrum, and measure the time width of a known ion peak (in this case, Xe[132]) after moving through the whole system. A similar measurement is done, but placing the detector at the exit of the ion source, where the flight path is minimal, thus minimizing, ℓ_f. The peak width here was 17ns compared to that of 18ns for a ion that has passed through the whole analyzing region.

We can summarize the information as follows;
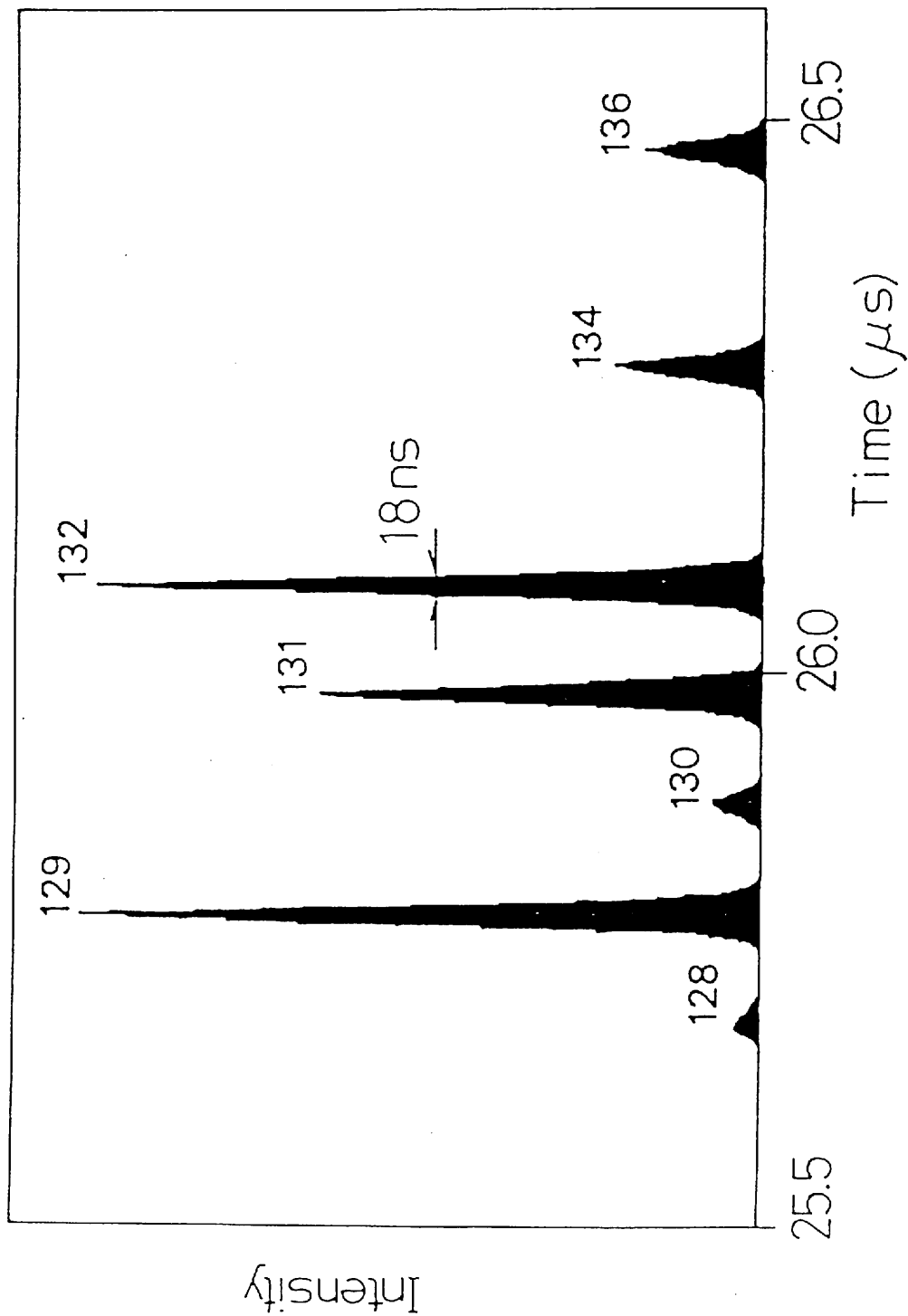
Fig. 5 - 2. TOF mass spectrum of xenon isotopes. The accelerating voltage, 3 kv; source slit 1 mm; maximum horizontal and vertical aperture angles, ±0.01 rad. The peak width of 18 ns corresponds to the mass resolution of 730.

1. the resolvable time width $\Delta t = \ell_f / v_0 + t_0 + t_d$,

2. t_0 is estimated to be < 15ns,

3. t_d is estimated to be < 5ns,

4. $\Delta t = 18$ns is obtained in xenon spectrum after traveling the analyzer,

5. $\Delta t = 17$ns is obtained by xenon at the exit of the ion source.

In the case of no flight in the analyzer, we can assume $\ell_f = 0$, so that $\Delta t = t_0 + t_d$. Comparing the result of 4 and 5, the time aberration caused by path length deviation in the analyzer can be seen to be small compared to the overall time aberration observed (18ns). This suggests that the first-order isochronous focusing is achieved and that higher-order aberrations are reasonably small.

Table 5-2.
Variation of mass resolution, $M/\Delta M$, with M/Z, in case of resolvable time width $\Delta t = 20$ns, flight length 1.7m, acceleration voltage 3kV.

M/Z	$M/\Delta M$
1	60
10	180
50	400
100	570
200	800
500	1300
1000	1300
2000	2500
3000	3100
4000	3600
5000	4000
10000	5800

The flight time, T_f, increases with an increment in the mass of ion. From Eq. 5-1, even though the same values of the resolvable time width, Δt, are obtained in different mass regions, the mass resolution increases with the mass. In case of $\Delta t = 20$ns, flight length 1.7m and acceleration voltage 3kV, the variation of the mass resolution with mass to charge ratio are given in Table 5-2.

An example of a TOF spectrum of a region of greater mass to charge ratio is shown in Fig. 5-3 (b). The peaks shown are the quasi-molecular ions of gramicidin-S (M.W.=1140.7) which are produced in the SIMS analysis. Experimental conditions were as follows: Primary ion beam, Ar^+, 10keV; frequency of oscillator, 5kHz; TAC time range, 8µs; start delay, 70µs; time channel width, 3.7ns; accumulation time 500s: The flight time of M/Z=1141.7 ions is 76.71µs. A time width of 19ns (FWHM) was obtained. This corresponds to a mass resolution of 2,000.

5-2. Ion transmission of the TOF mass spectrometer

Triple spatial focusing is demanded in the ion-optical design of the constructed TOF mass spectrometer, in order to increase the ion transmission efficiency. Ions with a wide-spread solid angle and energy distribution can be focused at the detector, and pass through the detector slit by the spatial focusing property of the electric sectors. A toroidal electric field, by which an ion beam diverging off the median plane can return to the detector, was adopted. As discussed in Chapter 4, the toroidal sector was produced by the combination of the cylindrical condenser and Matsuda plates. The c-value of the

(a)

(b)

[M+H]$^+$

19ns

1141.0   1142.0   1143.0   1144.0

M/Z
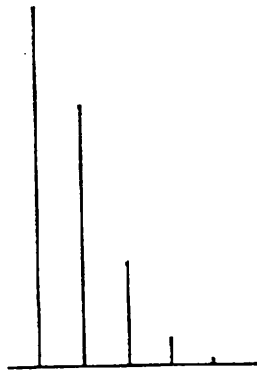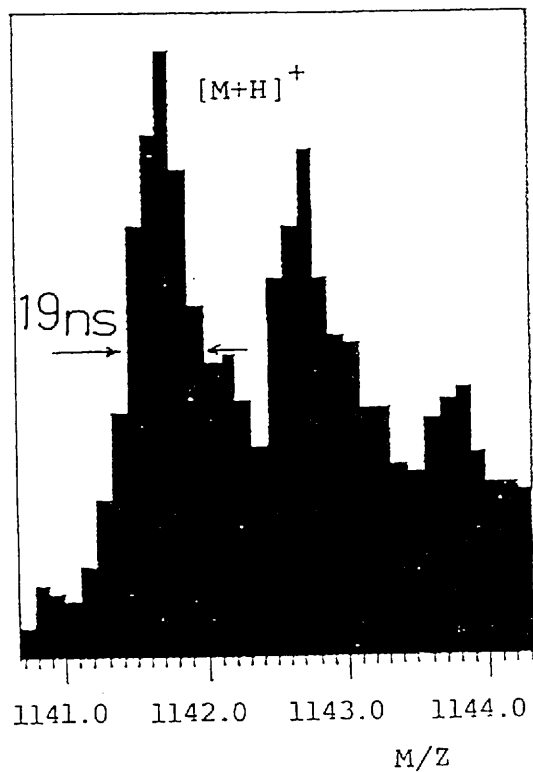
Fig. 5 - 3.   a) Mass distribution of the molecules of
gramicidin-S.

b) Molecular ion region of SIMS-TOF mass
spectrum of gramicidin-S. The time
width of 19 ns corresponds to the mass
resolution of 2,000.

toroidal field can be varied by changing potential applied to Matsuda plates. In the case of the structure of this electrode, the relationship between the c-value of the toroidal field and the applied voltage, V_m, were calculated by the computer simulation [4-2]. The results are shown in Fig. 5-4. The case of c=0 means a pure cylindrical field. For the designed value c=0.015, 13% of the potential of the outer electrode is demanded for V_m. For the case of 3kV ion acceleration, the voltage of the Matsuda plates corresponds to 62V.
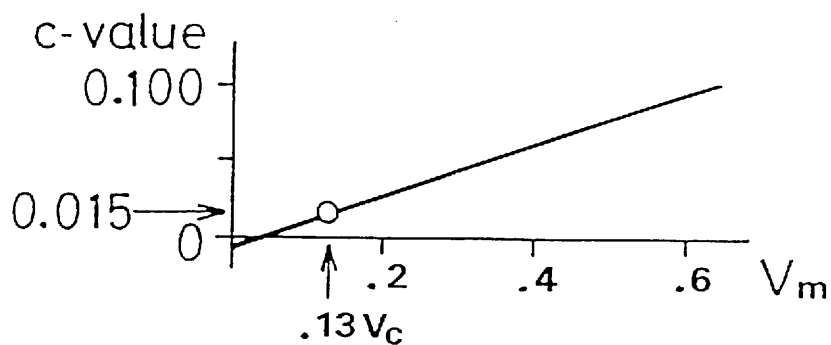
Fig. 5 - 4. Variation of c-value of the toroidal electric field with voltage of the Matsuda plates.

The effect of the potential of the Matsuda plates to the ion transmission efficiency is measured experimentally. The way of the experiment is as follows:

The EI source was used in continuous operation mode. The acceleration voltage was 3kV. The width of the source slit was

1mm and the maximum horizontal and vertical aperture angles were ±0.01rad. At the position of the detector, a faraday cage was used instead of the secondary-electron-multiplier. The quantity of the ions, which passed through the four condensers and reached to the faraday cage, was directly measured as an ion current by an electrometer. On the other hand, the quantity of the extracted ions just after leaving the ion source was also measured by using the first condenser as a faraday cage. The ratio of the two ion currents is defined as the ion transmission efficiency of the TOF mass spectrometer.

The results are shown in Fig. 5-5. It is clear from the figure that the ion transmission efficiency increases to 90% around V_m=60V while it is only 40% for V_m=0 (no use of the Matsuda plates). This voltage is in good agreement with the designed one (62V). The ion transmission of 90% indicates that the spatial focusing is satisfactory.

5-3. Mass calibration of TOF mass spectra

In mass spectrometry, accurate calibration of a mass to charge ratio scale is indispensable. Because time-of-flight mass spectrometry directly measures the flight time of an ion, the mass to charge ratio can be easily derived from using the relation expressed by Eq. 2-3, rewriting:

$$T_f = 72.0 \ L_f \ (\frac{M}{Z \ V})^{\frac{1}{2}} \qquad (\mu s) \qquad\qquad (5-3)$$

ION
TRANSMISSION
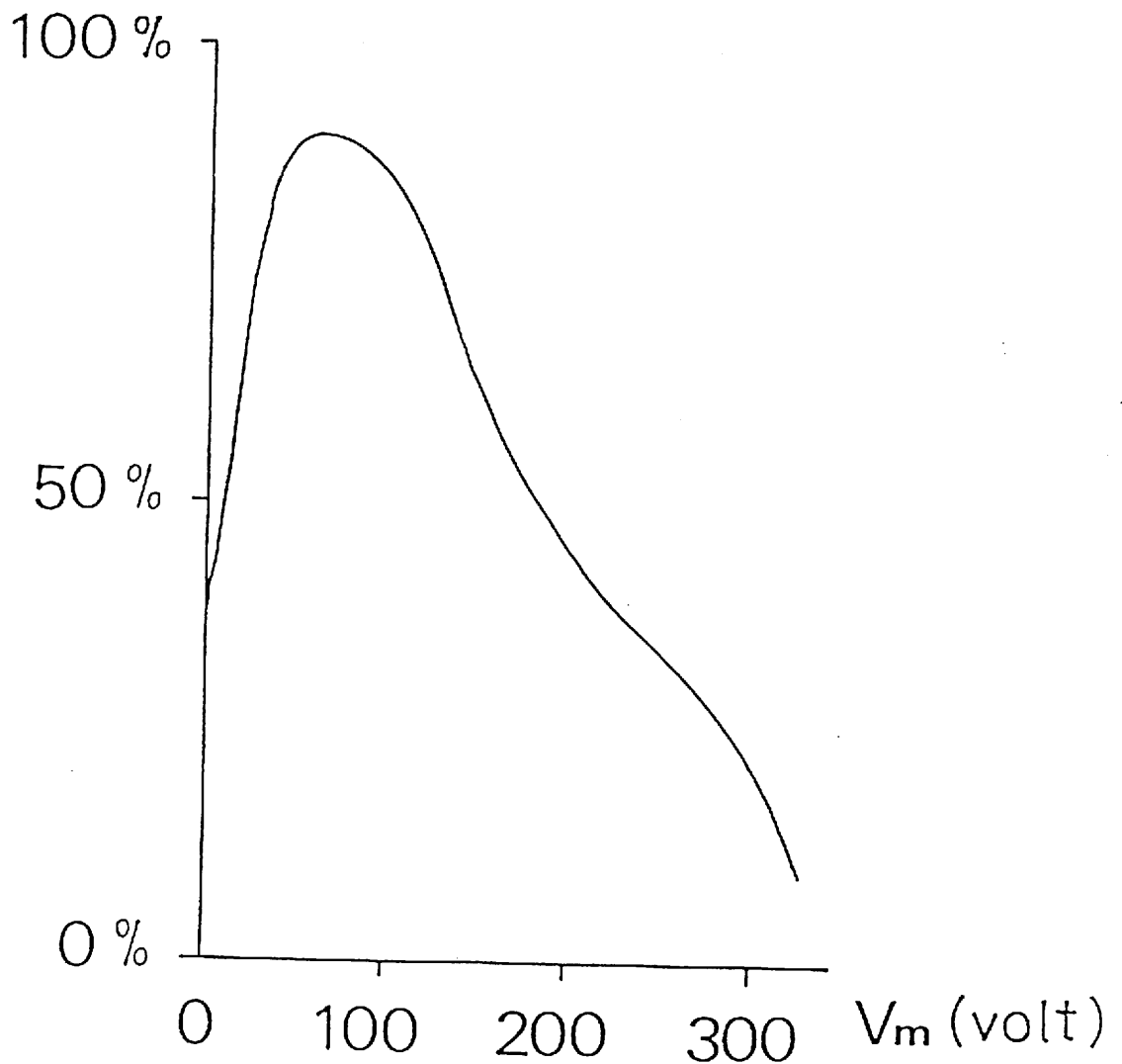
Fig. 5 - 5.   Variation of the ion transmission efficiency with
the voltage on the Matsuda plates.   Ion acceleration
voltage, 3 kV; source slit width, 1 mm; maximum
horizontal and vertical aperture angles, ±0.01rad.
An ion transmission of 90 % was obtained around
$V_m = 60$ V.

The principle of the mass calibration is as follows. The flight length, L_f, and the acceleration voltage, V, in Eq. 5-3 are constants for any ion. The channel number in the multi-channel analyzer (MCA) is proportional to the measured time. The origin of the channels does not usually coincide with the start point of the time-of-flight measurement. Therefore, if the number of the N-th channel is expressed as N, the relationship between the N and M/Z obtained from Eq. 5-3 is:

$$N = K \left(\frac{M}{Z}\right)^{\frac{1}{2}} + N_0$$

$$(5-4)$$

where K is the proportionality constant related to the flight length, the acceleration voltage and time channel width of the MCA, and N_0 corresponds to the origin of the TOF spectrum. From Eq. 5-4, only two constants, K and N_0, are need to be determined for mass calibration. Therefore, at least two standard points are necessary in order to determine K and N_0. After determination, the mass to charge ratio of the unknown peak obtained at the channel number N_{exp} is calculated as:

$$\frac{M}{Z} = \frac{(N_{exp} - N_0)^2}{K^2}$$

$$(5-5)$$

The accuracy and linearity of the time measuring system is very precise. Therefore, the accurate mass value can be predicted, even if the observed mass is far from the calibration region. In our experiment, a few standard points were

used for calibration to increase the accuracy. The two constants, K and N_0, were determined by the method of least squares by using these points.

The standard points are given by the use of either an internal standard or an external standard. The internal standard is utilized by the known peaks in the TOF mass spectrum that of the sample of interest, for instance the peak of a proton (M/Z=1.0078), that of a sodium ion (M/Z=22.990) and etc.. The external standard method uses the spectrum of a standard sample for the calibration that is independently taken under identical conditions of the unknown sample.

5-4. <u>Analysis of large molecule</u>

The possibility of the analysis for large molecules by the TOF mass spectrometer has been investigated. The pulsed primary ion gun for SIMS was developed. A detailed description of the primary gun has already been given in Chapter 4. The sample tip was made of copper, and its stage was coated with gold. The diameter of the sample stage was 2mm. In SIMS analysis for normally intractable compounds, the aid of a suitable liquid matrix is usually employed. In this case, glycerol was used as a matrix. Several compounds were then investigated by the TOF mass spectrometer.

The common conditions of these experiments are as follows. The species of the primary ion beam was argon, and its energy was 10keV. The ion current of the primary ion beam was 10-100nA in continuous operation mode. The duration time of the

ion gun was 5-10ns, and the frequency was 5kHz, The accelera-
tion voltage for secondary ions was 3kV. In the secondary ion
source, the extraction voltage was established at 1000-1500V,
in order to decrease the time spread at the ion extraction
even for heavier ions. The cluster ions of cesium iodide,
$[CsI]_n Cs^+$, were used as an external standard for mass
calibration.

A hepta-peptide, angiotensin-III, was used as sample com-
pound and its structure is shown in Fig. 5-6. The molecular
weight of the mono-isotopic angiotensin-III is 930.5 dalton.
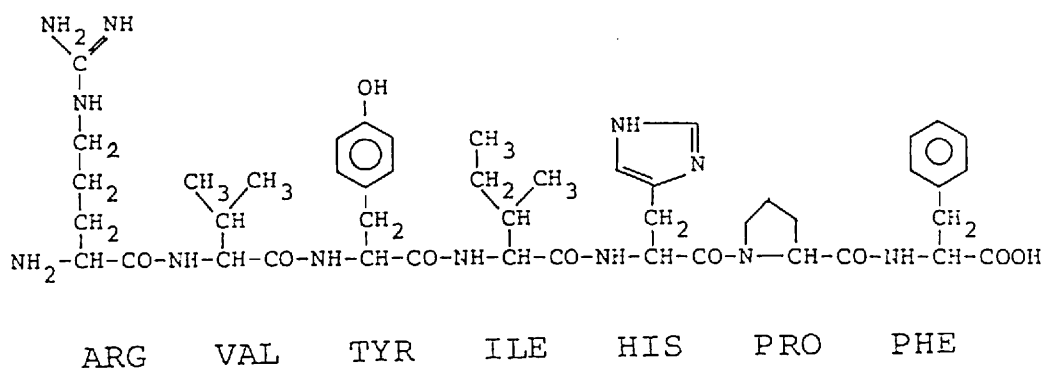
Fig. 5-6. The structure of angiotensin-III. The
molecular weight of the mono-isotopic
angiotensin-III is 930.5 dalton.

The sample was purchased from the Protein Research Foundation
(Minoh, Osaka, Japan). The full scale of the TAC was 80μs. No
delay time used for the TOF measuring start. The accumulation
time was 100s. The measuring time range was 0-80μs cor-
responded to the mass range of 0-1200. The SIMS-TOF mass
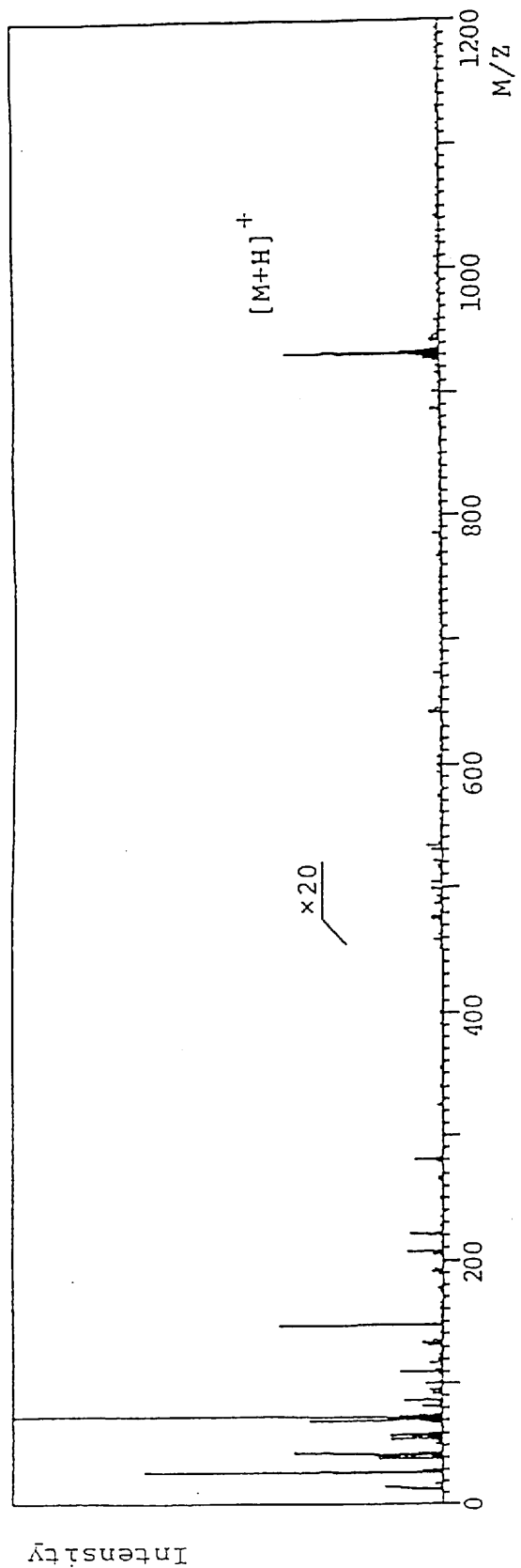
Fig. 5 - 7. SIMS-TOF mass spectrum of angiotensin - III. The flight time of the quasi-molecular ion is 69.29 μs.

spectrum of angiotensin-III is shown in Fig. 5-7. In the

spectrum, quasi-molecular ion, $(M+H)^+$, is clearly seen. The

flight time of the ion M/Z=931.5 was 69.29μs. In the lower

mass region, few peaks derived from fragments of the sample and

the matrix appeared.

A cyclic peptide, gramicidin-S was used for next sample,

which was purchased from Sigma Chemical Co. (St. Louis, MO USA).

The structure of gramicidin-S is shown in Fig. 5-8, and the

molecular weight of mono-isotopic compounds is 1140.7 dalton.
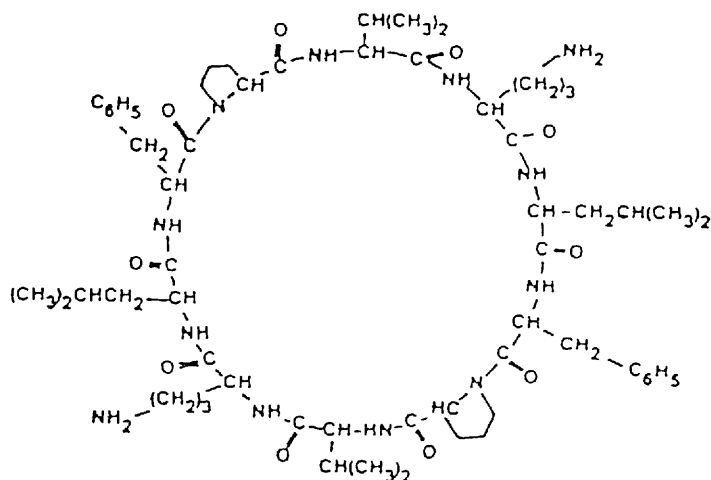
Fig. 5-8. Structure of gramicidin-S.
The molecular weight of the
mono-isotope is 1140.7 dalton.

The flight time of the quasi-molecular ion (M/Z=1141.7) was

76.71μs. The measuring time range was also 0-80μs. The time

channel width was 38ns. The accumulation time was 100s. The

SIMS-TOF mass spectrum of gramicidin-S is shown in Fig. 5-9.

The quasi-molecular ion is clearly observed.
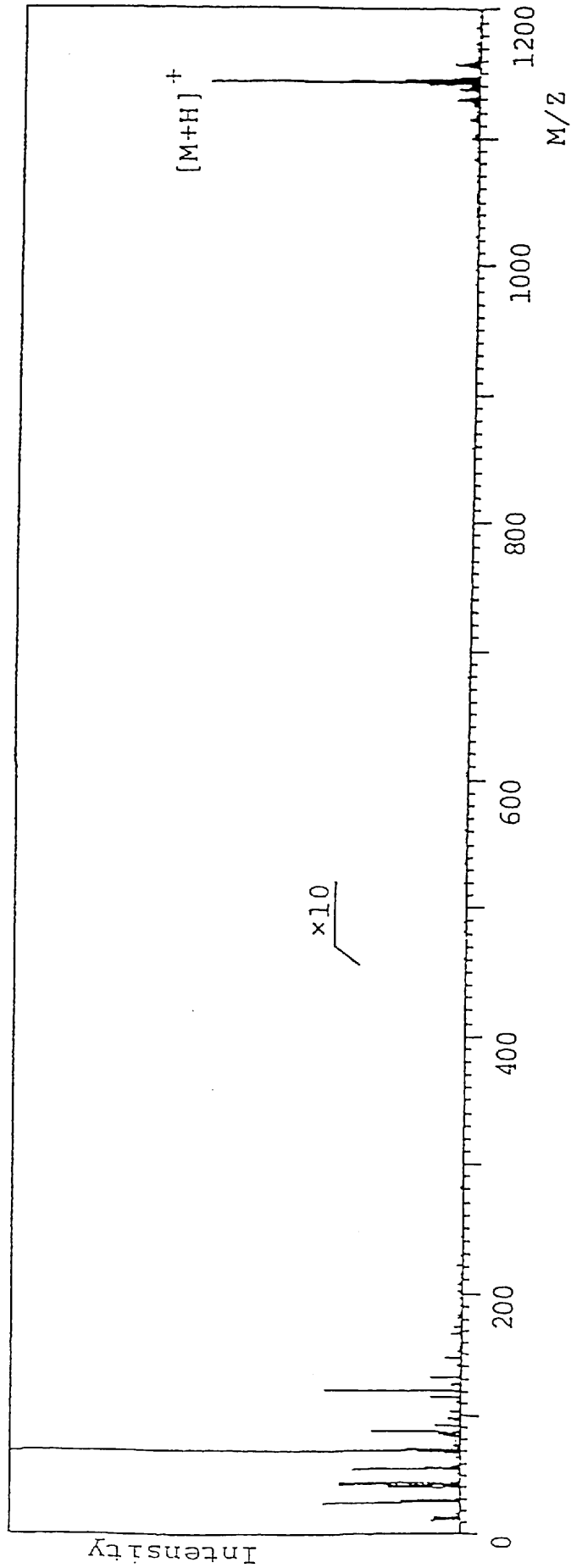
Fig. 5 - 9. SIMS-TOF mass spectrum of gramicidin-S. The flight time of the quasi-molecular ion is 76.71 µs.

The empirical formula of gramicidin-S is $C_{60}H_{92}O_{10}N_{12}$. The molecular weight is distributed by the effect of the natural isotope abundance of respective elements. The theoretical mass distribution of the gramicidin-S molecules was calculated by computer program [5-1], and the results are shown in Fig. 5-3 (a) with the major effect being due to the existence of carbon 13. The molecular ion region of TOF spectrum of gramicidin-S is shown in Fig. 5-3 (b), and in this spectrum, each isotopic peak can be clearly seen as resolved, showing a mass resolution of 2,000.

A more heavier compound, perfluoroalkayl phosphazine was investigated. This sample was presented by Prof. Cotter of the Johns Hopkins University (MD USA). This sample was a mixture of four compounds of families of perfluoroalkayl phosphazines, and these structures are shown in Fig. 5-10 (a-d). Their molecular weights are 4242, 3535, 2828 and 2121, respectively. The SIMS-TOF mass spectrum of perfluoroalkayl phosphazine was taken in the flight time of 100μs-180μs. The accumulation time was 500s. The mass spectrum with mass range of 2000-4500 is shown in Fig. 5-11. The molecular ions $(M)^+$ are detected at M/Z=3535, 2828 and 2121. The molecular ion of compound (a) is barely detected at M/Z=4242. The fragment ions of $(M-331)^+$, which are due to the loss of one side chain, also appeared at M/Z= 3911, 3204 and 2497. Other fragment peaks can also be seen.

TOF mass spectra of organic compounds can be obtained up to M/Z=4000 in the SIMS analysis by the four-sector TOF mass spectrometer. The mass resolution of 2,000 was obtained at M/Z=1141.7, where the peak of unit mass can be clearly resolved.
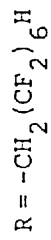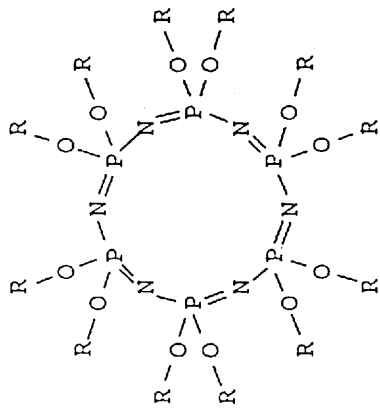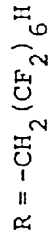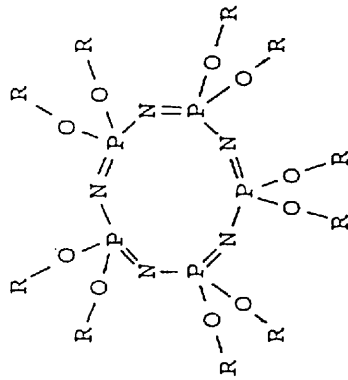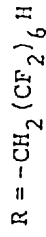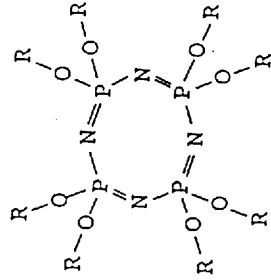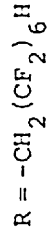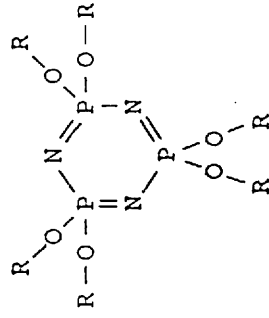
Fig. 5 - 10. Structure of the families of perfluoroalkayl phosphazine.

(a)   R = -CH$_2$(CF$_2$)$_6$H

(b)   R = -CH$_2$(CF$_2$)$_6$H

(c)   R = -CH$_2$(CF$_2$)$_6$H
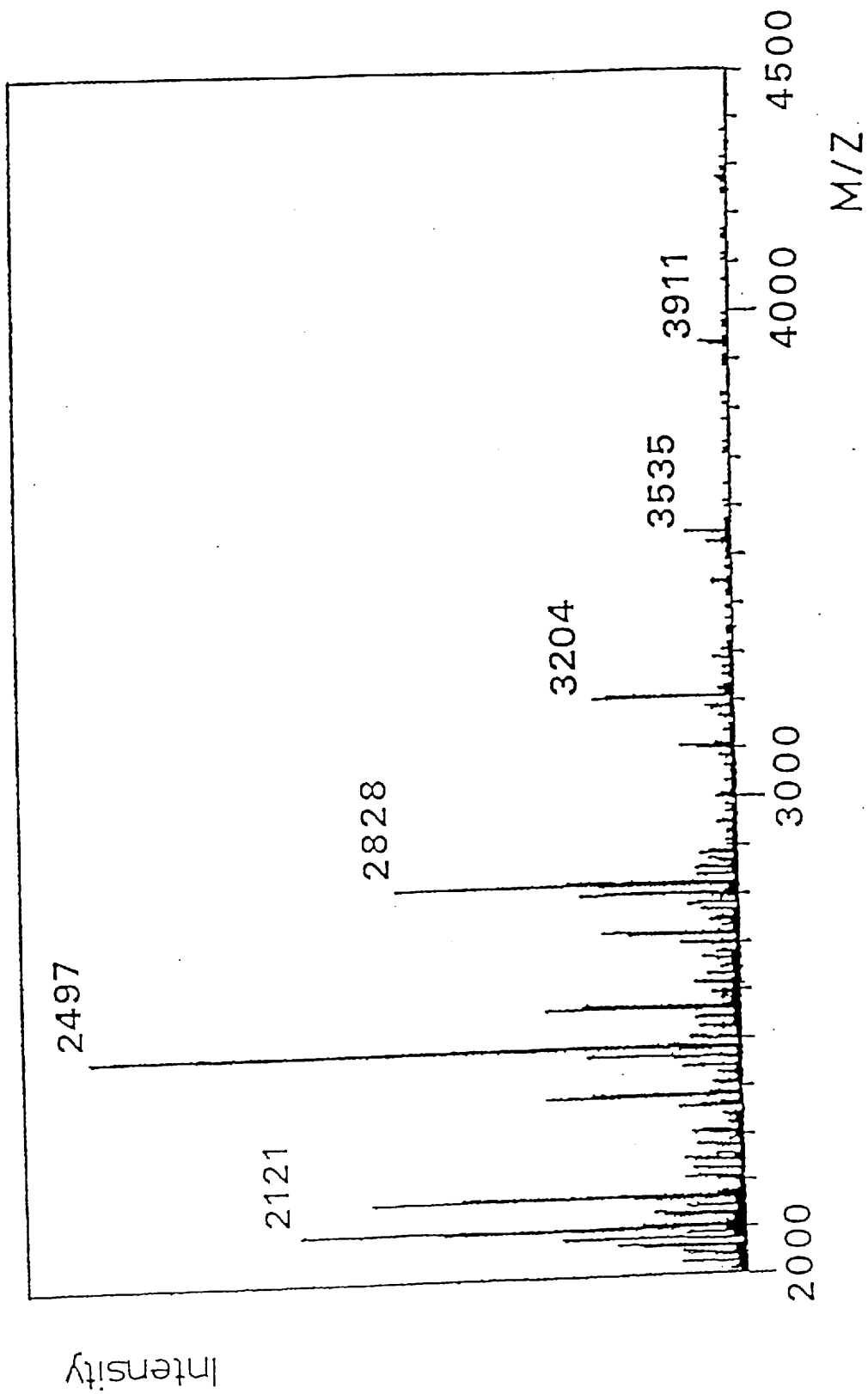
(d)   R = -CH$_2$(CF$_2$)$_6$H

Fig. 5 - 11. SIMS-TOF mass spectrum of perfluoroalkayl phosphazine. The flight time of M/Z = 3911 ion is 142.97 μs.

REFERENCE

5-1. T. Sakurai, T.Matsuo, H. Matsuda and H. Wollnik, Biomed.
Mass Spectom., 11 (1984) 396.

6. SUMMARY

A new time-of-flight mass spectrometer consisting of four electric sectors was investigated. The flight time of an ion in a TOF system is calculated as a power series expansion in a third-order approximation. The ion-optical design of the TOF mass spectrometer satisfies the triple isochronous focusing and the triple spatial focusing conditions, in order to improve the mass resolving power and the ion transmission efficiency. A TOF system with 1.7m flight path length was constructed and the ion-optical characteristics were examined experimentally. The results of the investigations described in this thesis are as follows:

1.) The calculation of the flight times in the toroidal electric sector and the electric quadrupole lens.

It is important to investigate the second and third-order characteristics in addition to the first-order characteristics for a high resolution TOF mass spectrometer. When the higher-order aberrations of a TOF system consisting of electric sector or quadrupole lens are estimated, the calculation of the flight times of ions is necessary. The flight times of the charged particles in a toroidal electric sector and an electric quadrupole lens are calculated. The effects of the fringing fields

are also investigated. The expression of the flight times is given as a path length deviation. The general transfer matrix, which includes an extra row and an extra column for the path length deviation, is introduced into the flight time calculations. The computer program is developed for the numerical calculation of the path length deviation. The ion-optical characteristics of the TOF mass spectrometer can be determined by this program.

2.) The investigation of ion-optical designs for a high
   performance TOF mass spectrometer.

The triple isochronous focusing and triple spatial focusing conditions are introduced to the TOF mass spectrometer, in order to increase the mass resolving power and ion transmission efficiency simultaneously. The possible solutions for satisfying these conditions are investigated in the ion-optical system consisting of toroidal electric sectors. Symmetrical arrangement of systems is introduced for the search of the solutions of the multiple focusing conditions. Many solutions are found for the systems with consisting of two, three and four electric sectors. The ion-optical characteristics for the higher-order aberration coefficients and geometrical properties are also considered.

3.) The proposal and construction of 'excellent' TOF mass

spectrometer consisting of four toroidal electric sectors.

An excellent ion-optical design for the high performance TOF mass spectrometer is proposed. The system consists of four toroidal electric sectors with 269° deflection. The system with 1.7m flight path length is constructed. The analyzing region with four sectors, the ion source and the ion detector are installed in a 41cm diameter vacuum chamber. The toroidal electric field is produced by the combination of cylindrical condenser and Matsuda plates. The fast timing circuits, which are available in practical nuclear physics, are used for the time measuring system. Two types of pulsed ion sources are attached to the mass spectrometer. One is of the electron impact type and other is a secondary ion source for SIMS.

4.) The proof of the ion optical characteristics of the TOF mass spectrometer and the capability of large molecule analysis.

The time width of 18ns at M/Z=132 is obtained by the EI ion source, even though the pulse width of the ion source is 17ns. This suggests that the isochronous focusing is satisfactory. The time width of 19ns at M/Z=1141.7 (quasi-molecular ion of gramicidin-S) is obtained. This corresponds to a mass resolution 2,000. The satellite of the carbon 13 isotope is clearly resolved.

The ion transmission efficiency is investigated by using

the EI ion source and 90% transmission is obtained. The spatial focusing of the TOF mass spectrometer is thus satisfied. Mass peaks up to $M/Z=4000$ are obtained in TOF mass spectrum for a heavier compounds (perfluoroalkayl phosphazine).

From these results, it becomes clear that the new TOF mass spectrometer has enough capability for the analysis of large molecules.

The functions F(m) are defined as $\int_0^\omega m\ d\omega$. The explicit results of calculation are given:

$$F(1) = \omega$$

$$F(s_x) = \frac{1}{k_x} - \frac{c_x}{k_x}$$

$$F(c_x) = \frac{s_x}{k_x}$$

$$F(\omega) = \frac{\omega^2}{2}$$

$$F(s_x s_x) = \frac{\omega}{2} - \frac{s_x c_x}{2k_x}$$

$$F(s_x c_x) = \frac{s_x s_x}{2k_x}$$

$$F(s_x \omega) = \frac{s_x}{k_x^2} - \frac{c_x \omega}{k_x}$$

$$F(c_x \omega) = \frac{-1}{k_x^2} + \frac{c_x}{k_x^2} + \frac{s_x \omega}{k_x}$$

$$F(s_y s_y) = \frac{\omega}{2} - \frac{s_y c_y}{2k_y}$$

$$F(s_y c_y) = \frac{s_y s_y}{2k_y}$$

$$F(s_x s_x s_x) = \frac{2}{3k_x} - \frac{2c_x}{3k_x} - \frac{s_x s_x c_x}{3k_x}$$

$$F(s_x s_x c_x) = \frac{s_x s_x s_x}{3k_x}$$

$$F(s_x s_x \omega) = \frac{\omega^2}{4} + \frac{s_x s_x}{4k_x^2} - \frac{s_x c_x \omega}{2k_x}$$

$$F(s_x c_x \omega) = \frac{-\omega}{4k_x} + \frac{s_x c_x}{4k_x^2} + \frac{s_x s_x \omega}{2k_x}$$

$$F(s_x \omega \omega) = \frac{-2}{k_x^3} + \frac{2c_x}{k_x^3} + \frac{2s_x \omega}{k_x^2} - \frac{c_x \omega \omega}{k_x}$$

$$F(c_x \omega \omega) \quad = \quad \frac{-2s_x}{k_x^3} + \frac{2c_x \omega}{k_x^2} + \frac{s_x \omega \omega}{k_x}$$

$$F(s_x s_y s_y) \quad = \quad \frac{\left(-2k_y^2/k_x + 2k_y^2 c_x/k_x + 2k_y s_x s_y c_y - k_x c_x s_y s_y\right)}{\left(k_x^2 - 4k_y^2\right)}$$

$$F(s_x s_y c_y) \quad = \quad \frac{\left(k_y s_x - 2k_y s_x s_y s_y - k_x c_x s_y c_y\right)}{\left(k_x^2 - 4k_y^2\right)}$$

$$F(c_x s_y s_y) \quad = \quad \frac{\left(-2k_y^2 s_x/k_x + k_x s_x s_y s_y + 2k_y c_x s_y c_y\right)}{\left(k_x^2 - 4k_y^2\right)}$$

$$F(c_x s_y c_y) \quad = \quad \frac{\left(-k_y + k_y c_x + k_x s_x s_y c_y - 2k_y c_x s_y s_y\right)}{\left(k_x^2 - 4k_y^2\right)}$$

$$F(s_y s_y \omega) \quad = \quad \frac{\omega^2}{4} + \frac{s_y s_y}{4k_y^2} - \frac{s_y c_y \omega}{2k_y}$$

$$F(s_y c_y \omega) \quad = \quad \frac{-\omega}{4k_y} + \frac{s_y c_y}{4k_y^2} + \frac{s_y s_y \omega}{2k_y} \quad .$$

APPENDIX 2

When the general transfer matrix [Q] is given by Eq. 3-7, the inverse matrix $[Q]^{-1}$ is expressed as:

$$
[Q]^{-1} = \begin{bmatrix}
(\alpha|\alpha) & -(x|\alpha) & 0 & 0 & (x|\alpha)(\alpha|\delta)-(x|\delta)(\alpha|\alpha) & 0 \\
-(\alpha|x) & (x|x) & 0 & 0 & -(x|x)(\alpha|\delta)+(x|\delta)(\alpha|x) & 0 \\
0 & 0 & (\beta|\beta) & -(y|\beta) & 0 & 0 \\
0 & 0 & -(\beta|y) & (y|y) & 0 & 0 \\
0 & 0 & 0 & 0 & 1 & 0 \\
-(\alpha|\alpha)(l|x) & (x|\alpha)(l|x) & 0 & 0 & -(l|\delta) & 1 \\
+(\alpha|x)(l|\alpha) & -(x|x)(l|\alpha) & & & -[(x|\alpha)(\alpha|\delta)-(x|\delta)(\alpha|\alpha)](l|x) & \\
& & & & +[(x|x)(\alpha|\delta)-(x|\delta)(\alpha|x)](l|\alpha) &
\end{bmatrix}
$$

The point symmetrical matrix [Q*] is created by inversing the signs of the second, fourth and fifth columns and rows of $[Q]^{-1}$.

$$
[Q^{\star}] = \begin{bmatrix}
(\alpha|\alpha) & (x|\alpha) & 0 & 0 & -(x|\alpha)(\alpha|\delta)+(x|\delta)(\alpha|\alpha) & 0 \\
(\alpha|x) & (x|x) & 0 & 0 & -(x|x)(\alpha|\delta)+(x|\delta)(\alpha|x) & 0 \\
0 & 0 & (\beta|\beta) & (y|\beta) & 0 & 0 \\
0 & 0 & (\beta|y) & (y|y) & 0 & 0 \\
0 & 0 & 0 & 0 & 1 & 0 \\
-(\alpha|\alpha)(l|x) & -(x|\alpha)(l|x) & 0 & 0 & (l|\delta) & 1 \\
+(\alpha|x)(l|\alpha) & +(x|x)(l|\alpha) & & & +[(x|\alpha)(\alpha|\delta)-(x|\delta)(\alpha|\alpha)](l|x) & \\
& & & & -[(x|x)(\alpha|\delta)-(x|\delta)(\alpha|x)](l|\alpha) &
\end{bmatrix}
$$

The plane symmetrical matrix [Q'] is obtained by inversing the signs of the second, fourth and sixth columns and rows of $[Q]^{-1}$:

$$[Q'] = \begin{bmatrix} (\alpha|\alpha) & (x|\alpha) & 0 & 0 & (x|\alpha)(\alpha|\delta)-(x|\delta)(\alpha|\alpha) & 0 \\ (\alpha|x) & (x|x) & 0 & 0 & (x|x)(\alpha|\delta)-(x|\delta)(\alpha|x) & 0 \\ 0 & 0 & (\beta|\beta) & (y|\beta) & 0 & 0 \\ 0 & 0 & (\beta|y) & (y|y) & 0 & 0 \\ 0 & 0 & 0 & 0 & 1 & 0 \\ \begin{array}{l}(\alpha|\alpha)(l|x)\\ -(\alpha|x)(l|\alpha)\end{array} & \begin{array}{l}(x|\alpha)(l|x)\\ -(x|x)(l|\alpha)\end{array} & 0 & 0 & \begin{array}{l}(l|\delta)\\ +[(x|\alpha)(\alpha|\delta)-(x|\delta)(\alpha|\alpha)](l|x)\\ -[(x|x)(\alpha|\delta)-(x|\delta)(\alpha|x)](l|\alpha)\end{array} & 1 \end{bmatrix}$$

ACKNOWLEDGMENTS